SANDIA REPORT

SAND95–1736 • UC–814
Unlimited Release
Printed January 1997

Yucca Mountain Site Characterization Project

Mechanical Properties of Fractures from Drillholes UE25-NRG-4, USW-NRG-6, USW-NRG-7, USW-SD-9 at Yucca Mountain, Nevada

William A. Olsson, Stephen R. Brown

Prepared by
Sandia National Laboratories
Albuquerque, New Mexico 87185 and Livermore, California 94550
for the United States Department of Energy
under Contract DE-AC04-94AL85000

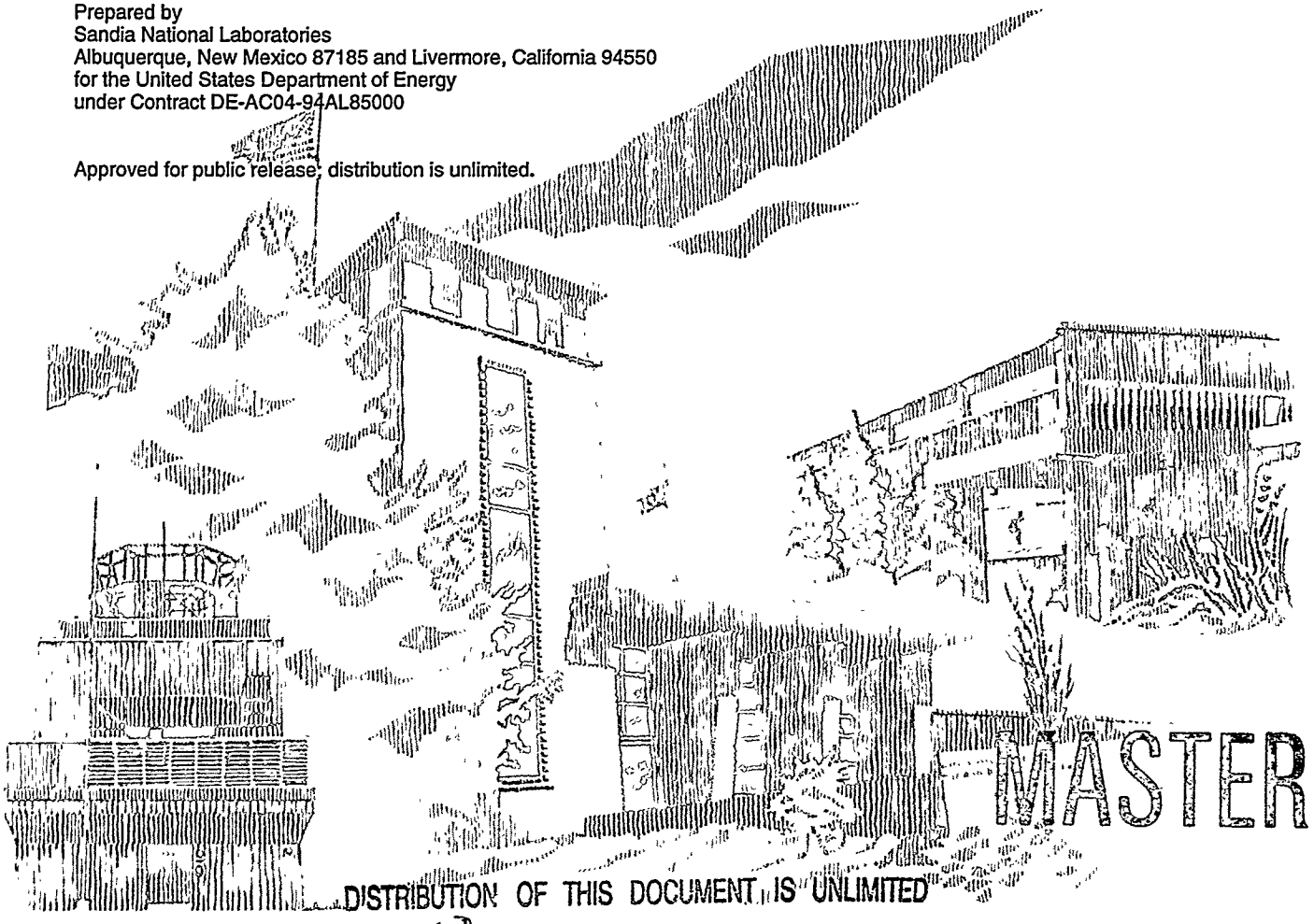

"Prepared by Yucca Mountain Site Characterization Project (YMSCP) participants as part of the Civilian Radioactive Waste Management Program (CRWM). The YMSCP is managed by the Yucca Mountain Project Office of the U.S. Department of Energy, DOE Field Office, Nevada (DOE/NV). YMSCP work is sponsored by the Office of Geologic Repositories (OGR) of the DOE Office of Civilian Radioactive Waste Management (OCRWM)."

Issued by Sandia National Laboratories, operated for the United States Department of Energy by Sandia Corporation.

Available to DOE and DOE contractors from
Office of Scientific and Technical Information
PO Box 62
Oak Ridge, TN 37831

Prices available from (615) 576-8401, FTS 626-8401

Available to the public from
National Technical Information Service
US Department of Commerce
5285 Port Royal Rd
Springfield, VA 22161

NTIS price codes
Printed copy: A05
Microfiche copy: A01

Distribution
Category UC-814

SAND95–1736
Unlimited Release
Printed January 1997

Mechanical Properties of Fractures from Drillholes

UE25-NRG-4
USW-NRG-6
USW-NRG-7
USW-SD-9

at Yucca Mountain, Nevada

William A. Olsson and Stephen R. Brown
Geomechanics Department
Sandia National Laboratories
Albuquerque, New Mexico 87185-0751

ABSTRACT

Rock cores from drillholes UE25-NRG-4, USW-NRG-6, USW-NRG-7, and USW-SD-9 containing natural fractures were obtained from the Sample Management Facility at Yucca Mountain, Nevada. All recoverable fractures were sheared at constant normal stresses from 2.5 to 15 MPa, in the as-received condition (air-dry). Detailed profilometer data were collected from each fracture surface before testing. The tests yielded the normal closure as a function of normal stress, and the shear stress and dilation as functions of shear offset. The constitutive properties obtained from these stress-displacement relations were: normal stiffness, shear stiffness, shear strength, and dilation angle at peak shear stress. Shear strength plotted against normal stress for four thermomechanical units shows that friction angle varies from 37° to 46° and cohesion varies from 0.02 to 1.71 MPa.

This report was prepared under the Yucca Mountain Project WBS number 1.2.3.2.7.1.4. The planning documents that guided this work activity are Site Characterization Plan Section 8.3.1.15.1.4 and Work Agreement WA-0091. The information and data documented in this report are qualified and have been submitted to YMP in TDIF numbers 304186, 304192, and 304529.

Contents

List of Tables

List of Figures

This page intentionally left blank.

1 Introduction

The Yucca Mountain Site Characterization Project (YMP) of the Office of Civilian Radioactive Waste Management (OCRWM) Program has been assigned the task of determining the suitability of the Yucca Mountain site. Among the concerns being investigated, the characterization of the mechanical properties of the fractures present in the host rock has direct relevance to repository design, and the pre- and post-closure performance assessment. This report is the second in a series beginning with Olsson and Brown (1994), and includes data collected on natural fractures from drillholes: UE25-NRG-4, USW-NRG-6, USW-NRG-7, and USW-SD-9. This work is in support of design of the Experimental Studies Facility and Repository as well as performance assessment of the Repository System.

Most rock masses contain natural fractures that are called joints if they show little or no visible offset. The presence of these features in the rock mass has important effects on the overall thermomechanical/hydromechanical response of the mass. They can increase the compliance, reduce the strength, alter the thermal conductivity, and act as pathways for fluid movement. Because of their potential importance in design and performance assessment, the Site Characterization Plan (SCP) calls for the measurement of certain fracture properties: normal stiffness, shear stiffness, cohesion, and coefficient of friction. Normal stiffness is defined as the derivative of normal stress with respect to closure; shear stiffness is defined as the derivative of shear stress with respect to joint slip. Shearing the joint at a constant slip rate while holding the normal stress constant will give all specified data, provided that shear and normal displacements are recorded.

We report for each test: normal stress, shear and normal stiffness functions, shear strength, residual shear strength, and dilation angle at peak shear stress. Also, the friction angle Φ and cohesion C are obtained from plots of shear strength against normal stress for four thermomechanical units. There is a variety of possible plots of shear strength against normal stress, i.e., for a given thermomechanical unit or for a specific drill hole; we have chosen to compare Φ and C for the various thermomechanical units. The depth for each specimen is included in its ID number so that the user may examine the data in terms of the detailed stratigraphy or any other grouping. The fracture dilation, though not called for, is nevertheless critical to coupled thermomechanical or hydromechanical modeling. Furthermore, we include data on reversed shearing and cyclic loading. Because shear and normal stiffnesses are functions of stress they are plotted against stress; and either stiffness may be read directly from the curves in the figures at any stress desired.

In anticipation of needs brought out by further developments in theoretical models relating surface topography to joint hydromechanical and thermomechanical response, we also report detailed topographic data for each joint. The resolution of the topographic data is greater than that specified in related rock mechanics testing standards (e.g., the ASTM D 5607-94, governing direct shear tests). The mathematical characteristics of detailed surface profiles such as those reported herein have been related to the more qualitative joint roughness measurements by Tse and Cruden (1979).

This page intentionally left blank.

2 Experimental Technique and Specimen Preparation

The results reported here were obtained in rotary shear. This technique has been used for at least twenty years and has certain advantages over other configurations used for shear testing. Details on implementation of this test technique along with discussions of its relative advantages and disadvantages and many important results can be found in a number of papers (Biegel *et al.*, 1992; Christensen *et al.*, 1974; Kutter, 1974; Olsson, 1987, 1988; Olsson and Brown, 1993; Xu and Frietas, 1988; Tullis and Weeks, 1986; Weeks and Tullis, 1985; Yoshioka and Scholz, 1989). In this type of experiment, the specimen is composed of two, short, hollow tubes of rock that are pressed together under controlled load. Torque is then applied to cause sliding on the interface (Fig. 1). Further details may be obtained from (Olsson, 1987).

Specimens were recieved packaged for shipping in molded styrofoam and wrapped in plastic wrap. No shipping damage to the core boxes or the core itself was evident. The discontinuities appeared to be fractures and possibly some bedding surfaces. Fracture orientations with respect to the core were not measured, but because the tested specimens were replaced in their original locations in the core boxes these data remain available. Being outside the scope of the present investigation, geologic descriptions of the individual specimens were not obtained; however, the lithostratigraphic unit assignments are given in Table 1 and descriptions of these units are given in Geslin and Moyer (1995). The core was stored in the laboratory in the as-recieved condition.

Test specimens were short hollow cylinders divided at mid-height by the fracture. They were prepared from the as-received core by subcoring perpendicular to the fracture. Outer diameters of the test specimens were constrained by the size of the recovered core and by the orientations of the fractures. In each case, the largest possible test specimen was obtained. Outer diameters ranged from 44.3 mm to 82.0 mm. The hollow center was created by removing a concentric subcore with a diameter about one half that of the test specimen. Test specimens were potted into metal specimen holders with gypsum cement (Fig. 1); the metal specimen holders were then bolted into the load-frame.

In the usual direct shear tests, rotations of the shear box around axes in the plane of the fracture are accounted for by mounting LVDTs at the corners of the rectangular shear box to measure normal displacements (ASTM 5607-94); the readings from the 4 LVDTs are averaged to compute the normal displacement. In rotary shear, however, rotations about axes that lie in the fracture plane are absent so that only two LVDTs are used. The specimens were tested in the air-dry condition and thus no encapsulants were used. No photographs were taken, but all test materials were saved. The test period was July 29, 1994 to May 17, 1995.

Measured values of torque and axial load were used to compute, respectively, the shear stress and normal stress. The shear stress during sliding is given by

$$\tau = \frac{3T}{2\pi(R_o^3 - R_i^3)} \tag{1}$$

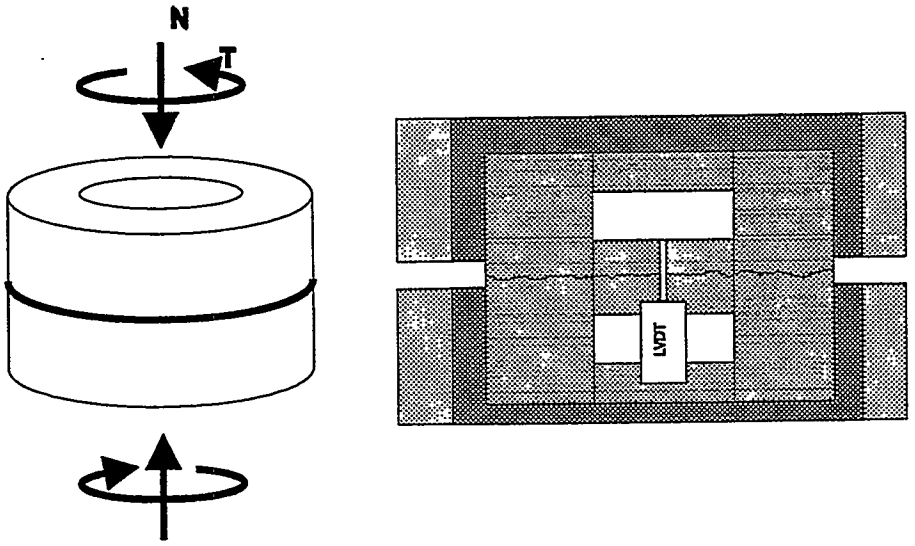

Figure 1: The specimen configuration for rotary shear experiments on joints. Left is a perspective view showing applied forces. Right is a cross-section; light grey is aluminum holder, dark grey is gypsum cement, medium grey is rock specimen, white is LVDT body and core, and mounting supports. Setup also included LVDTs mounted to the outside of aluminum ring to measure displacement across the joint. Not to scale.

here T is the torque, and R_o and R_i are, respectively the outer and inner diameters.

In the first phase of a test, the normal stress was increased from zero to the pre-selected normal stress and then unloaded. This normal stress cycle provided information on the inelasticity of the normal closure process. In the second phase of the test, the joint was reloaded to the previous maximum value of normal stress; then, monotonically increasing shear displacement was applied while the torque was recorded. Tests in which the specimen halves were pushed through a complete cycle of forward slip, reverse slip, and repeated forward slip, show that shear strength is a strong function of stress history (e.g., Figs. 19 or 51, for example). Thus it would be inappropriate, for the specimens tested in this study, to determine the shear strength as a function of pressure (Φ and C) by running several tests at incrementally increased normal stress on the same joint, as sometimes done (cf. ASTM 5607-94).

3 Profilometer Data

In anticipation of needs brought out by further developments in theoretical models relating surface topography to joint hydromechanical and thermomechanical response, we have made detailed measurements of the surface topography for most specimens. The methods of measurement and data analysis are the same as those described in Brown (1995). It is beyond the scope of this report

Mechanical Property Summary

Test ID	T-M Unit	Lithologic Unit Unit	Specimen ID Number	σ MPa	τ_p MPa	τ_r MPa	β_p degrees
M3	TCw	Tpcpll	NRG-6-27.6–28.1-SNL	5.0	5.16	4.93	10.22
YM8	TCw	Tpcplnc	NRG-6-102.9-103.4-SNL	15.0	15.46	10.20	7.35
YM13	TSw1	Tptrl	NRG-4-670.5-671.1-SNL	2.5	3.49	2.59	11.05
YM10	TSw1	Tptrn	NRG-6-380.9-381.3-SNL	2.5	3.68	2.95	16.02
YM4	TSw1	Tptrn	NRG-4-537.8-538.2-SNL	5.0	5.48	5.21	5.72
YM2	TSw1	Tptrn	NRG-4-608.7-609.2-SNL	5.0	4.44	4.17	7.39
YM1	TSw1	Tptrn	NRG-6-297.4-297.7-SNL	5.0	5.16	5.01	7.15
YM5	TSw1	Tptrn	NRG-6-424.0-424.5-SNL	5.0	5.28	3.98	5.23
YM18	TSw1	Tptrn	NRG-7-367.2-367.8-SNL	5.0	6.47	4.2	15.9
YM14	TSw1	Tptrn	NRG-7-408.8-409.6-SNL	5.0	4.18	3.71	1.19
YM12	TSw1	Tptrn	NRG-6-296.0-296.4-SNL	10.0	11.89	6.59	13.41
YM7	TSw1	Tptrn	NRG-6-401.5-401.9-SNL	10.0	11.10	7.84	7.03
YM6	TSw1	Tptpul2	NRG-6-485.9-486.3-SNL	10.0	10.19	7.82	8.95
YM19	TSw1	Tptrn	NRG-7-434.7-435.3-SNL	10.0	6.85	6.02	-13.1
YM15	TSw1	Tptrn	NRG-7-447.2-448.1-SNL	10.0	9.45	5.41	4.18
YM17	TSw1	Tptrn	NRG-7-317.3-317.8-SNL	15.0	11.5	10.70	2.03
YM16	TSw1	Tptrn	NRG-7-430.2-430.9-SNL	15.0	13.26	9.09	1.28
YM9	TSw2	Tptpmn	NRG-6-782.3-782.6-SNL	2.5	1.92	1.80	1.11
YM24	TSw2	Tptpln	SD-9-1255.9-1256.3-SNL	2.5	2.37	2.29	8.48
YM30	TSw2	Tptpll	SD-9-1132.2-1132.9-SNL	5.0	5.45	4.53	17.3
YM22	TSw2	Tptpll	SD-9-1171.1-1171.8-SNL	5.0	5.48	4.81	1.23
YM23	TSw2	Tptpln	SD-9-1254.7-1255.2-SNL	10.0	7.68	7.10	33.4
YM25	TSw2	Tptpln	SD-9-1254.7-1255.2-SNL	10.0	8.97	8.34	18.4
YM11	TSw2	Tptpll	NRG-6-935.0-935.3-SNL	15.0	11.89	8.56	10.22
YM31	TSw2	Tptpll	SD-9-1141.2-1141.5-SNL	15.0	14.0	14.0	15.7
YM29	TSw2	Tptpll	SD-9-1144.2-1145.1-SNL	15.0	15.5	10.2	27.2
YM28	CHn1	Tac	SD-9-1480.7-1481.8-SNL	2.5	3.52	2.89	4.44
YM26	CHn1	Tac	SD-9-1480.7-1481.8-SNL	5.0	4.35	3.66	11.0
YM27	CHn1	Tac	SD-9-1480.7-1481.8-SNL	10.0	9.45	5.46	16.0

Table 1: Experiment identifier, thermomechanical unit, lithostratigraphic unit (Geslin and Moyer, 1995), specimen number and strength data for each experiment. TCw = Tiva Canyon welded unit; TSw1 = Topopah Spring welded unit, lithophysal rich; TSw2 = Topopah Spring welded unit, lithophysal poor; CHn1 = Calico Hills. σ normal stress; τ_p peak shear stress; τ_r residual shear stress; β_{peak} dilation angle at peak stress. *Note*: Data from tests YM1 through YM7 (Olsson and Brown, 1994) are included here for completeness and ease of use.

to describe the data analysis procedures in detail, so only a brief discussion is given here. For more detail, the interested reader is referred to the paper by Brown (1995) and the references included therein.

The topography of each fracture surface was measured with a non-contacting laser profilometer. This instrument consists of a precision three-axis positioning system which moves a laser distance measurement probe over the surface, recording surface height. The probe is moved along parallel lines to record a series of one-dimensional surface profiles. Each sample consists of two hollow tubes with the joint surfaces exposed on the ends. Three surface profiles were taken in a circular path around each of the two surfaces comprising a sample. The three profiles were separated from each other along the sample radius. Figure 4a (and its companions for other tests) shows a circular representation of these profiles, where topographic height is represented as deviations in radius around a circular path. The radius of the outer profile and the separation between profiles is given in Table 2. The topographic heights were sampled at an increment of every 0.06 degrees for a total of 360 degrees. Using Table 2, given the radius of a profile in millimeters R, the spacing between data points on each profile in millimeters, dx, can be calculated by the expression $dx = 0.06dR\pi/180$.

The samples were mounted in the profilometer in such a way as to allow matched pairs of profiles from each surface to be closely refitted in the subsequent analysis. Several preliminary data processing steps were done once the profiles were taken. First, each pair of profiles from the two halves of the fracture was fitted together and the standard deviation of the "composite topography" (negative of the aperture distribution or the local distance between the surfaces as defined by Brown, 1995) was computed. Then the two profiles were repeatedly shifted relative to one another, one sample interval at a time, and the composite topography was recomputed. The best match is found when the standard deviation of the composite topography computed at each offset reaches a minimum. The mean level and the linear slope were then removed from both profiles and the composite topography. Figure 4b (and its companions for other tests) show the matched profiles and composite topography for the center scan around the sample surface. Following the simple surface topography model presented by Brown (1995), several surface roughness statistics were calculated and are presented in Table 2. Figures 5c,d (and their companions for other tests) show two of the more important statistical functions calculated from the profile data: the power spectral density of surface profiles and the probability density function for heights of the composite topography. The probability density function describes the distribution of heights about the mean value without regard to the horizontal spatial position, and the the power spectrum describes the texture or spatial correlation of heights on the surface. Details of how these functions are computed and their significance to surface roughness characterization are given by Brown (1995). The roughness characteristics of the fracture surfaces derived from the profiles from this study agree qualitatively with the simple mathematical model of Brown (1995) derived from fracture data in many other rock types. The surfaces themselves have approximately power-law power spectral density functions indicating self-affine fractal geometry. The two surfaces comprising most fractures are closely matched at length scales above a few millimeters. Many fractures have Gaussian aperture distributions.

Profilometer Data for Each Sample

Test ID	R_o mm	dR mm	D_{lin}	D_{log}	λ_c^1 mm	λ_c^2 mm	σ_p mm	σ_a mm
YM8	21.12	5.0	1.44	1.26	3.58	1.44	0.36	0.16
YM9	21.12	5.0	1.57	1.29	NA	NA	0.14	0.33
YM10	21.12	5.0	1.47	1.28	6.73	2.33	0.38	0.26
YM11	21.12	5.0	1.74	1.36	1.17	0.75	0.18	0.04
YM12	21.12	5.0	1.47	1.37	4.47	0.49	0.38	0.30
YM13	21.12	5.0	1.53	1.36	3.38	1.22	0.34	0.33
YM14	38.25	7.0	1.56	1.41	NA	NA	0.66	0.86
YM15	–properties unknown, noisy data–							
YM16	37.00	6.0	1.48	1.32	9.41	1.61	0.66	0.59
YM17	20.38	4.0	1.36	NA	5.49	0.31	0.28	
YM18	20.38	4.0	1.51	1.24	2.71	1.03	0.82	0.28
YM19	20.38	4.0	1.45	1.38	7.67	2.33	0.27	0.29
YM22	20.38	4.0	1.41	1.28	24.8	3.64	0.27	0.25
YM23	20.38	4.0	1.51	1.36	11.8	3.85	0.17	0.14
YM24	36.38	7.0	1.56	1.30	NA	3.20	0.19	0.28
YM25	20.38	4.0	1.52	1.26	6.14	1.52	0.38	0.16
YM26	20.38	4.0	1.38	1.27	NA	0.41	0.22	0.31
YM27	20.38	4.0	1.48	1.40	7.12	1.24	0.15	0.17
YM28	20.38	4.0	1.46	1.39	1.13	0.28	0.22	0.08
YM29	20.38	3.0	1.36	1.12	3.14	0.85	1.05	0.24
YM30	20.38	4.0	1.38	1.16	2.33	1.03	0.31	0.12
YM31	20.38	4.0	1.50	1.20	1.07	0.31	0.43	0.05

R_o – Radius of outside profile.
dR – Radius increment between profiles.
D_{lin} – fractal dimension with uniform weights in least squares fit.
D_{log} – fractal dimension with logarithmic weights in least squares fit.
λ_c^1, λ_c^2 – estimates of mismatch length scale.
σ_p – standard deviation of surface for a 23 mm profile segment.
σ_a – standard deviation of aperture for a 23 mm profile segment.
Note: 'NA' indicates a mismatch length scale λ greater than the profile length.

Table 2: Profilometer data for each sample. Refer to Brown (1995) for a further explanation of each roughness parameter.

This page intentionally left blank.

4 Results of Compression and Shear Experiments

The mechanical data for all tests are summarized in Table 1 and the profilometric data are given in Table 2. To simplify nomenclature, a short experiment identification number was used; the correlation between experiment number and sample number is given in Table 1. The lithostratigraphic unit assignments (defined in Geslin and Moyer (1995)) are also given. The stress-deformation data from each test are summarized in a separate set of 3 figures. All data sets follow the example of test YM8 whose data are presented in Figures 2, 3, and 4. All the rest of the tests are shown in figures in Appendix A. For test YM8 the resulting closure curve is shown in the upper left of Figure 2. The normal stiffness, that is, the instantaneous slope of the normal stress-closure curve, is plotted in the upper right (Fig. 2).

The shear stress *vs.* slip up to peak shear stress is shown in the lower left part of Figure 2. The shear stress is plotted against the shear stiffness, i.e., the instantaneous slope of the shear stress-slip curve, on the lower right (Fig. 2). The full shear stress-slip data set is shown in Figure 3. Also, in Figure 3, the dilation is plotted against the slip. The dilation angle is defined as the arctangent of the instantaneous slope of the dilation *vs.* slip curve, and the value at peak stress β_p is given in Table 1. Profilometric data are summarized in Figure 4.

Each sample was subjected to a normal compression cycle in the mated condition before shearing. Test data are given in Table 1. All normal compression curves show hysteresis and permanent closure after the first cycle. Only the first loading in compression, the range over which the stiffness was computed, is shown in the figures. The second loading up to the normal stress required for the shear test was, as expected, always stiffer.

All samples were sheared at constant normal stress at room temperature and in the air-dry condition (prevailing laboratory relative humidity in the neighborhood of 20%). Most shear stress-slip curves are characterized by peak stress, τ_p, followed by a more or less gradual descent to a residual value, τ_r. The load-point slip was corrected to joint slip when necessary by subtracting shear stress/unloading modulus from the load-point values. The stiffness of the machine/mounting system was very large compared to most specimens so that the correction was not often necessary. Because shear stiffness is defined in terms of slip, its magnitude is infinitely high when no slip is occurring at the begining of a test, and drops smoothly to zero at peak stress.

All dilation curves start at a negative value because of the finite normal stress application. Furthermore, all show an initial decrease to a local minimum with the onset of slip. Then the dilation angle becomes positive and nearly constant for the remainder of the first loading phase. The reported value of dilation angle (Table 1) is computed at the slip corresponding to peak stress.

Figure 5 summarizes graphically the friction angle Φ and the cohesion C for each of the specimens and groups the data by thermomechanical unit. The wide variation in strength at a given normal stress for TSw1, the unit represented by the most data, suggests that reliable conclusions

with regard to Φ and C for the other 3 units cannot be made at this time. It is important to note that the data for CHn1 were measured on specimens collected from the same fracture, within half a dozen centimeters of each other. About the only preliminary conclusion that can be drawn with this limited number of samples, is that there may be a systematic difference in cohesion between the four units, ranging from 0.02 to 1.71 MPa; and very little difference in tan Φ, which averages 0.82 for the four units.

5 Summary

Cores from drillholes UE25-NRG-4, and USW-NRG-6 and USW-NRG-7, and USW-SD-9 containing natural fractures were obtained from the Sample Management Facility at Yucca Mountain, Nevada. Selected fractures were sheared at constant normal stress, either 2.5, 5, 10, or 15 MPa, in the as-received condition (air-dry). Detailed profilometer data were collected from each fracture surface before testing. The tests yielded the normal closure as a function of normal stress, and the shear stress and dilation as functions of shear offset. The constitutive properties resulting from the measurements at selected normal stresses were: normal stiffness, shear stiffness, shear strength, and dilation. At this point there is insufficient data to identify systematic variations in the mechanical parameters except that over the limited range of normal stress accessed, the shear stress-normal stress relation is linear and characterized simply by the slope (tan Φ) and the intercept (C). The roughness characteristics of the fracture surfaces agree qualitatively with the simple mathematical model of Brown (1995) derived from fracture data in many other rock types.

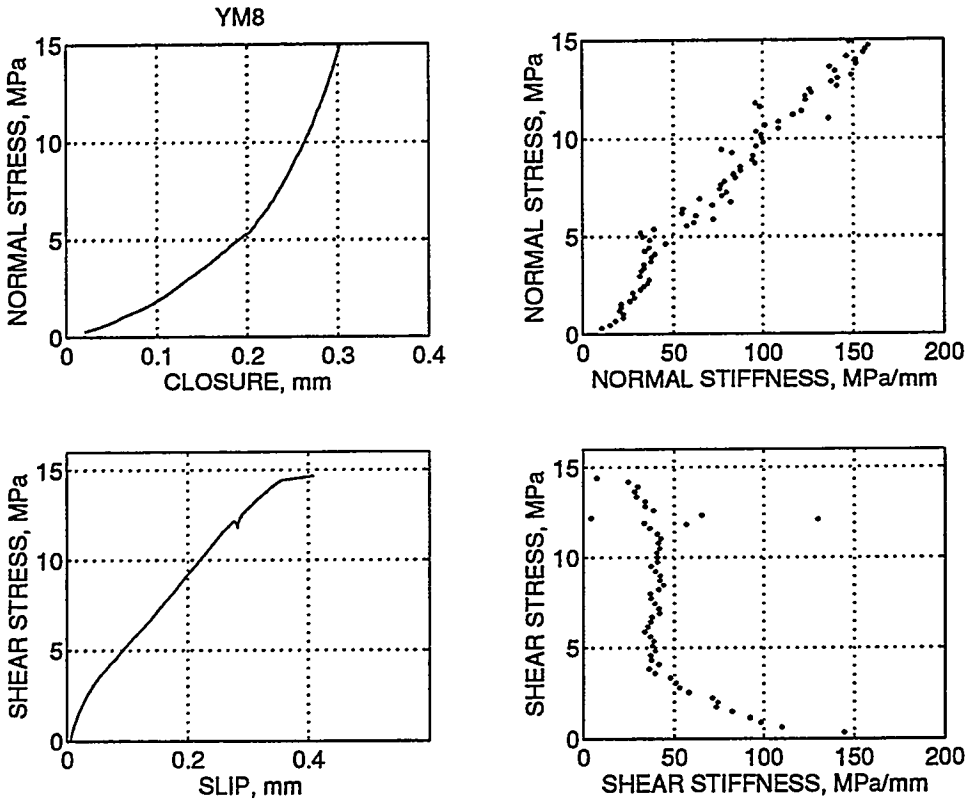

Figure 2: Shear and normal stiffness data for YM8. Upper left: normal stress *vs.* closure. Upper right: normal stress *vs.* normal stiffness. Lower left: shear stress *vs.* slip. Lower right: shear stress *vs.* shear stiffness. The corresponding data set for each test is displayed in the same manner.

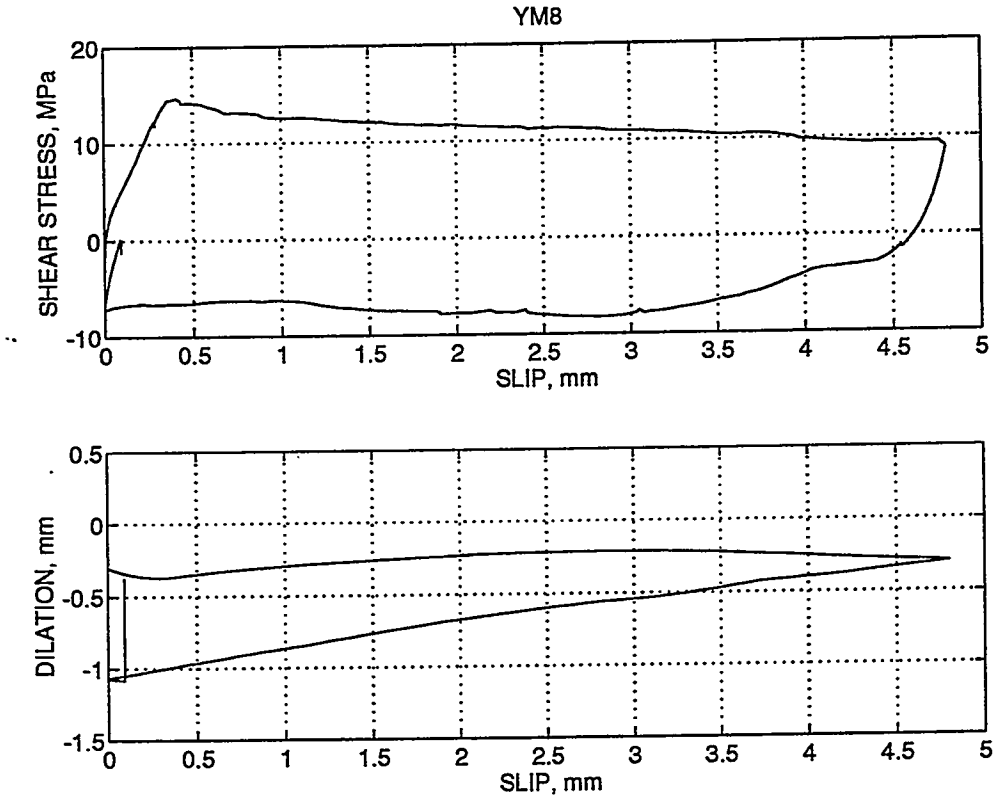

Figure 3: Shear strength and dilation data for YM8. Top: shear stress *vs.* slip at constant normal stress. Bottom: Dilation *vs.* slip. Corresponding data set for each test is displayed in the same manner.

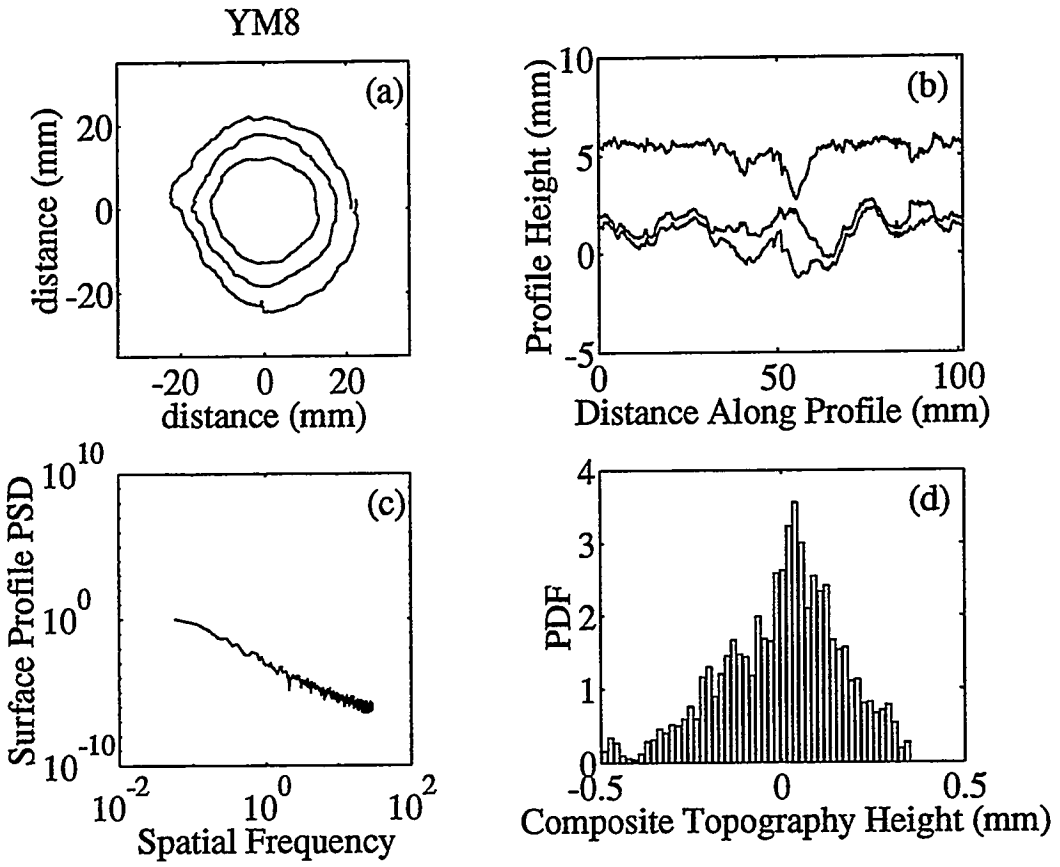

Figure 4: Profilometer data for YM8. **(a)** Three circular profiles on one fracture surface. The average (circular) radius of each profile represents the position of the profile in millimeters from the center of the sample. The radial variation from this circle represents the topographic height in millimeters. Variations in the topography of the surfaces around the sample surface can be seen in this representation. **(b)** The center profiles on each surface are unwrapped and matched in the two bottom curves. The "composite topography" (negative of the aperture) is plotted in the upper curve. This curve has a mean value of zero, but has been offset along the ordinate by an arbitrary amount for clarity. The local maxima of the composite topography are potential contact spots. **(c)** Average power spectral density function for all profiles on both fracture surfaces. The nearly linear form of this function on a log-log plot indicates that this surface is a self-affine fractal where the slope is proportional to the fractal dimension. **(d)** Probability density function for heights on the composite topography averaged over all three pairs of matched profiles.

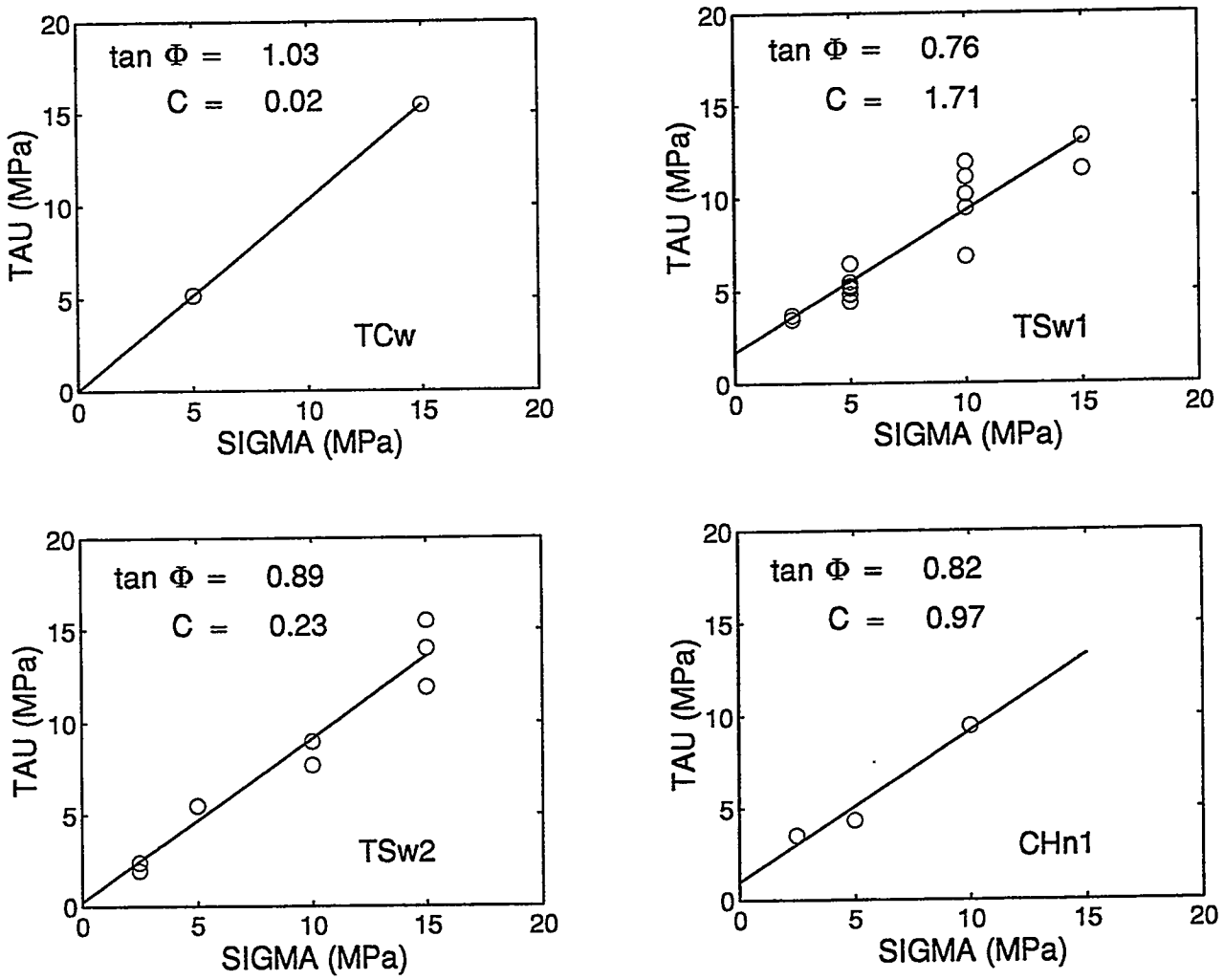

Figure 5: Mohr-Coulomb Parameters. Shear strength plotted against normal stress for the various thermomechanical units.

6 Acknowledgements

The authors thank D.E. Cox and T.V. Tormey for sample preparation, calibration, and testing. R.D. Hardy maintained and operated the profilometer and measured the profiles. R.D. Hardy and D.E. Cox carried out the mechanical testing. Nancy Brodsky's comments on the manuscript were very helpful.

7 References

Biegel, R. L., W. Wang, C. H. Scholz, and B. N. Boitnott, Micromechanics of Rock Friction 1. Effects of surface roughness on initial friction and slip hardening in Westerly granite, *J. Geophys. Res., 97*, 8951–8964, 1992.

Brown, S. R., Simple mathematical model of a rough fracture, *J. Geophys. Res., 100*, 5941–5952, 1995.

Christensen, R. J., S. R. Swanson, and W. S. Brown, Torsional shear measurements of the frictional properties of Westerly granite, in *Advances in Rock Mechanics, Proc. 3rd Cong. Intern. Soc. Rock Mech.*, National Academy of Sciences, Washington, D. C., 221–225, 1974.

Geslin, J.K., and T.C. Moyer, Summary of Lithologic Logging of New and Existing Boreholes at Yucca Mountain, Nevada, March 1994 to June 1994, U.S. Geological Survey Open-File Report 94-451, U.S. Department of the Interior, Denver, Colorado, 1995.

Kutter, H. K., Rotary shear testing of rock joints, in *Advances in Rock Mechanics, Proc. 3rd Cong. of the Intern. Soc. for Rock Mech.*, National Academy of Sciences, Washington, D.C., 254–262, 1974.

Olsson, W. A., Rock Joint Compliance Studies, *Sandia National Laboratories Tech. Rep., SAND86–0177*, Albuquerque, NM, 1987. (NNA.891019.0291)

Olsson, W. A., Compliance and Strength of Artificial Joints in Topopah Spring Tuff, *Sandia National Laboratories Tech. Rep., SAND88–0660*, Albuquerque, NM, 1988. (NNA.881202.0205)

Olsson, W. A., and S. R. Brown, Hydromechanical response of a fracture undergoing compression and shear, in *Int. J. Rock Mech. Min. Sci. & Geomech. Abstr., 30*, 845–851, 1993.

Olsson, W. A., and S. R. Brown, Mechanical Properties of Seven Fractures from Drillholes NRG-4 and NRG-6 at Yucca Mountain, Nevada, *Sandia National Laboratories Tech. Rep., SAND94–1995*, Albuquerque, NM, 1994. (MOL.19941007.0081)

Tse, R., and D.M. Cruden, Estimating joint roughness coefficients, *Int. J. Rock Mech. Min. Sci. & Geomech. Abstr., 16*, pp. 303–307, 1979.

Tullis, T. E., and J. D. Weeks, Constitutive behavior and stability of frictional sliding of granite, *PAGEOPH, 124*, 383–414, 1986.

Weeks, J. D., and T. E. Tullis, Frictional sliding of dolomite: a variation in constitutive behavior, *J. Geophys. Res., 90*, 7821–7826, 1985.

Xu, S., and M. H. de Frietas, Use of a rotary shear box for testing the shear strength of rock joints, *Geotechnique, 38*, 301–309, 1988.

Yoshioka, N., and C. H. Scholz, Elastic properties of contacting surfaces under normal and shear loads 2. Comparison of theory with experiment, *J. Geophys. Res., 94*, 17691–17700 1989.

8 Appendix A: Data Plots

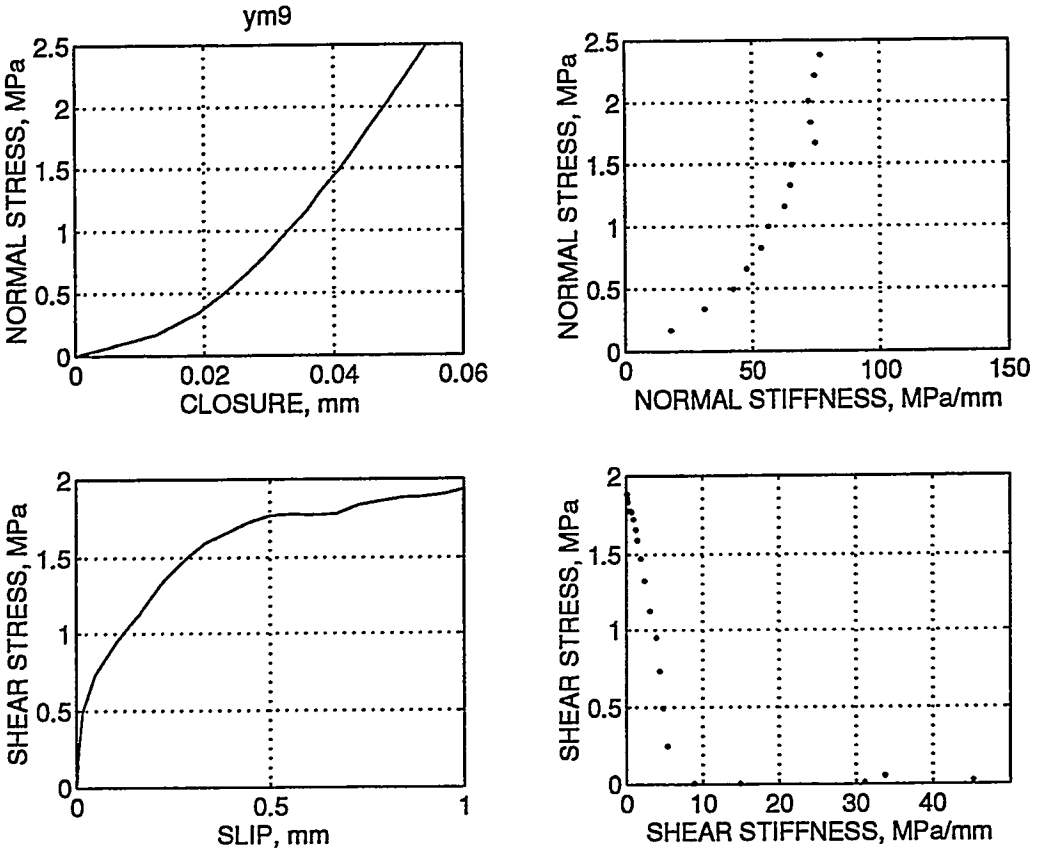

Figure 6: Shear and normal stiffness data for YM9.

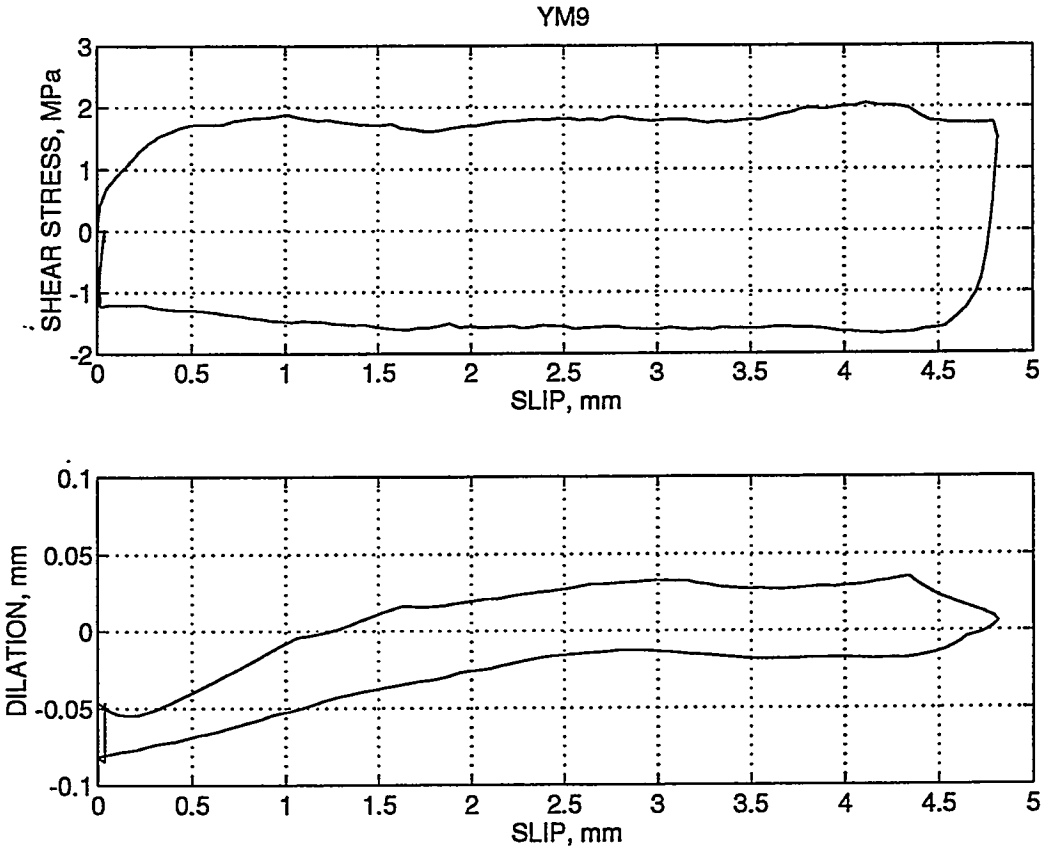

Figure 7: Shear strength and dilation data for YM9.

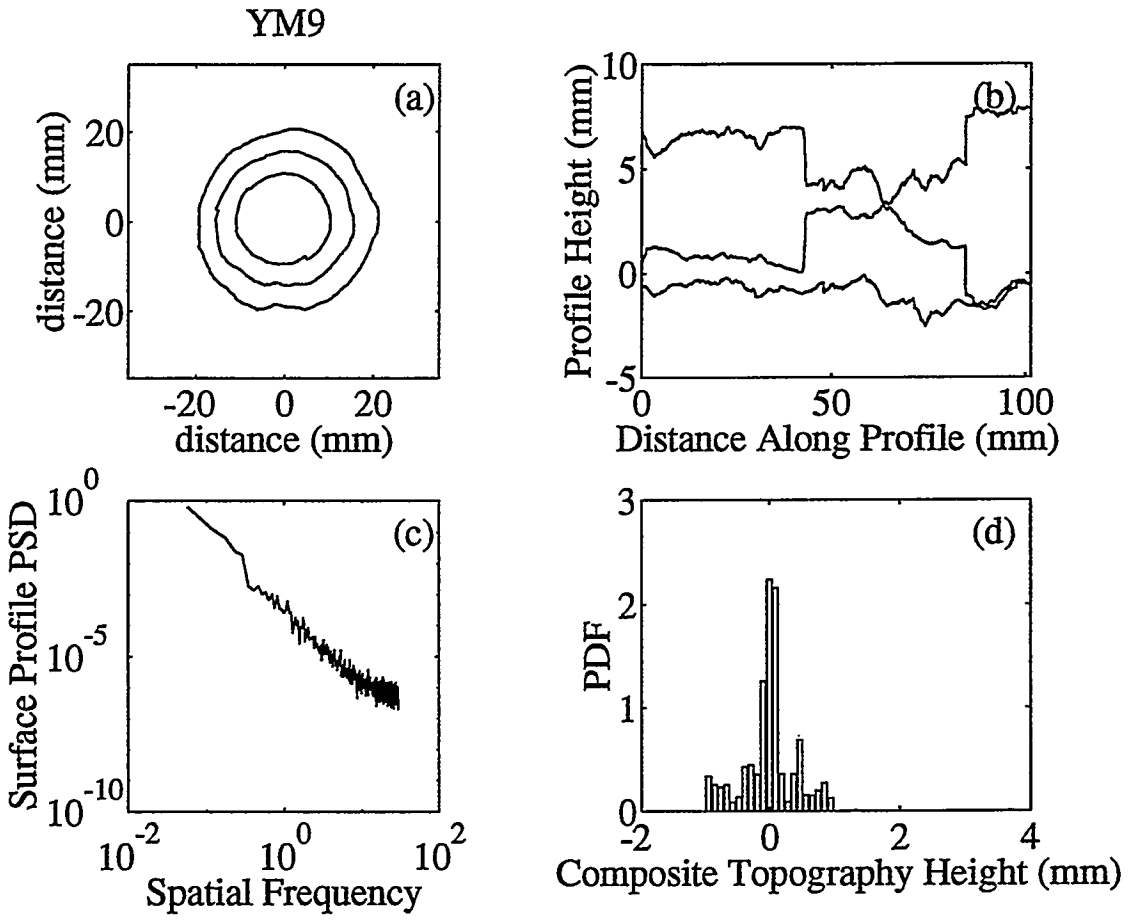

Figure 8: Profilometer data for YM9.

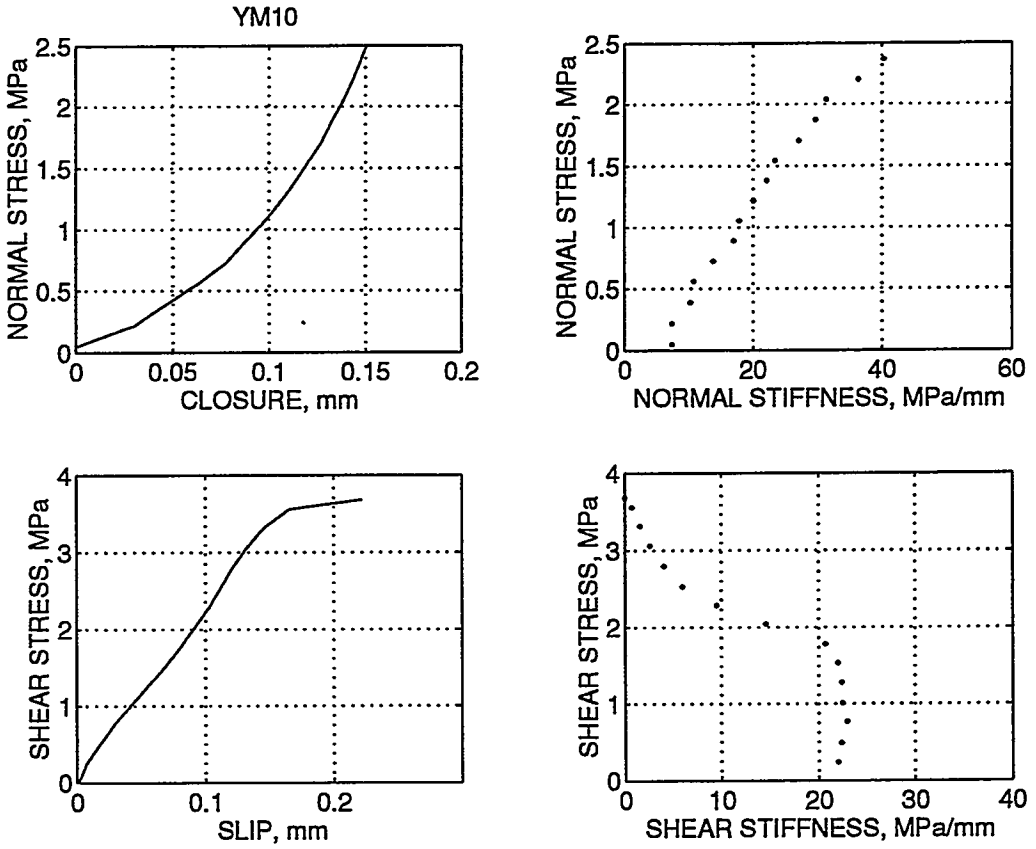

Figure 9: Shear and normal stiffness data for YM10.

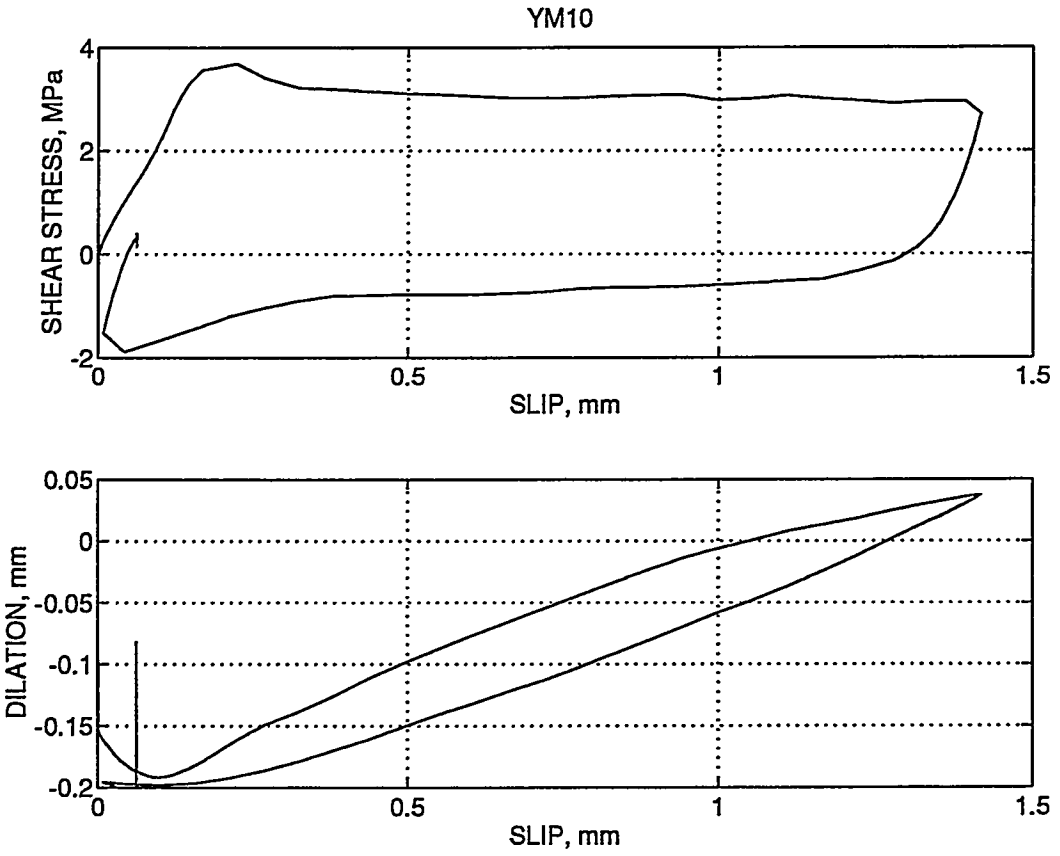

Figure 10: Shear strength and dilation data for YM10.

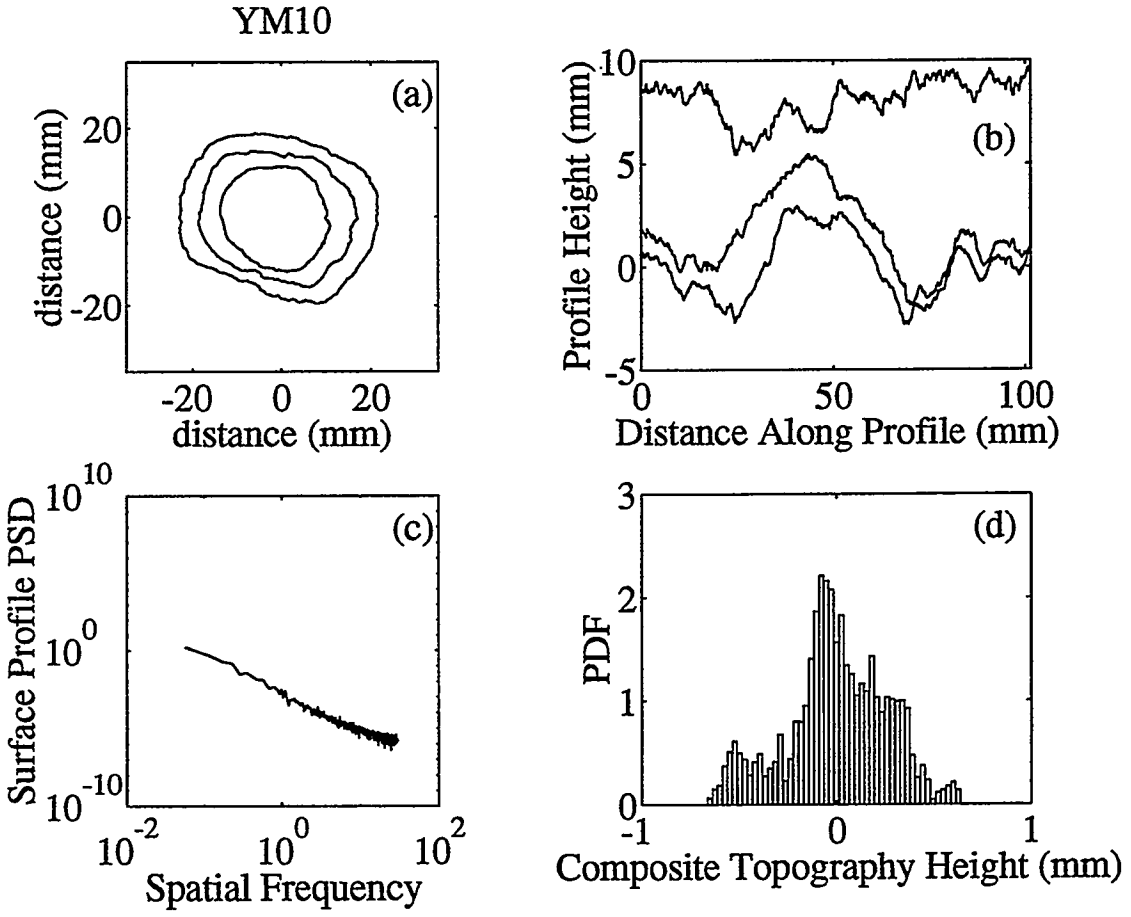

Figure 11: Profilometer data for YM10.

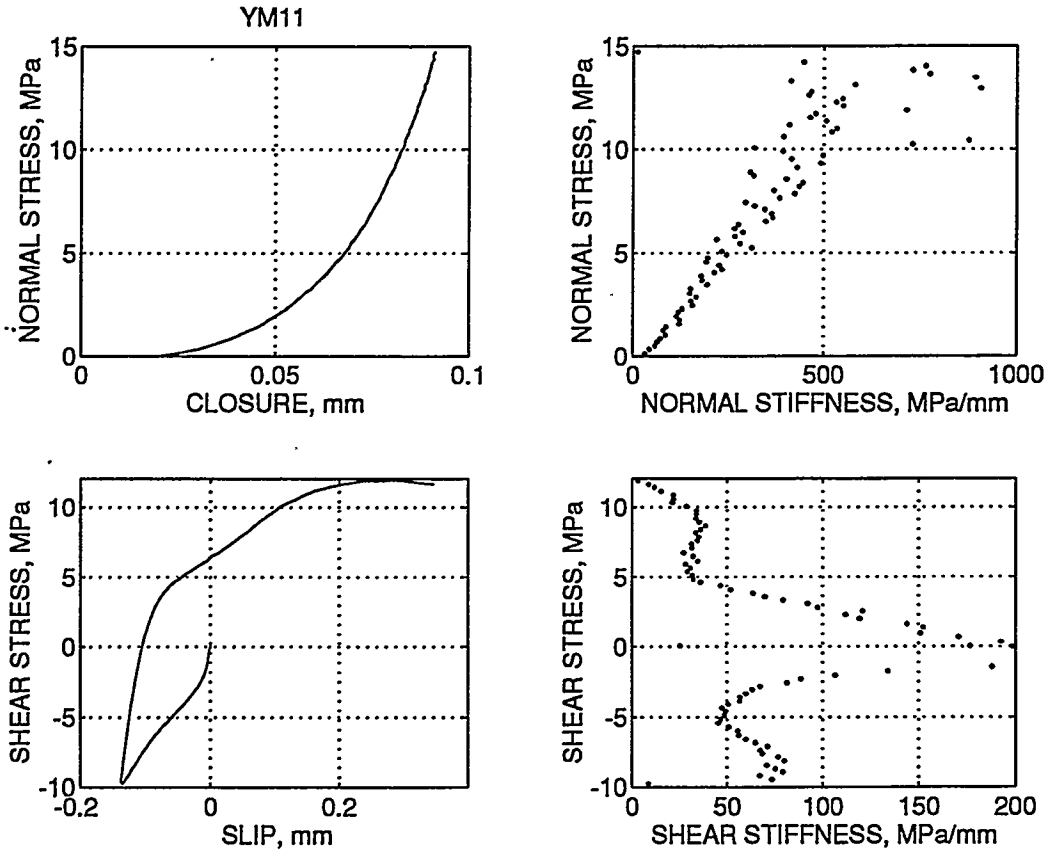

Figure 12: Shear and normal stiffness data for YM11.

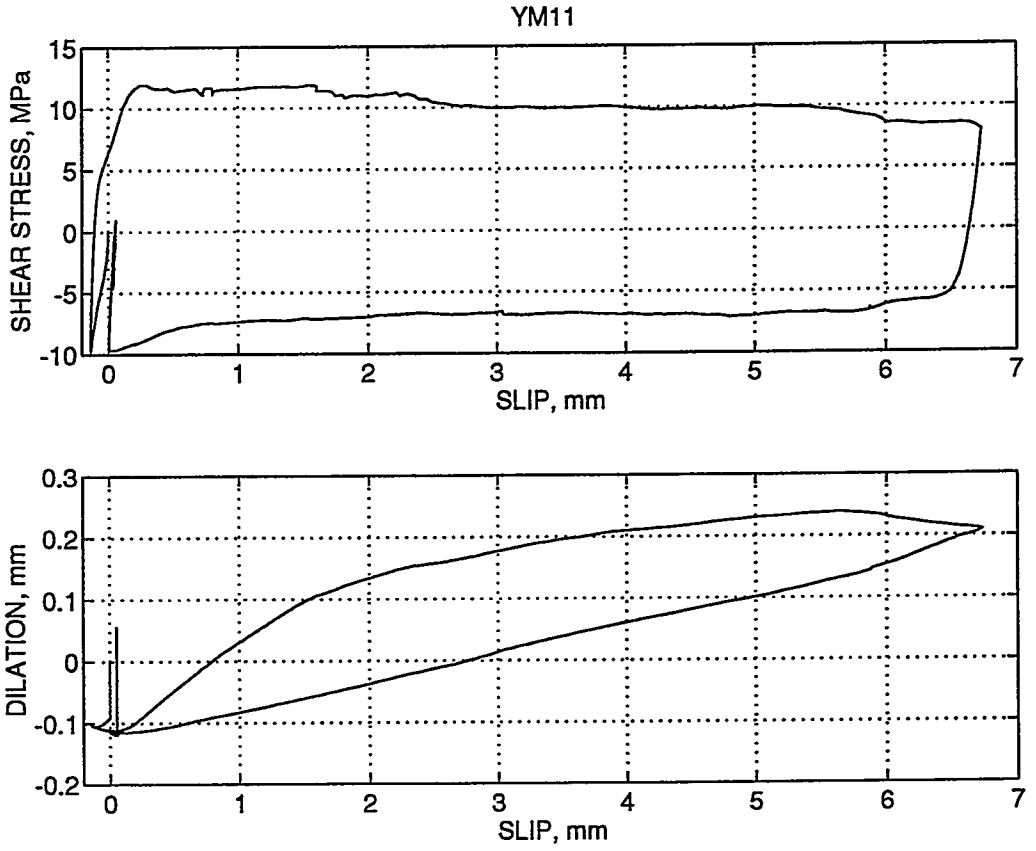

Figure 13: Shear strength and dilation data for YM11.

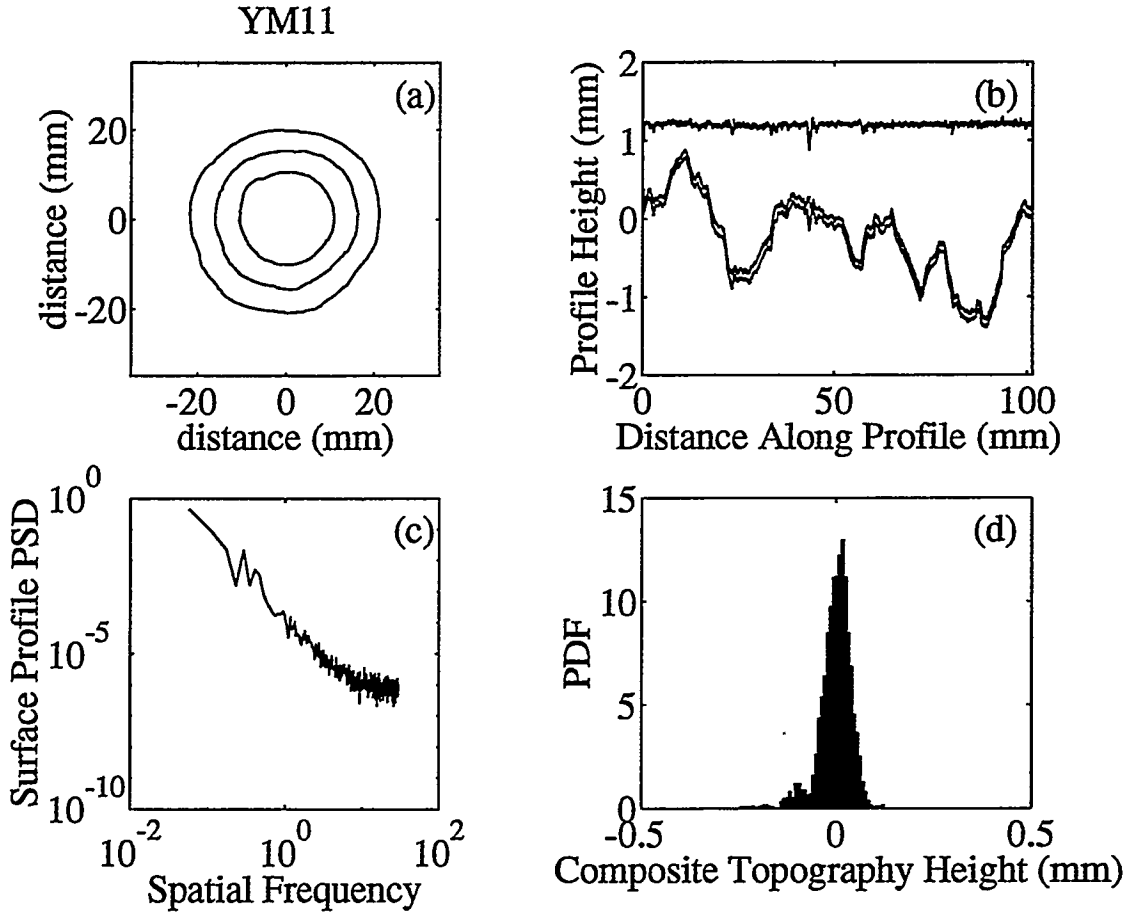

Figure 14: Profilometer data for YM11.

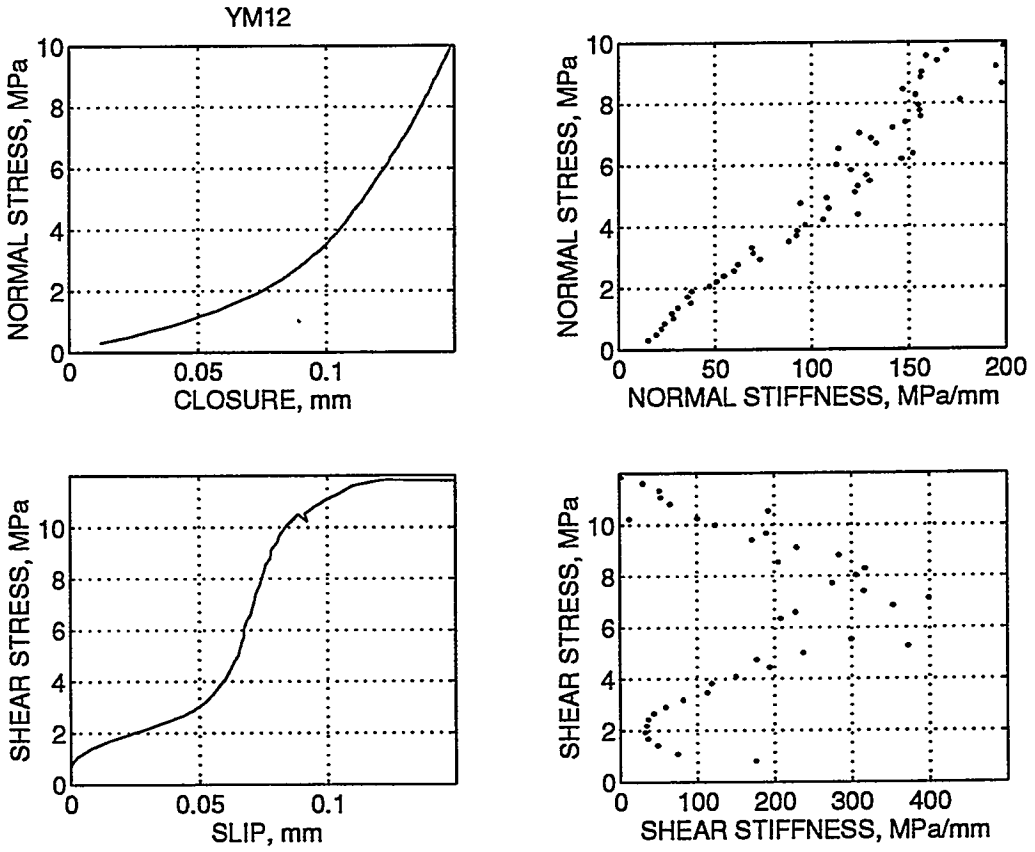

Figure 15: Shear and normal stiffness data for YM12.

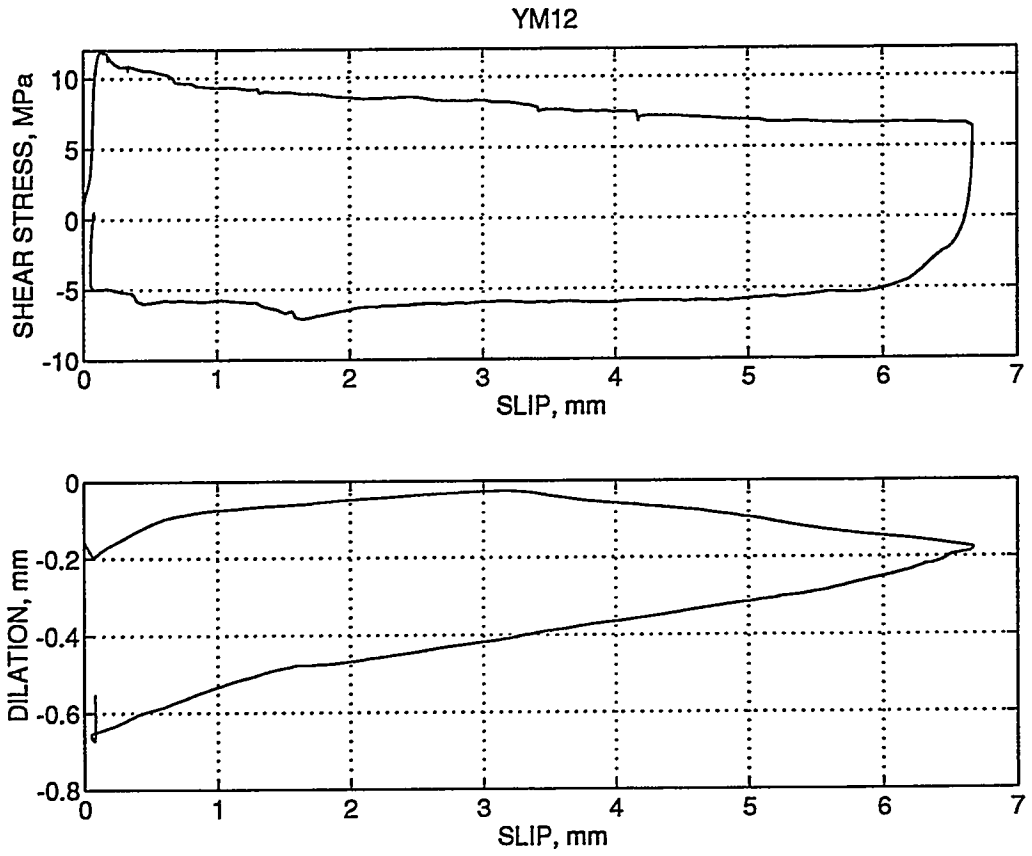

Figure 16: Shear strength and dilation data for YM12.

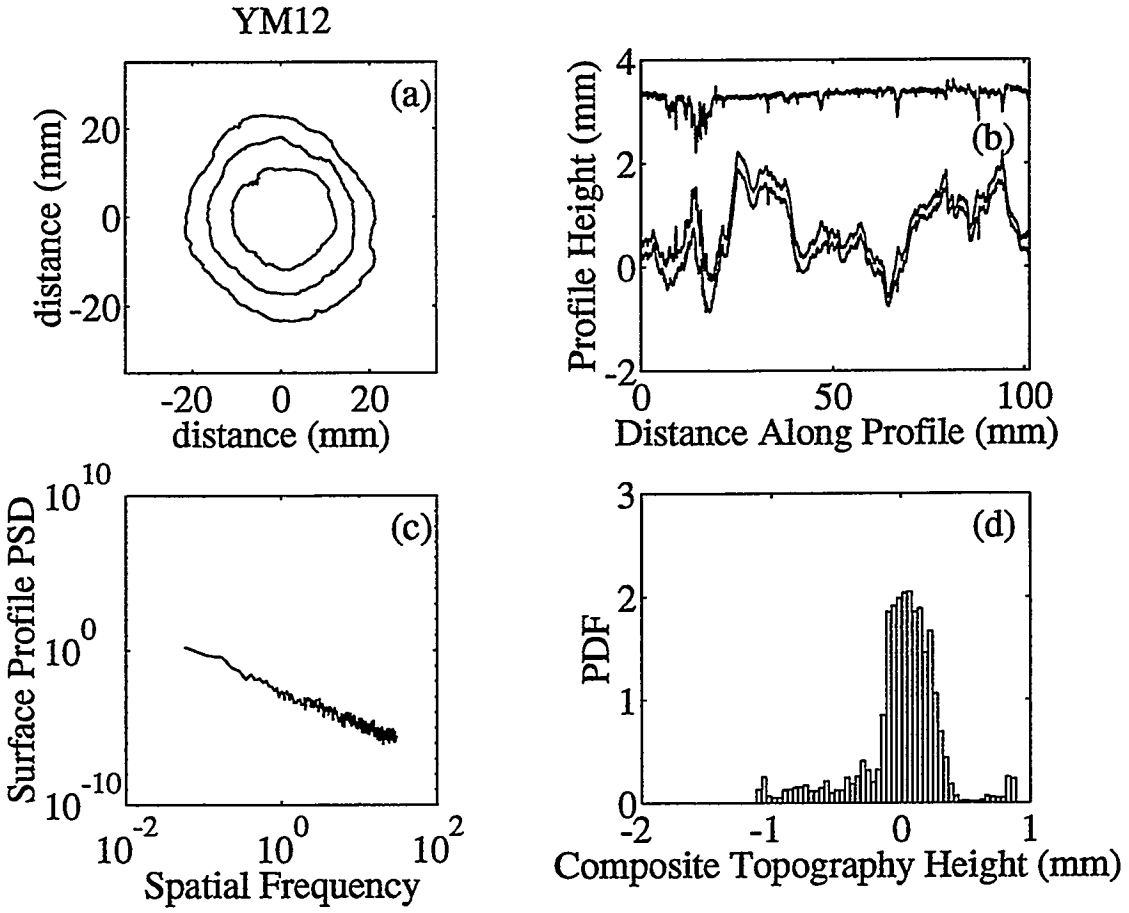

Figure 17: Profilometer data for YM12.

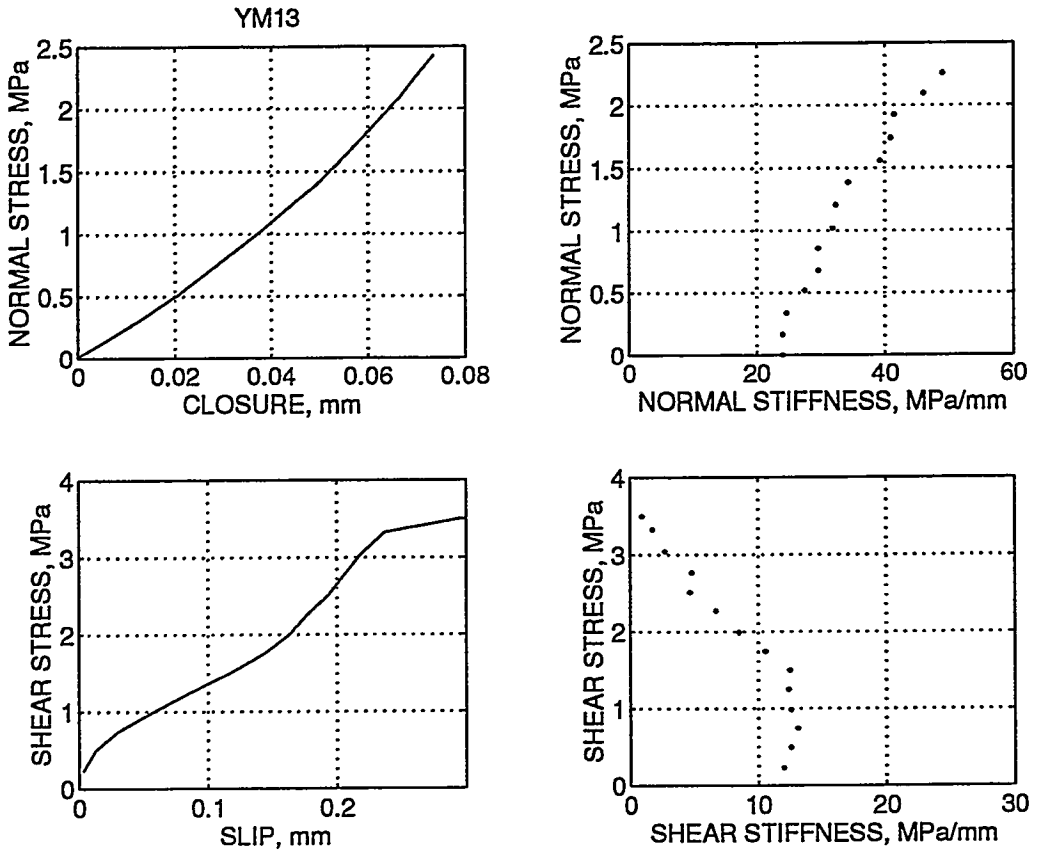

Figure 18: Shear and normal stiffness data for YM13.

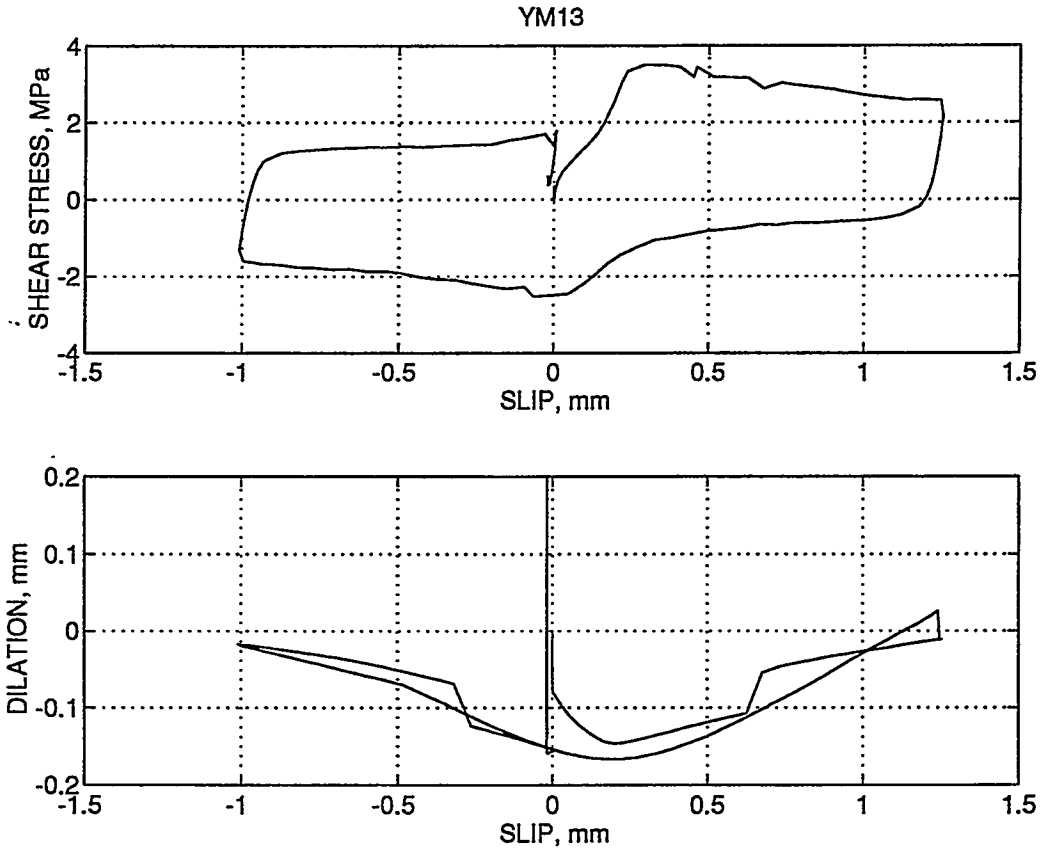

Figure 19: Shear strength and dilation data for YM13.

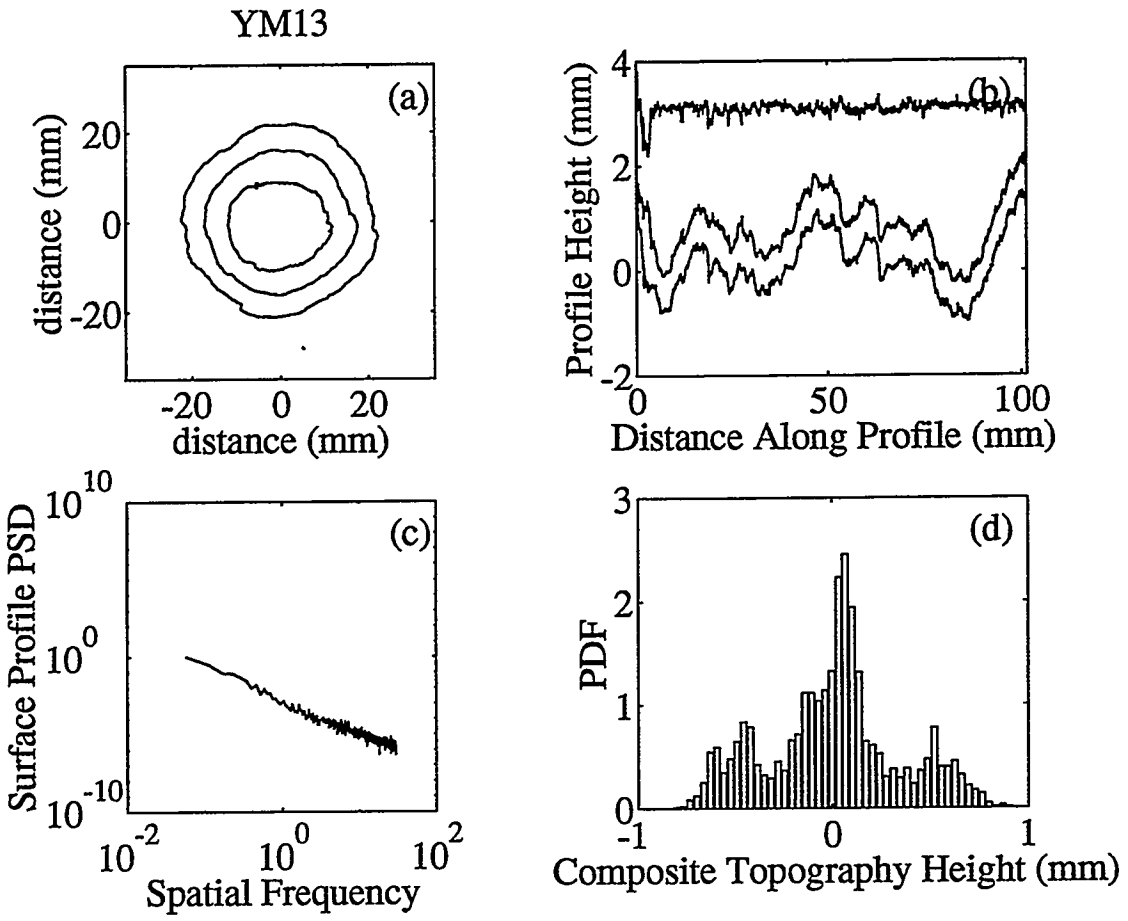

Figure 20: Profilometer data for YM13.

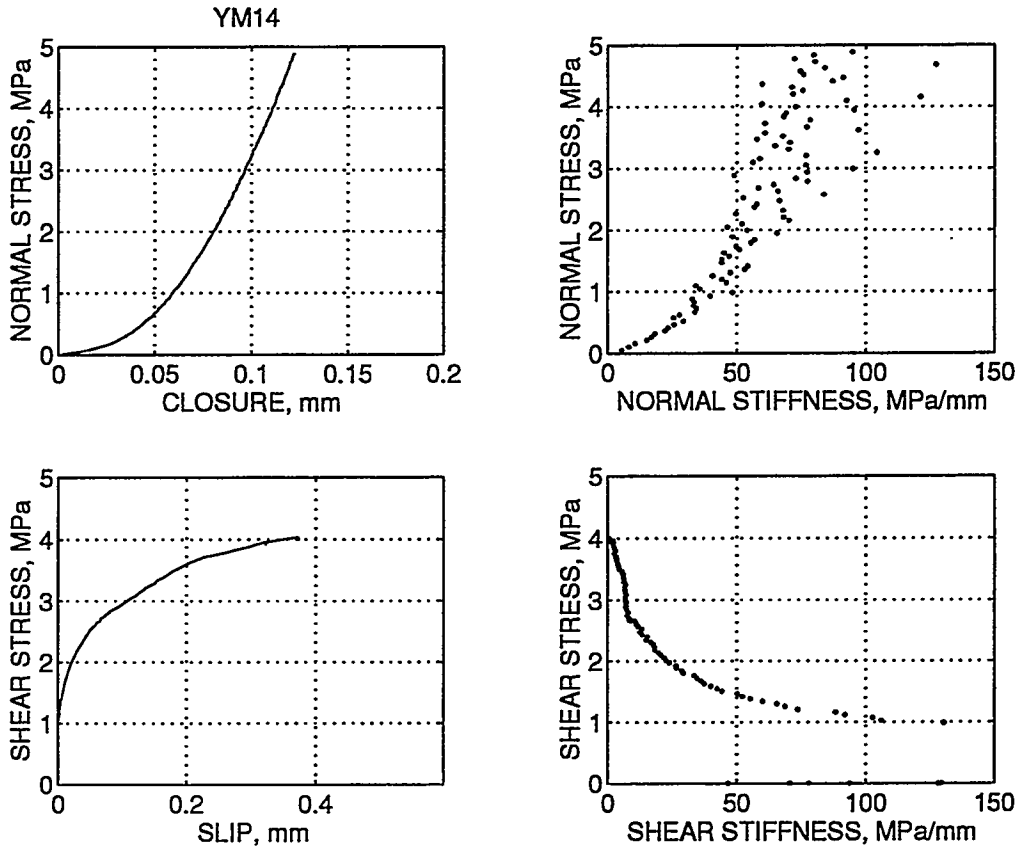

Figure 21: Shear and normal stiffness data for YM14.

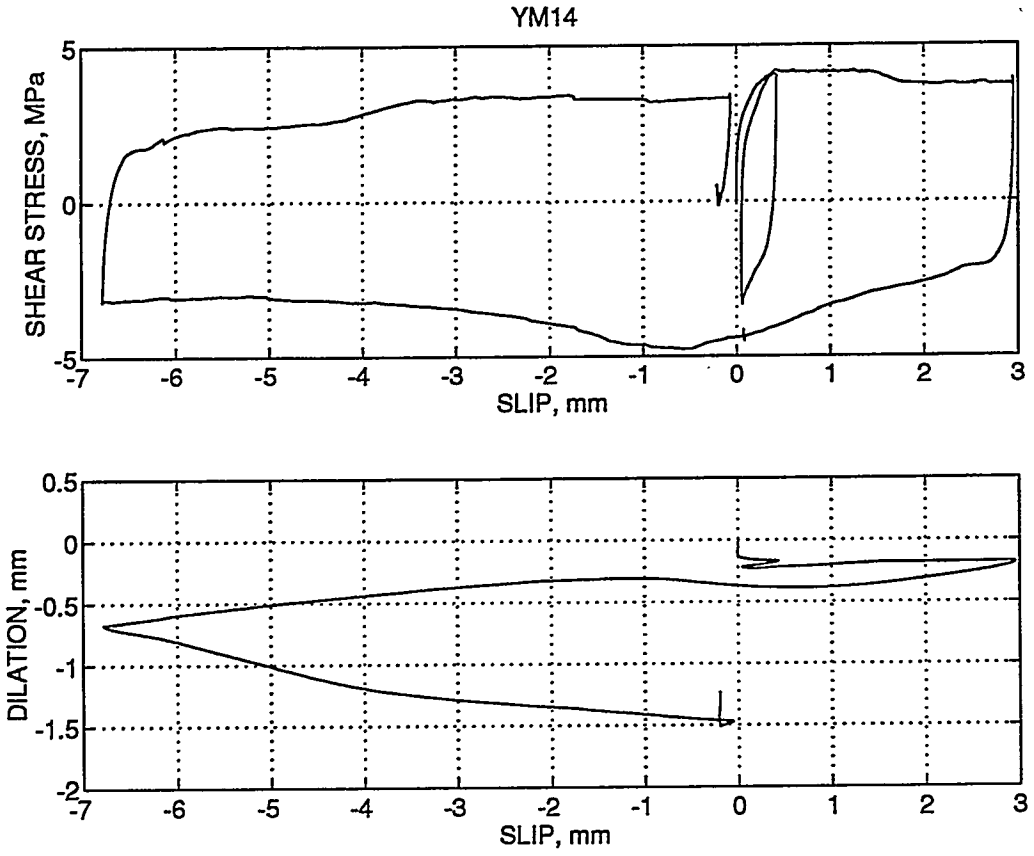

Figure 22: Shear strength and dilation data for YM14.

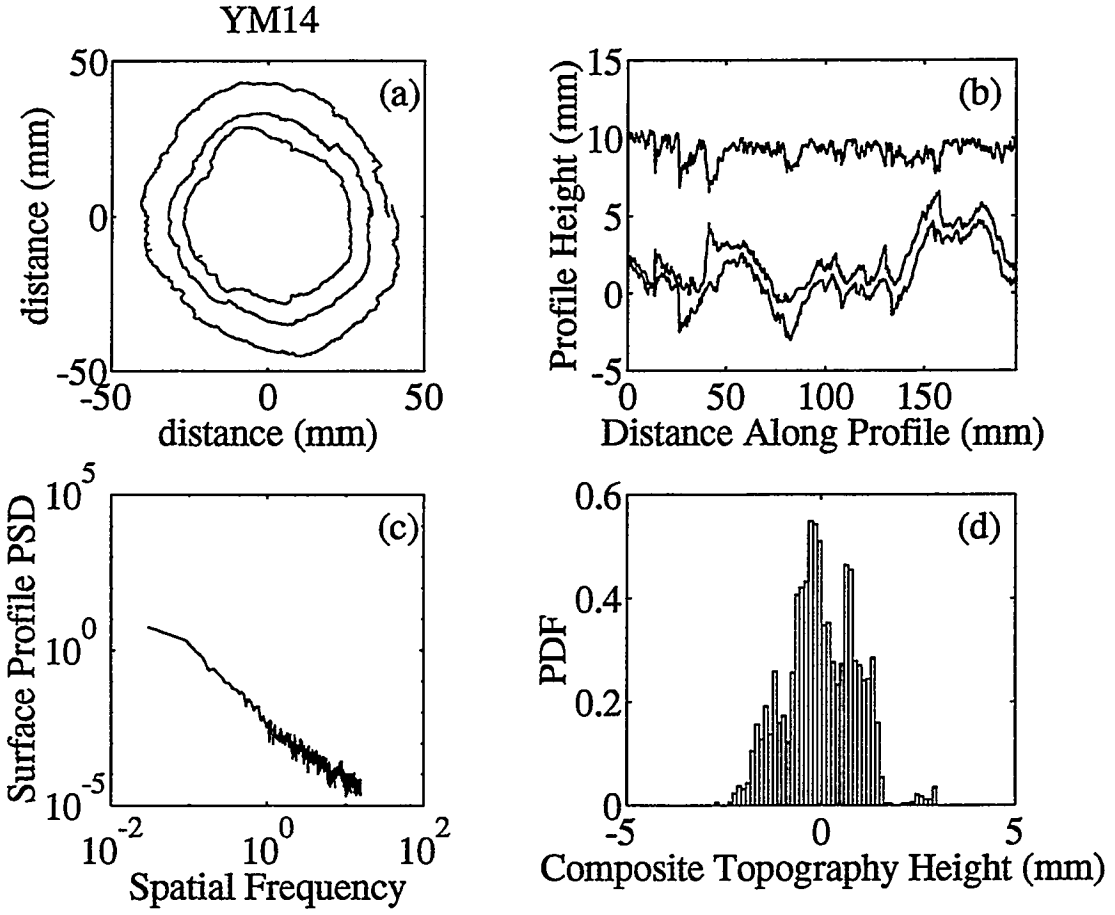

Figure 23: Profilometer data for YM14.

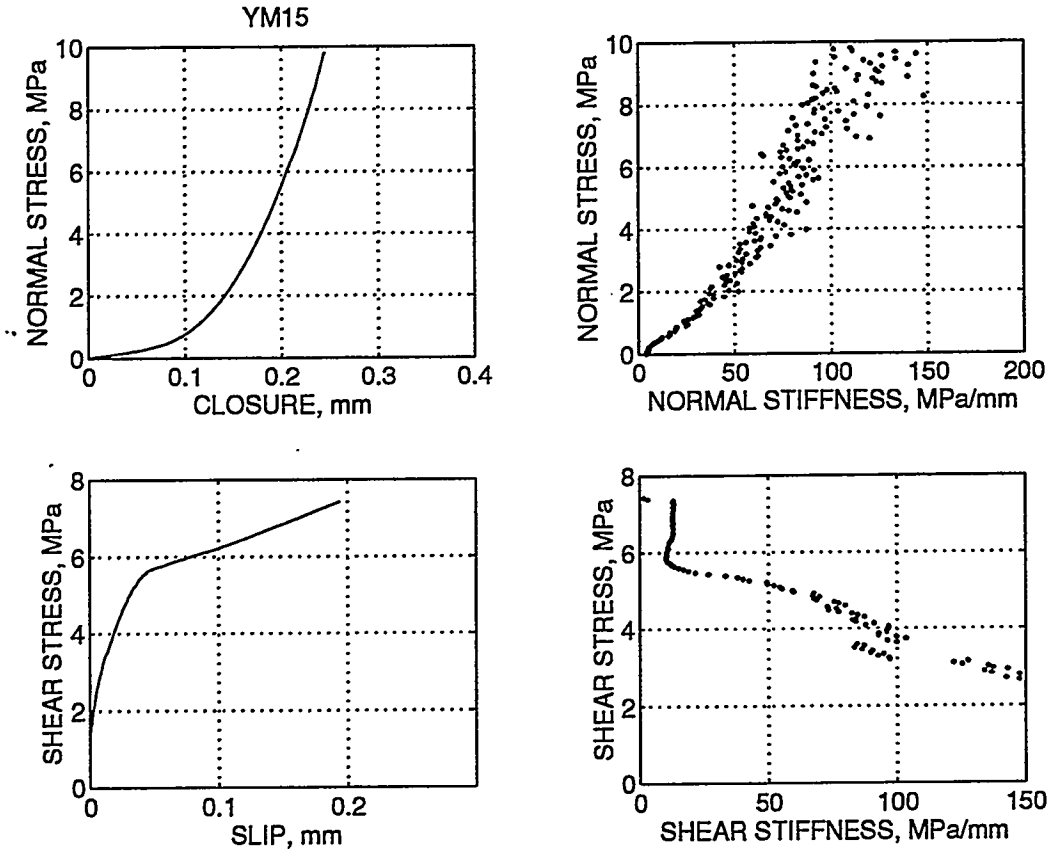

Figure 24: Shear and normal stiffness data for YM15.

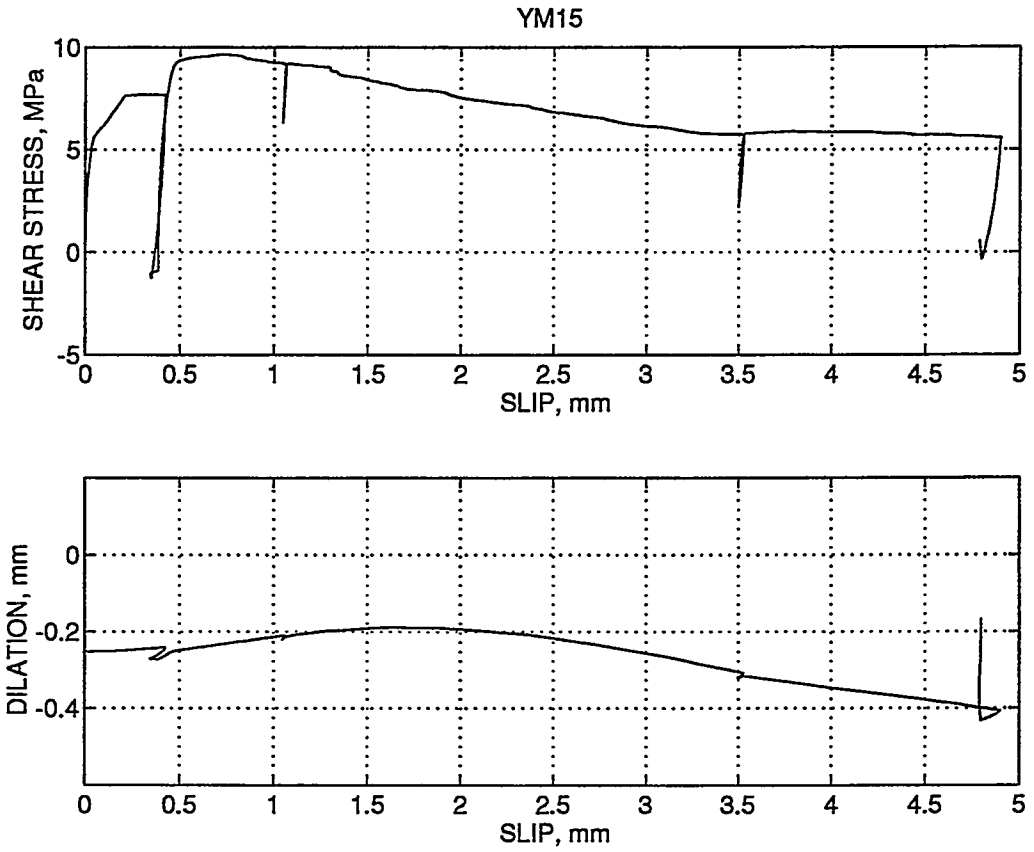

Figure 25: Shear strength and dilation data for YM15.

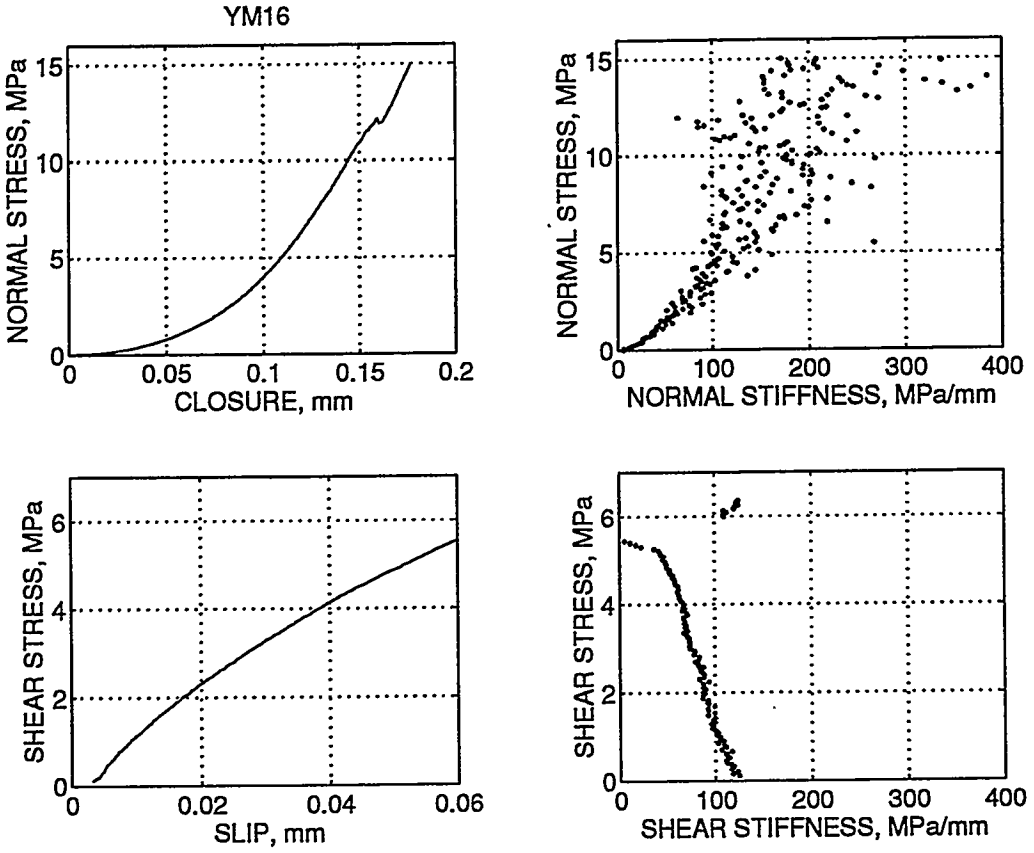

Figure 26: Shear and normal stiffness data for YM16.

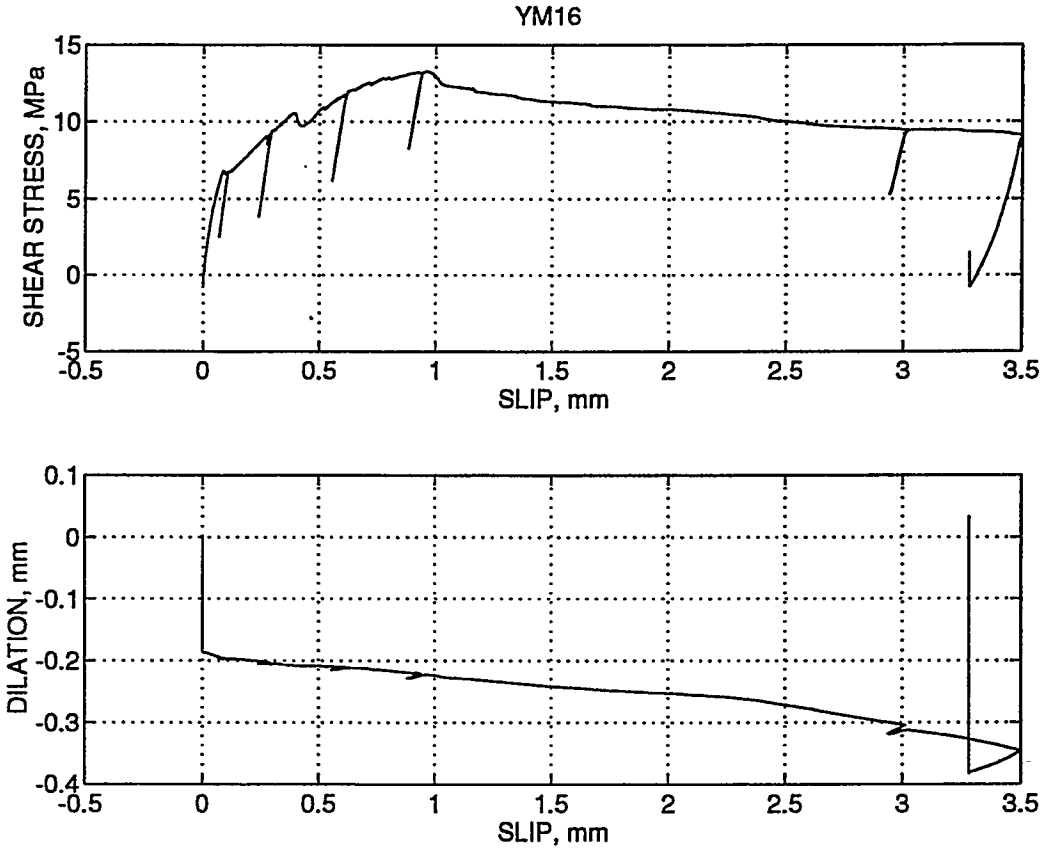

Figure 27: Shear strength and dilation data for YM16.

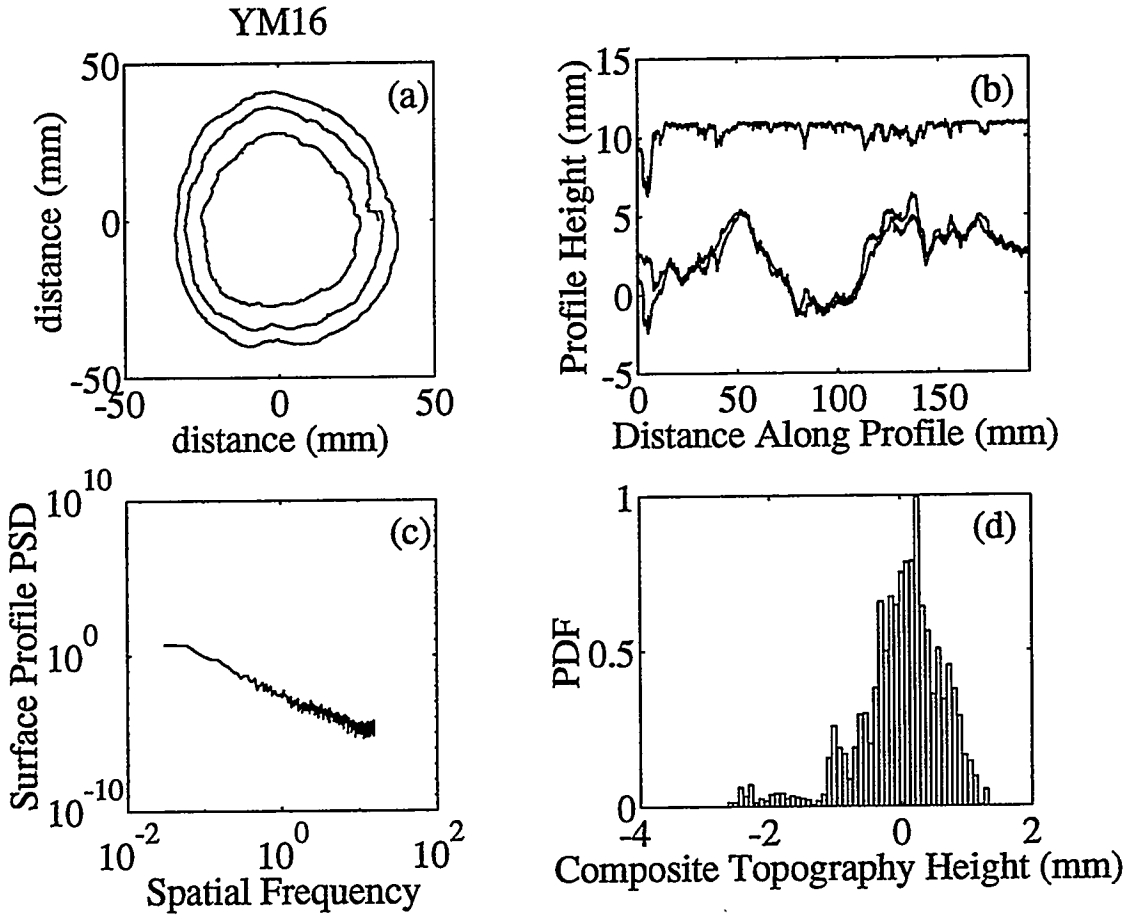

Figure 28: Profilometer data for YM16.

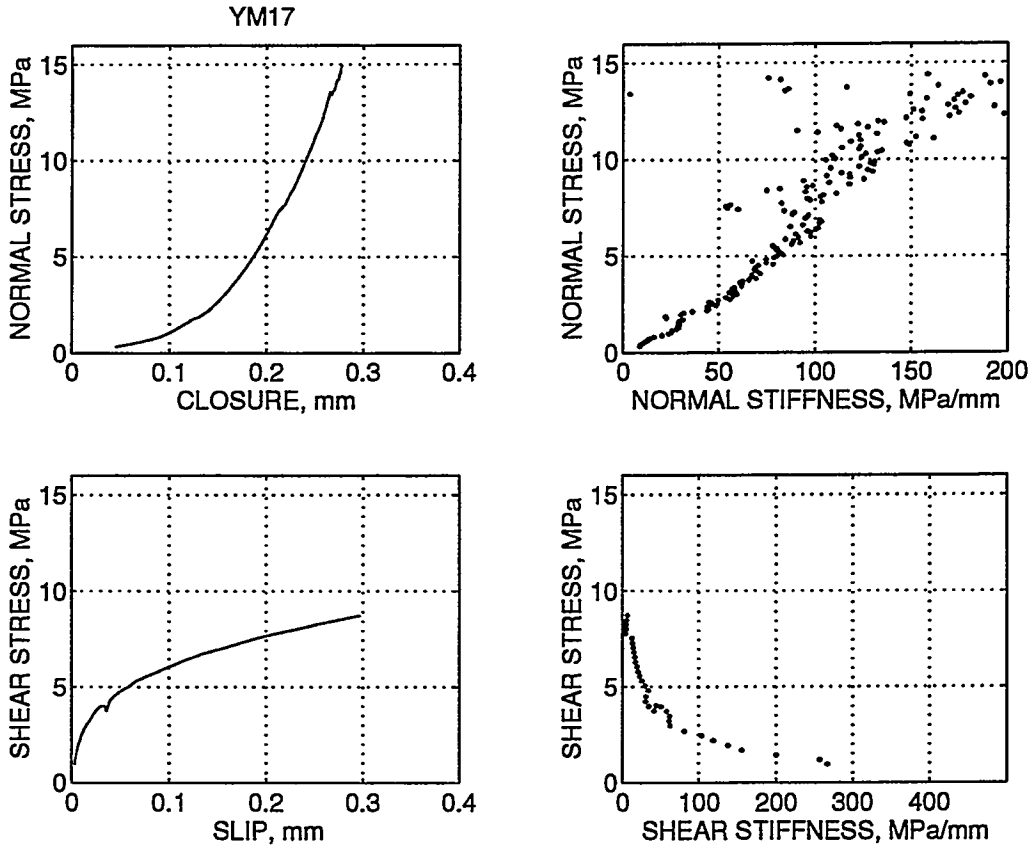

Figure 29: Shear and normal stiffness data for YM17.

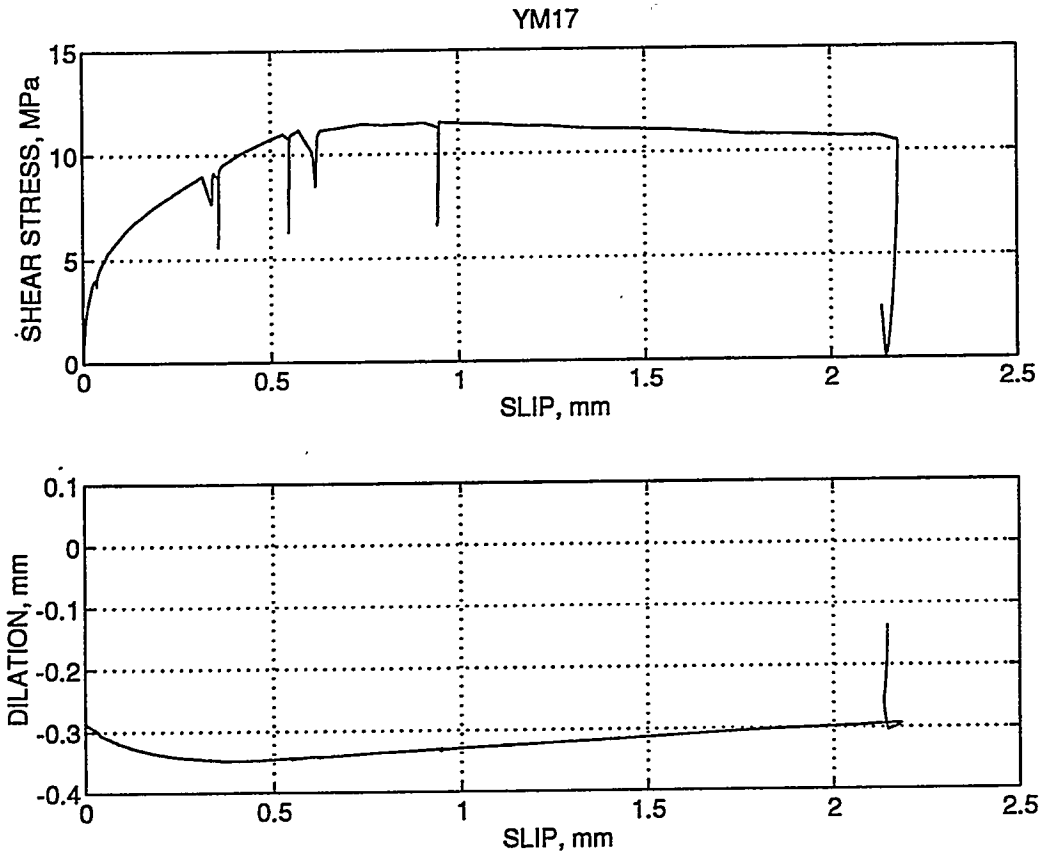

Figure 30: Shear strength and dilation data for YM17.

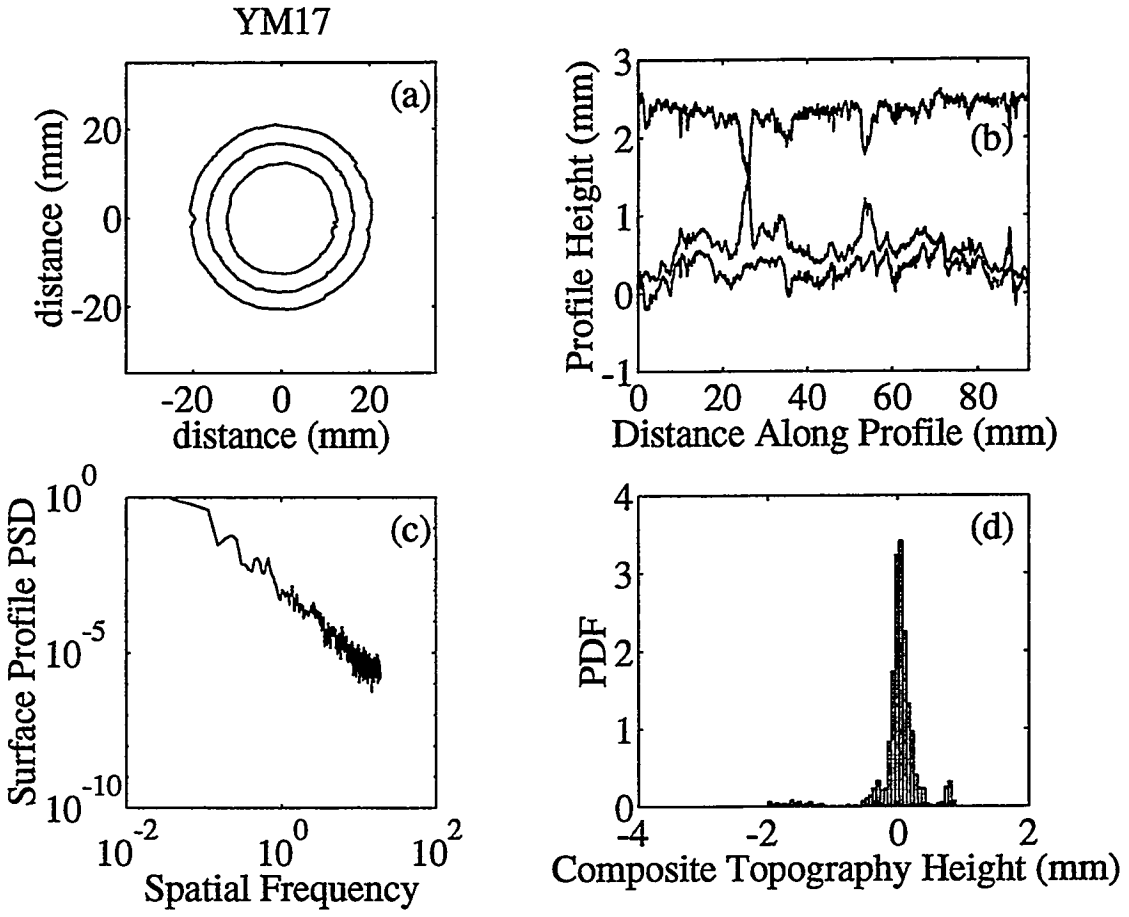

Figure 31: Profilometer data for YM17.

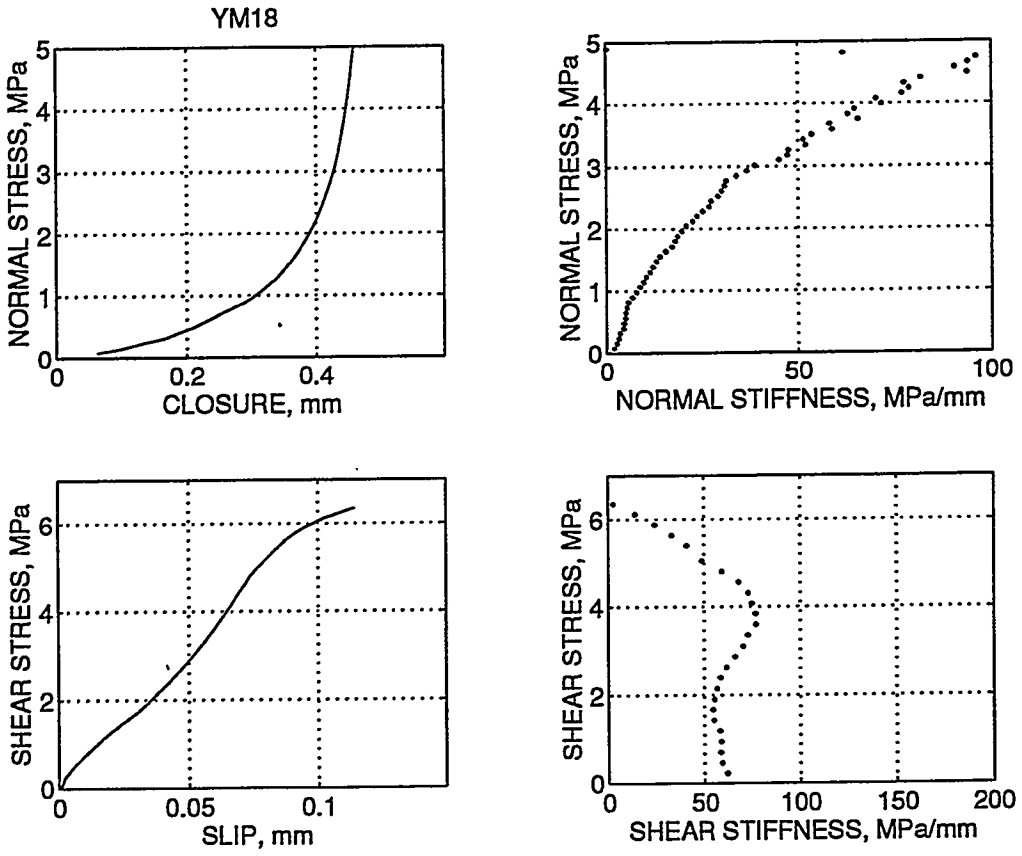

Figure 32: Shear and normal stiffness data for YM18.

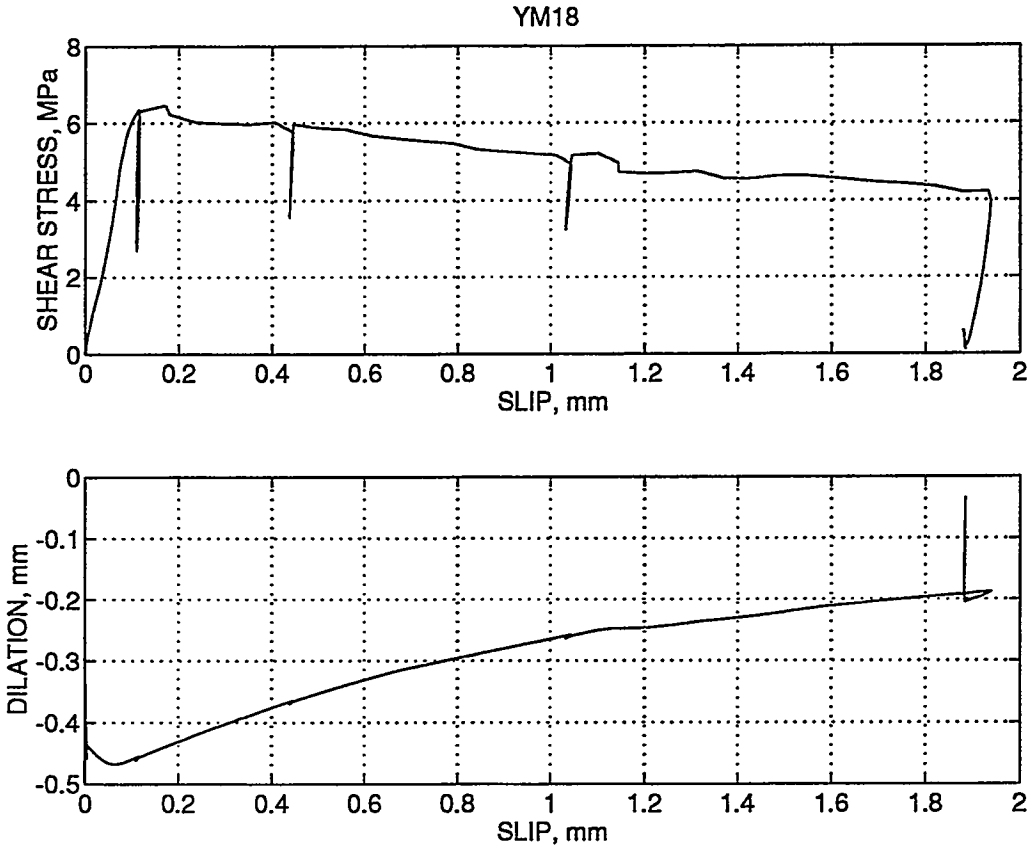

Figure 33: Shear strength and dilation data for YM18.

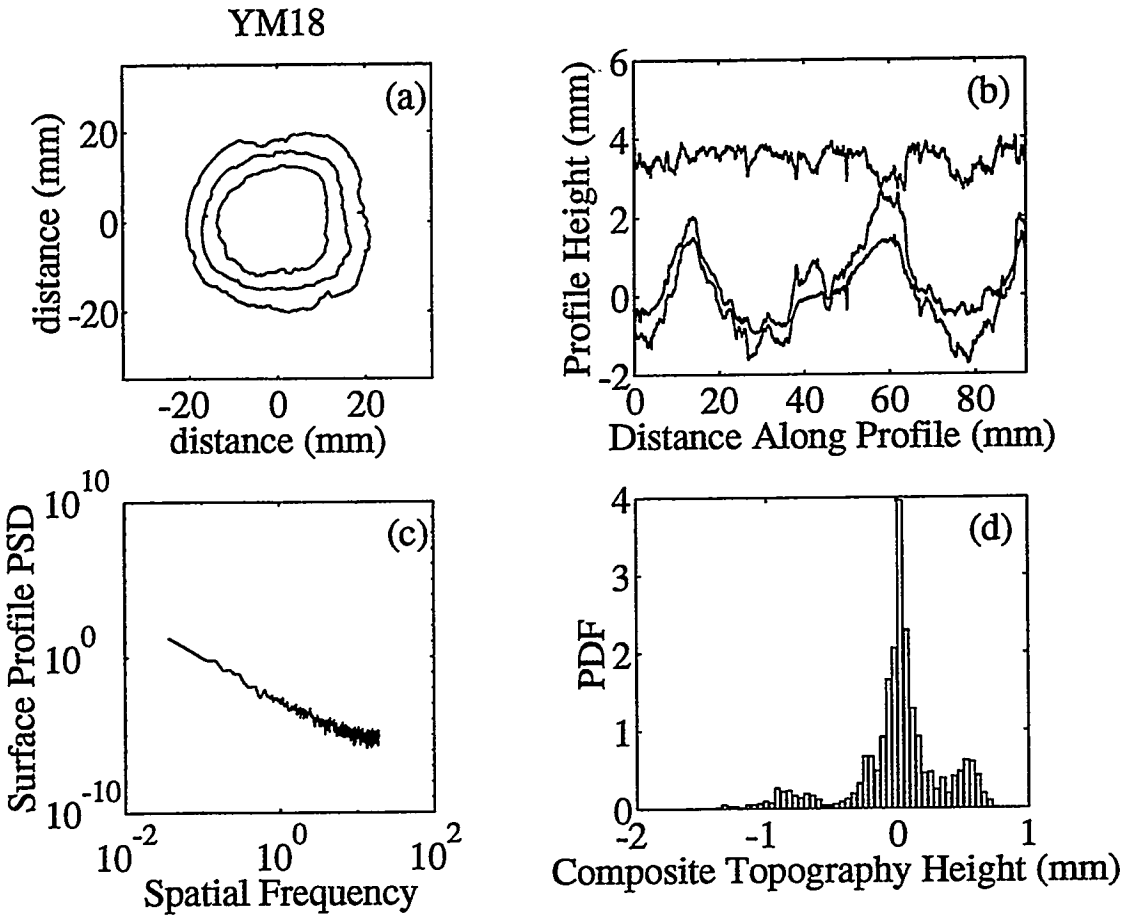

Figure 34: Profilometer data for YM18.

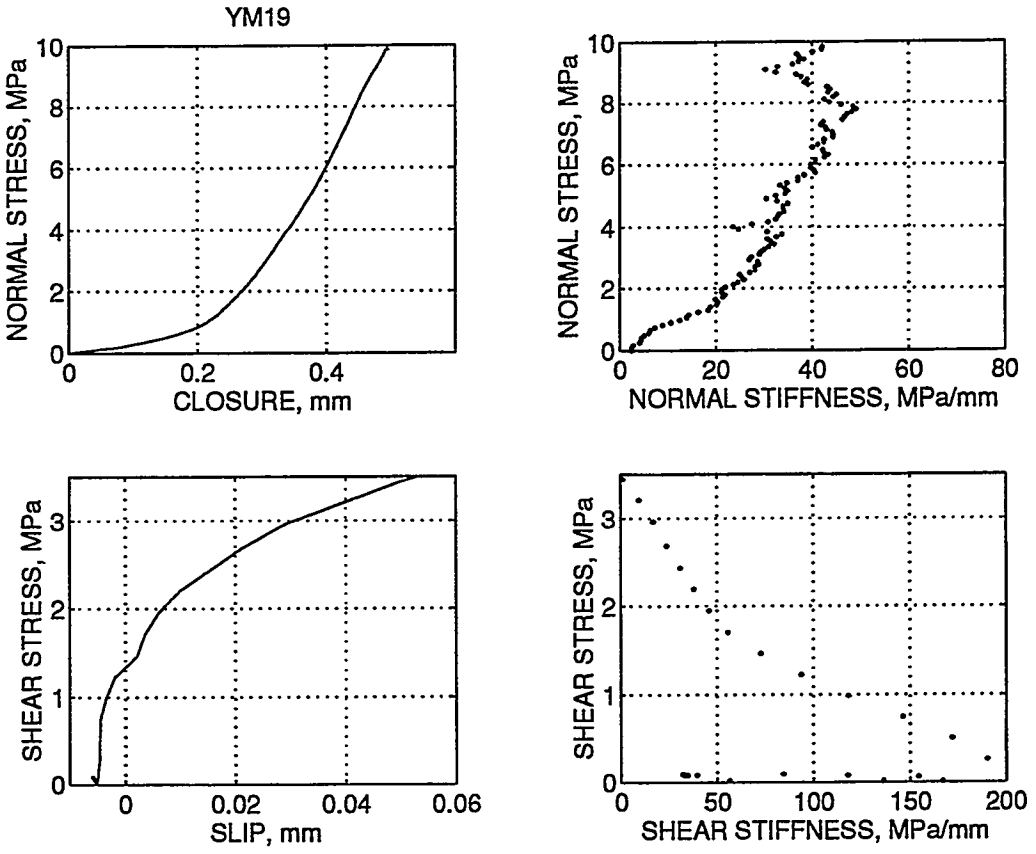

Figure 35: Shear and normal stiffness data for YM19.

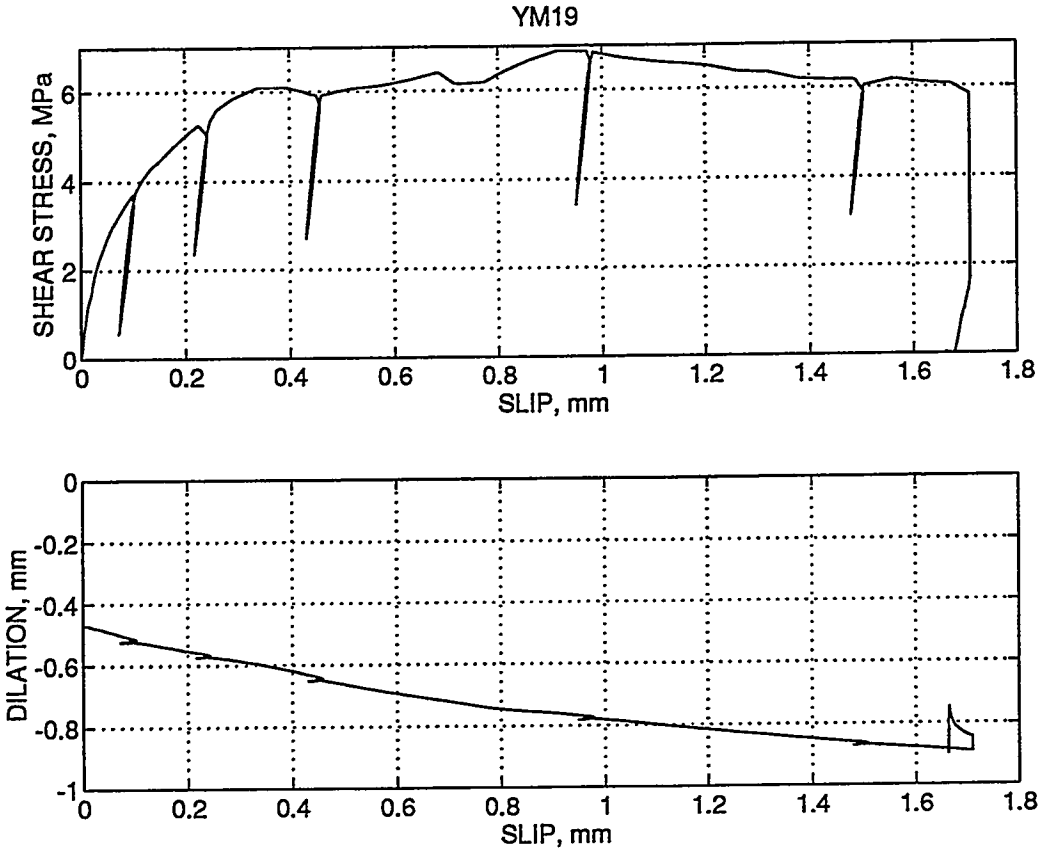

Figure 36: Shear strength and dilation data for YM19.

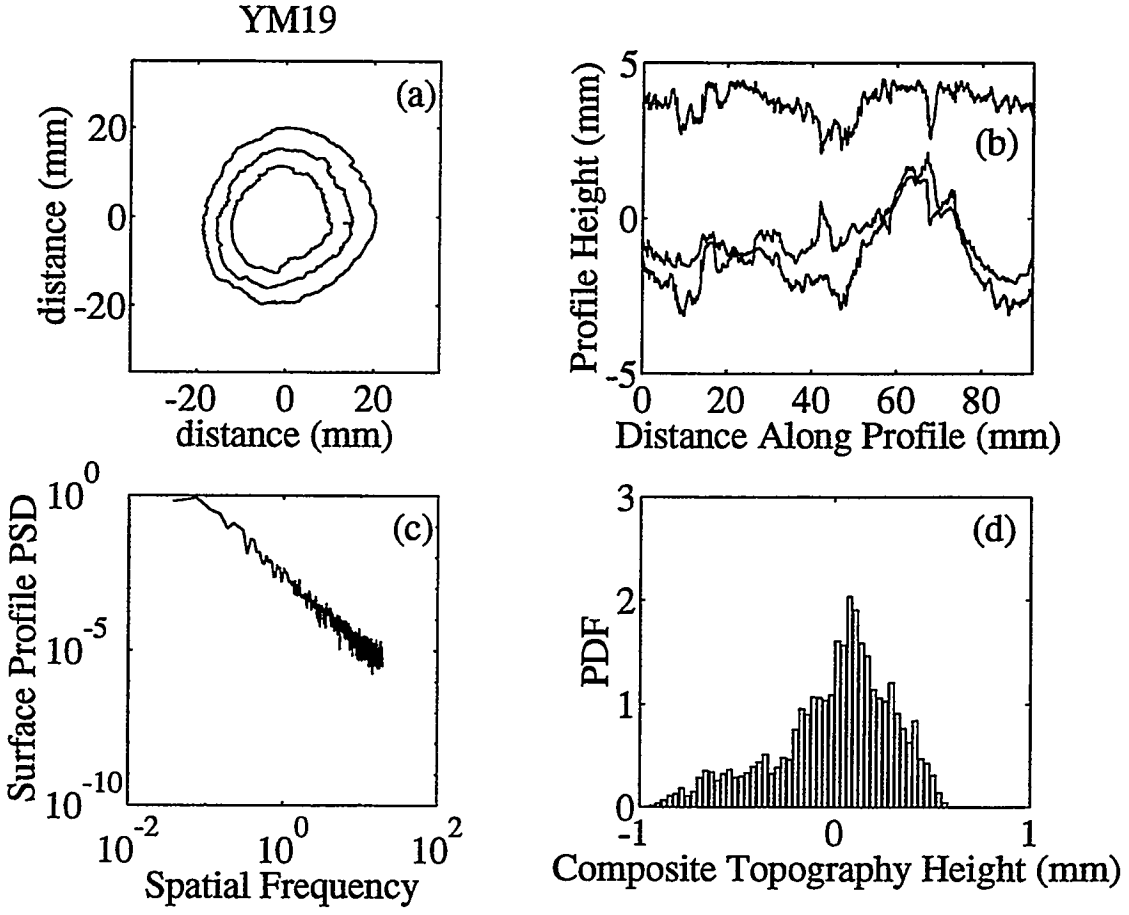

Figure 37: Profilometer data for YM19.

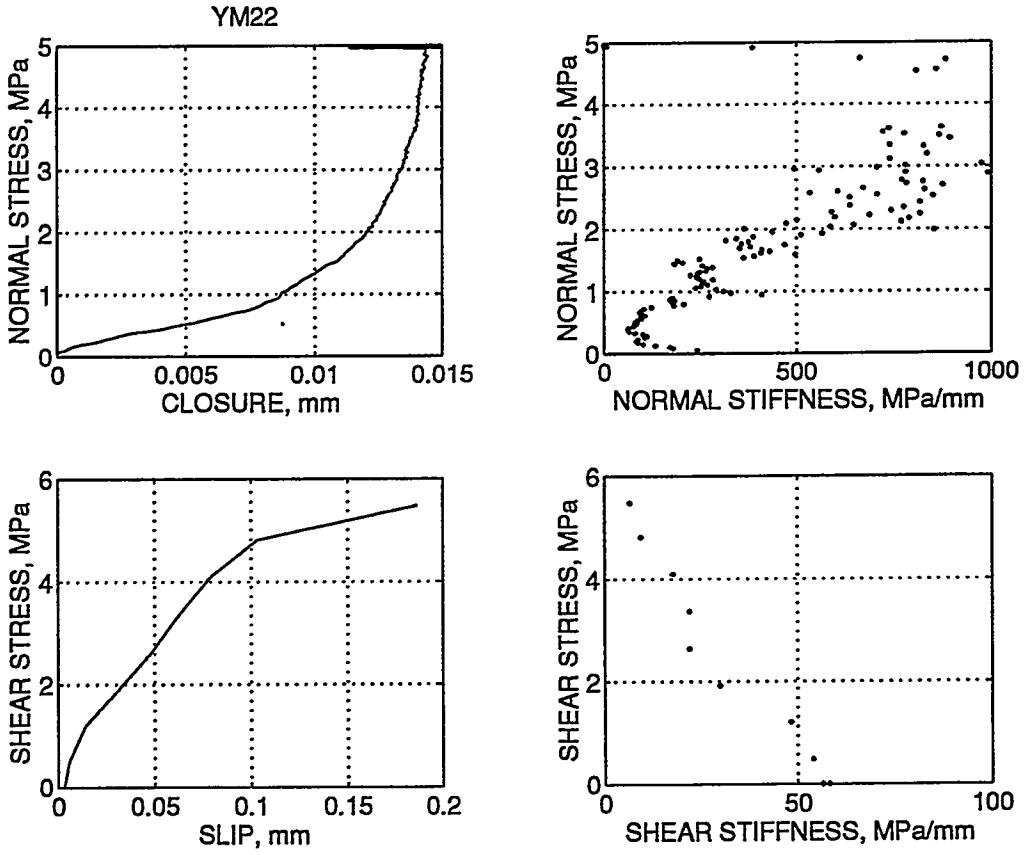

Figure 38: Shear and normal stiffness data for YM22.

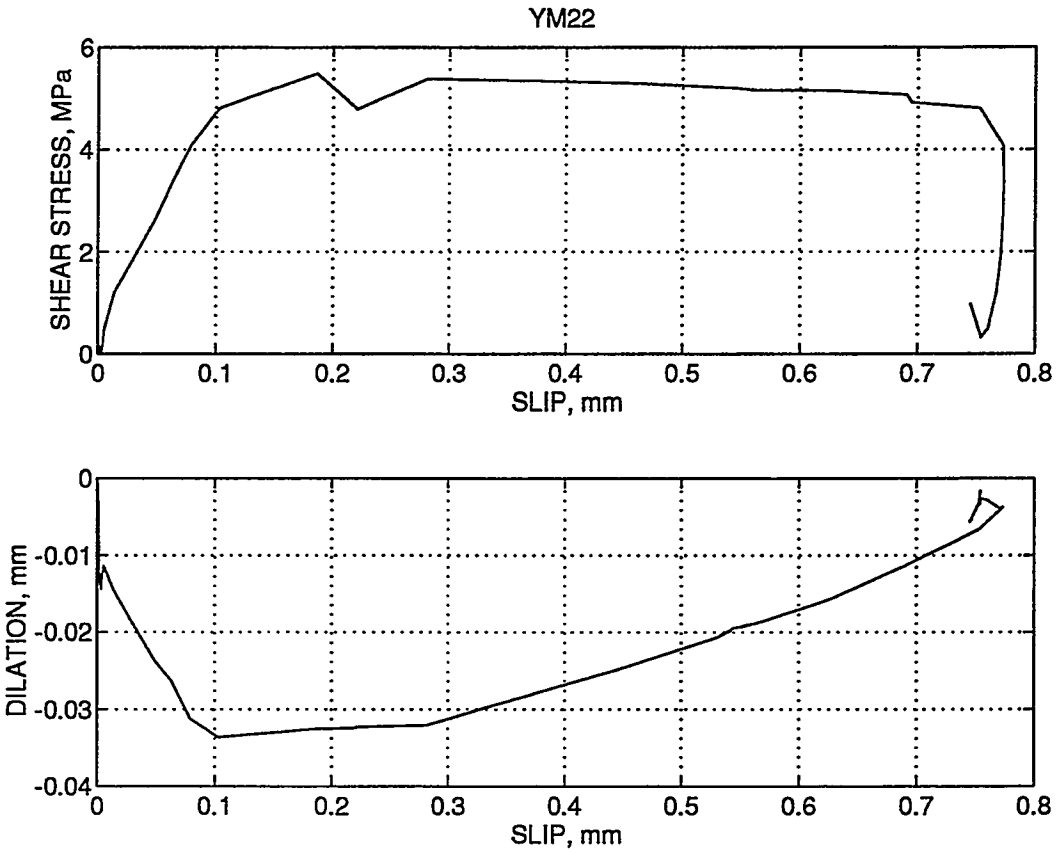

Figure 39: Shear strength and dilation data for YM22.

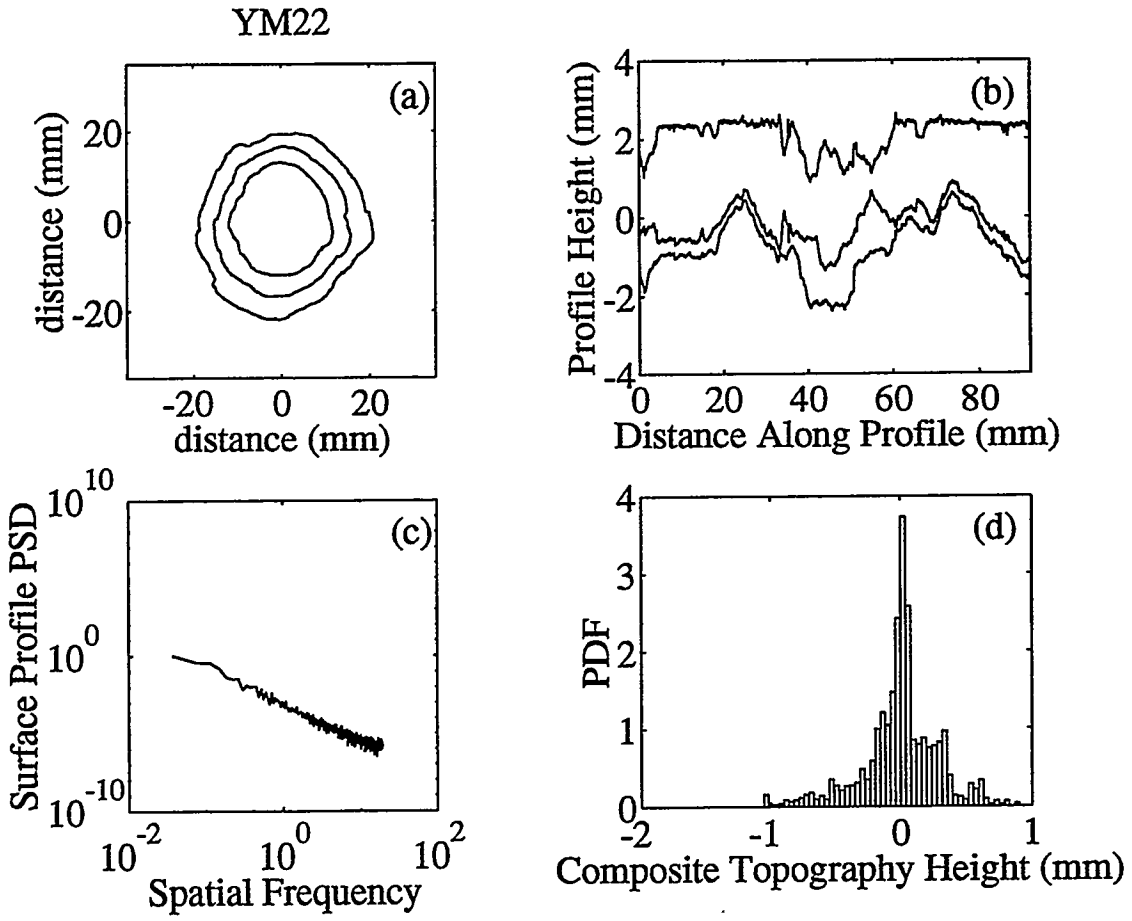

Figure 40: Profilometer data for YM22.

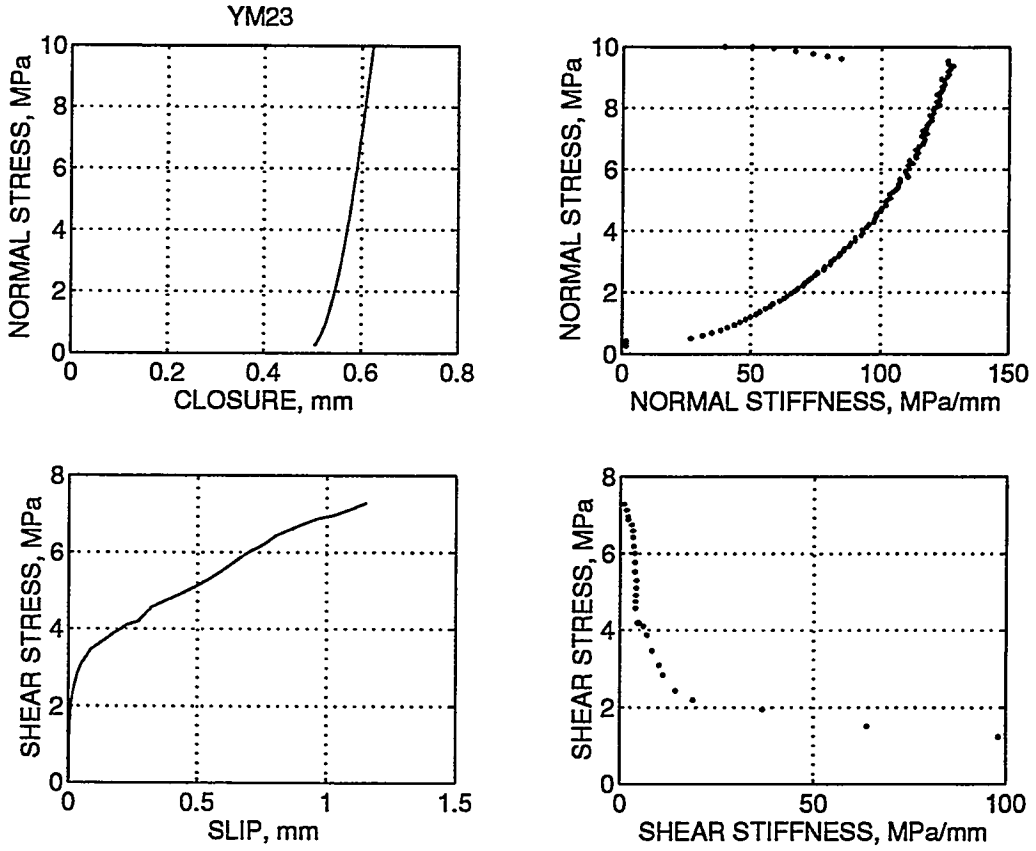

Figure 41: Shear and normal stiffness data for YM23.

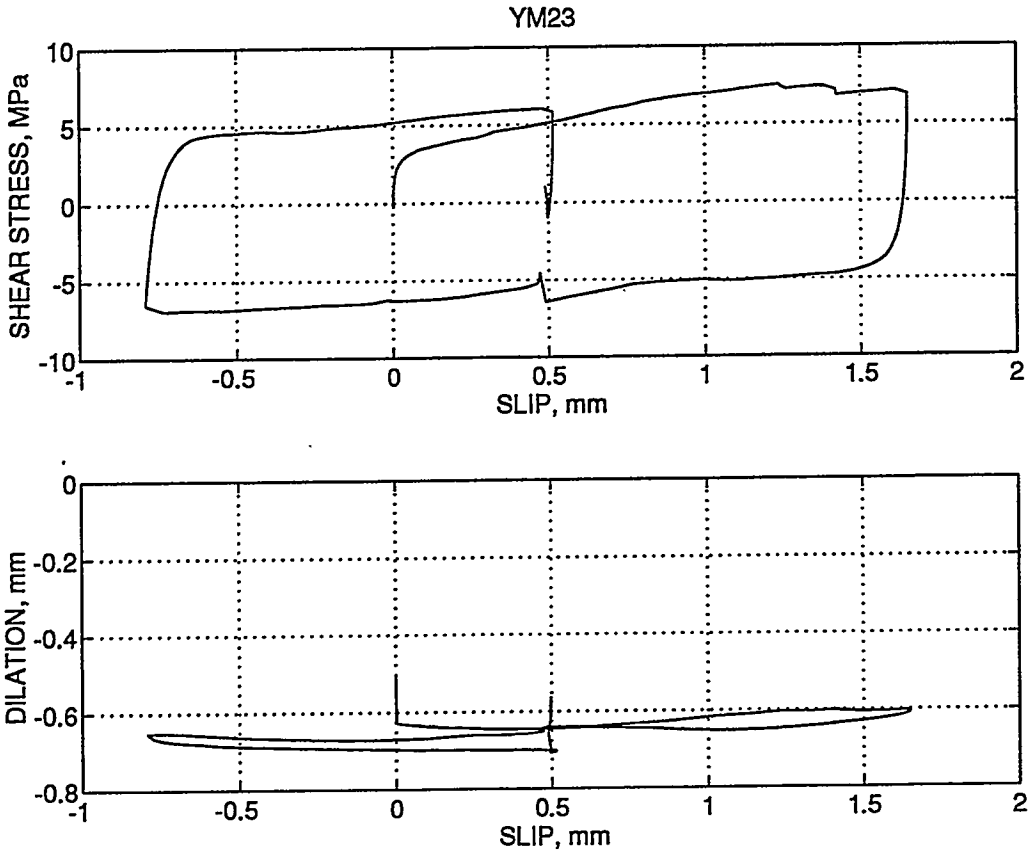

Figure 42: Shear strength and dilation data for YM23.

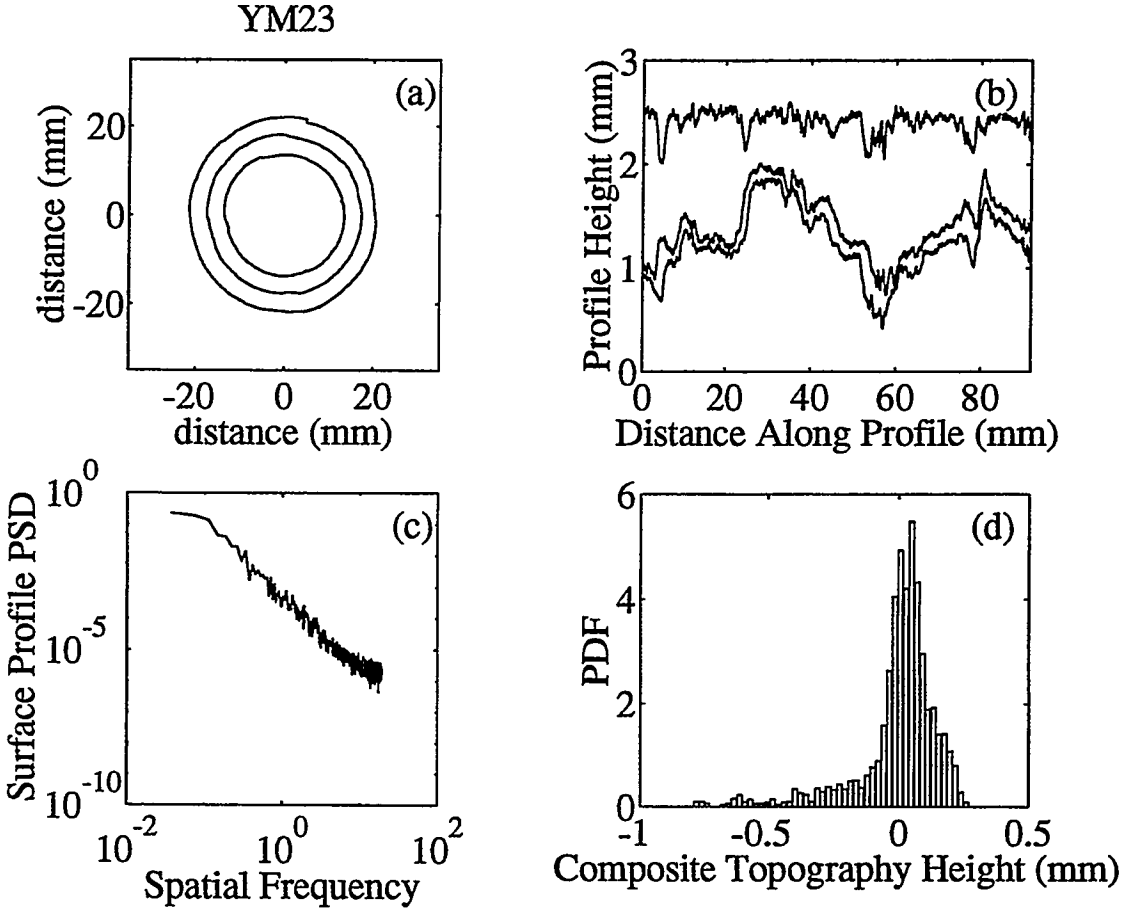

Figure 43: Profilometer data for YM23.

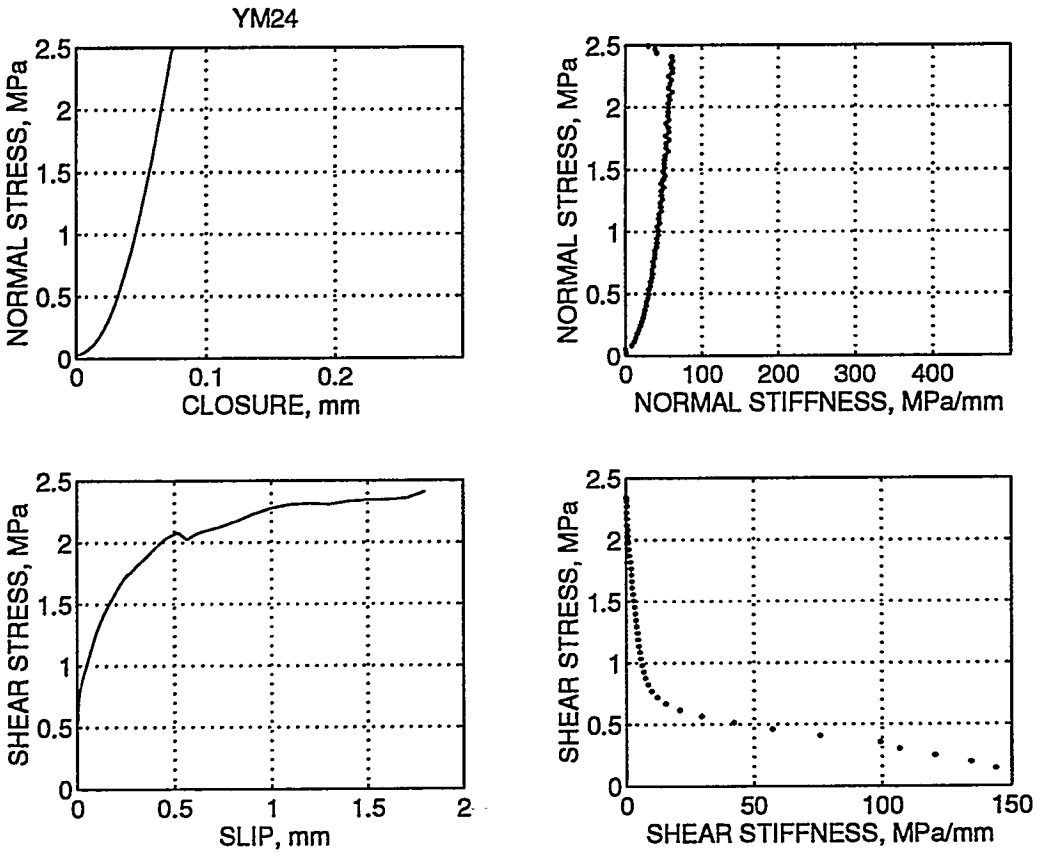

Figure 44: Shear and normal stiffness data for YM24.

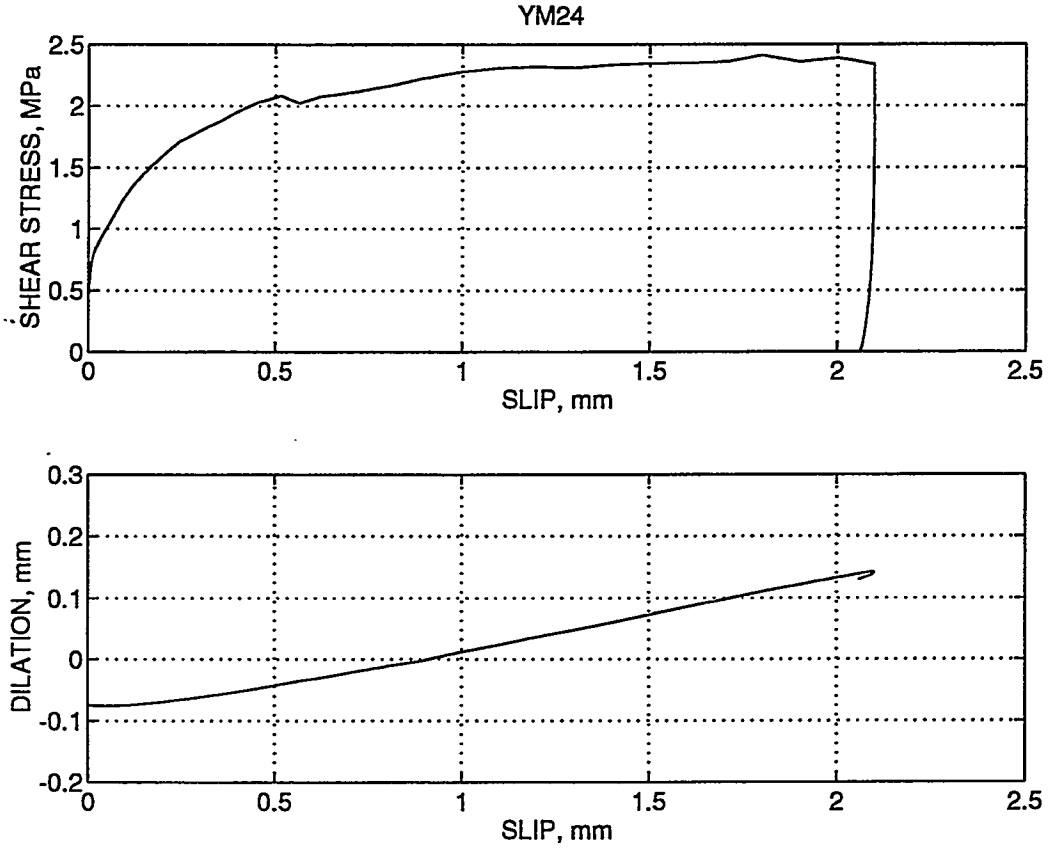

Figure 45: Shear strength and dilation data for YM24.

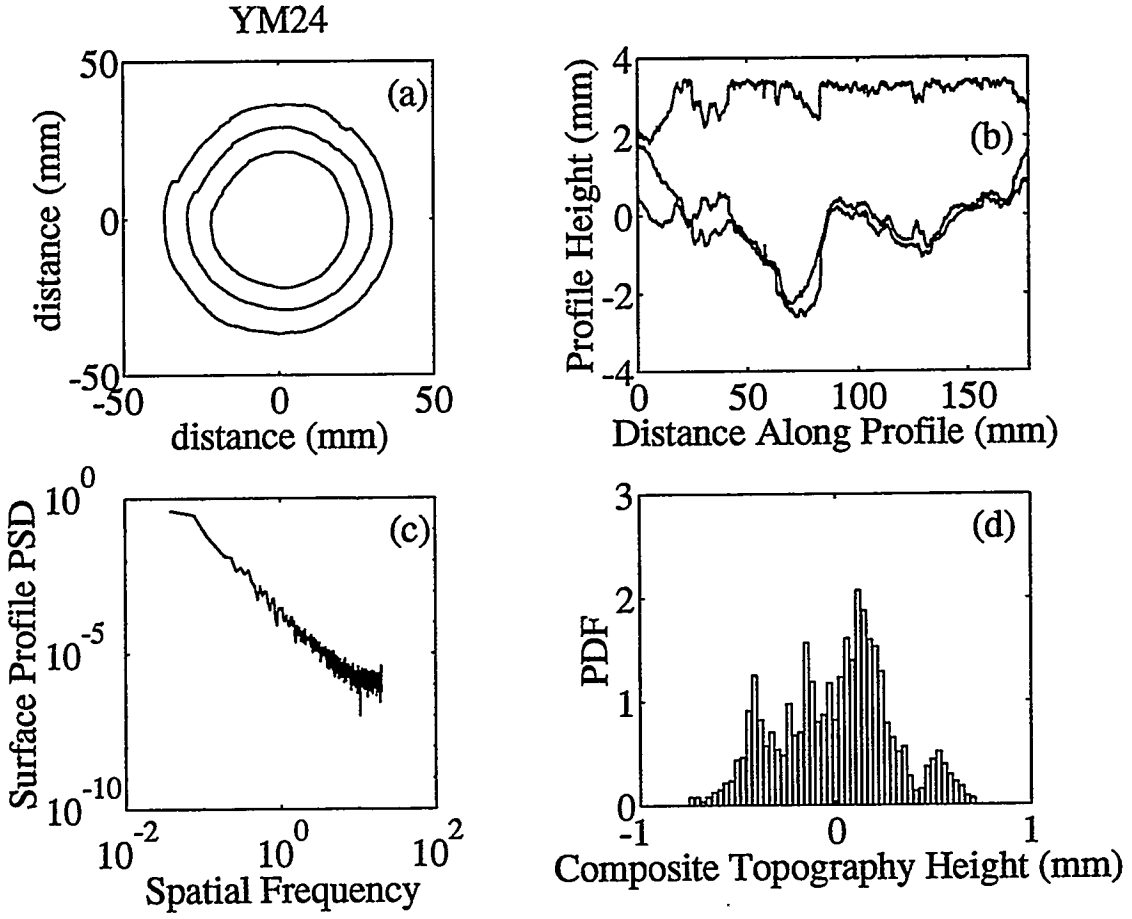

Figure 46: Profilometer data for YM24.

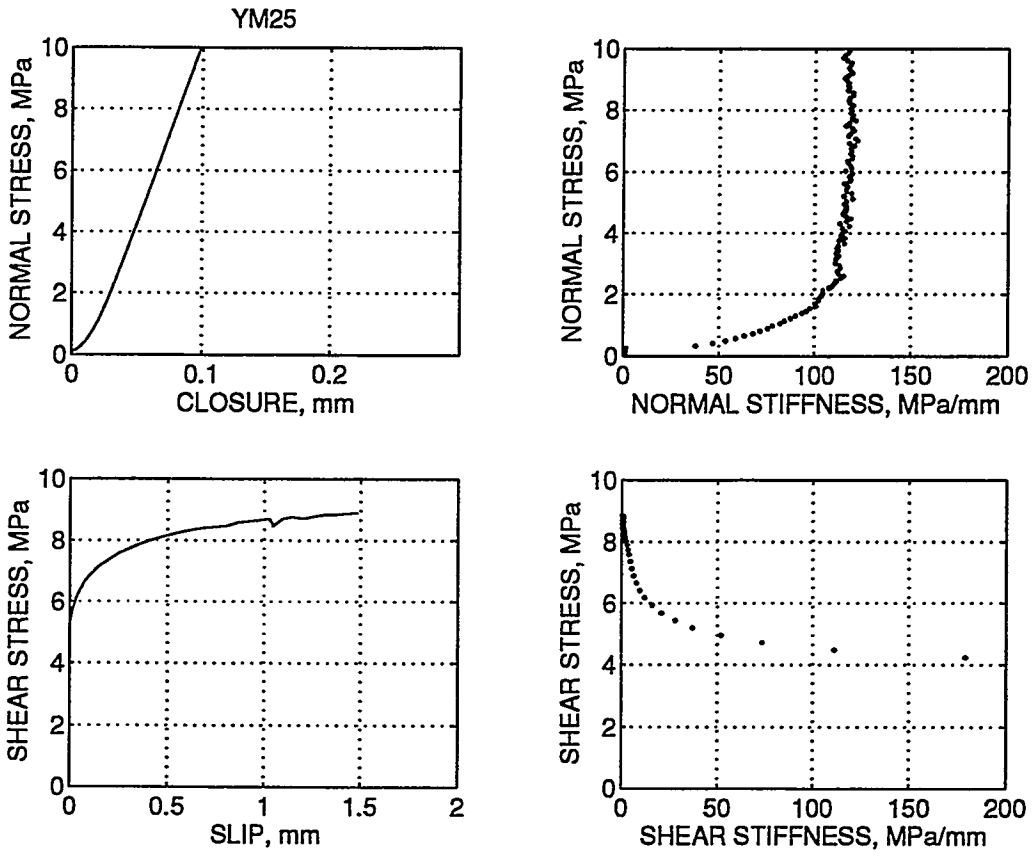

Figure 47: Shear and normal stiffness data for YM25.

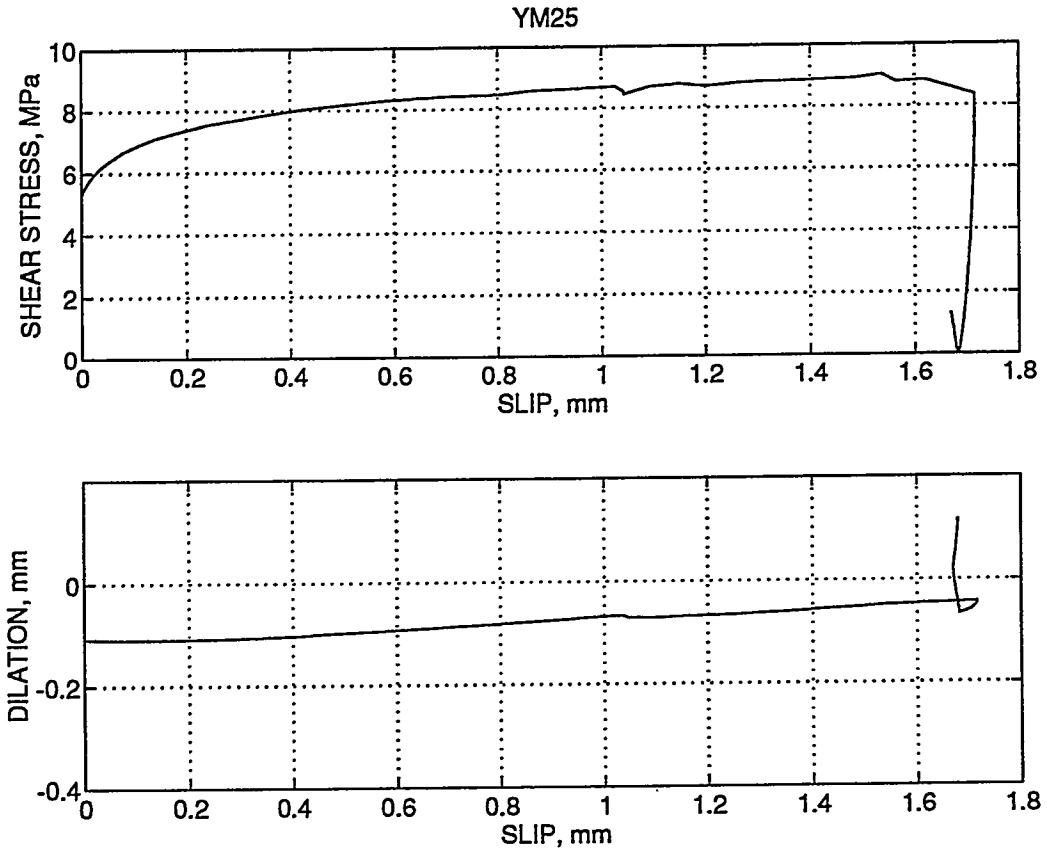

Figure 48: Shear strength and dilation data for YM25.

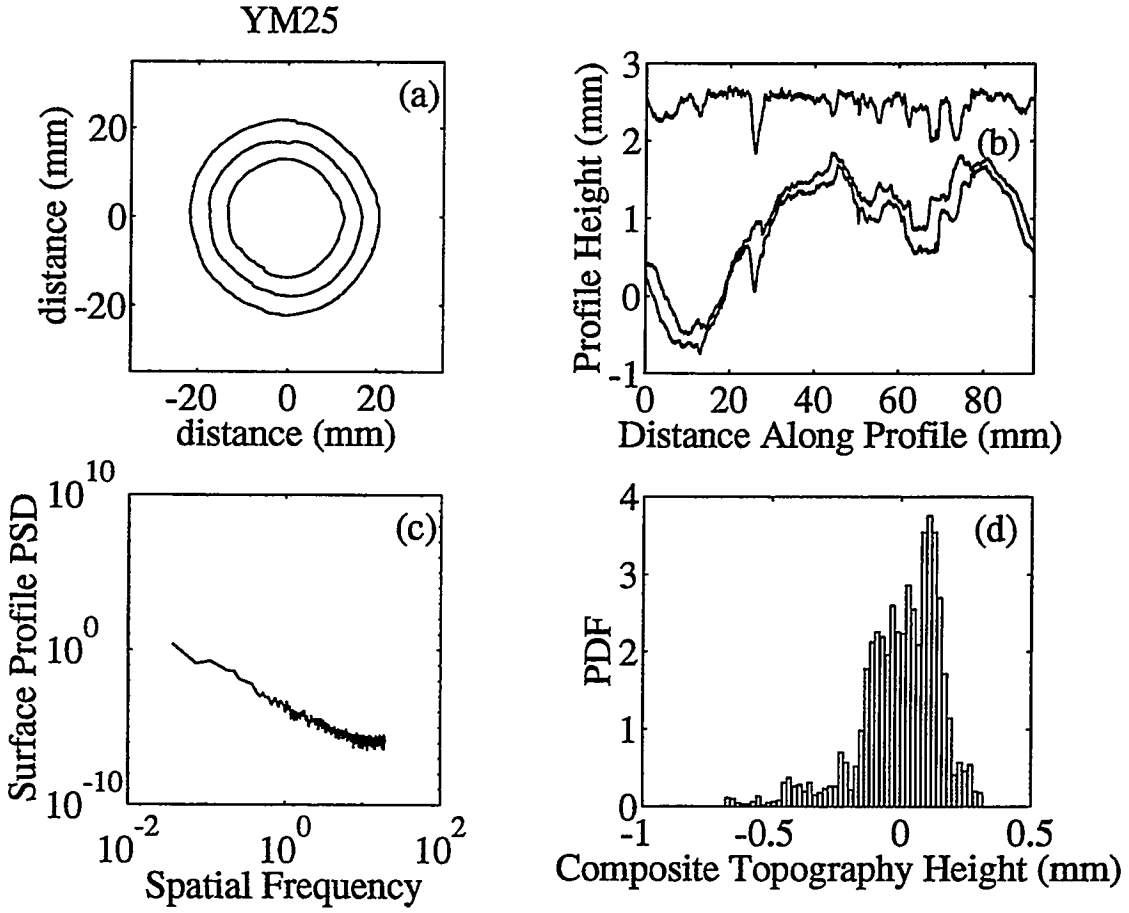

Figure 49: Profilometer data for YM25.

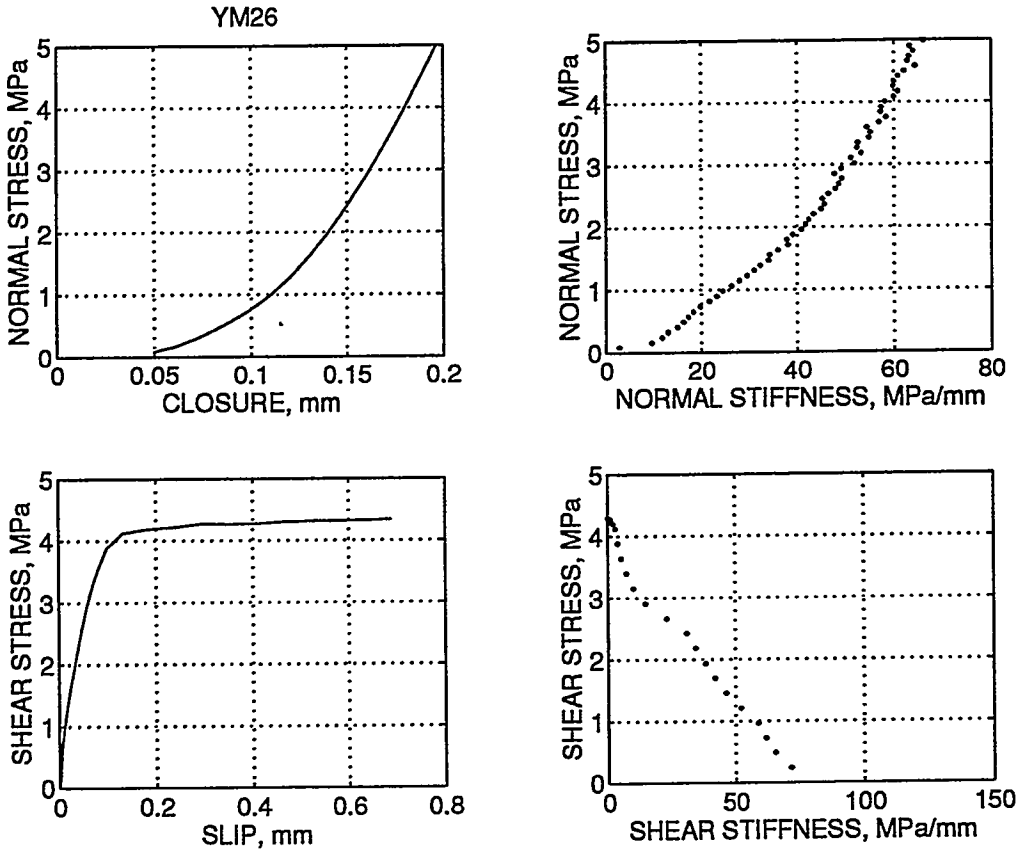

Figure 50: Shear and normal stiffness data for YM26.

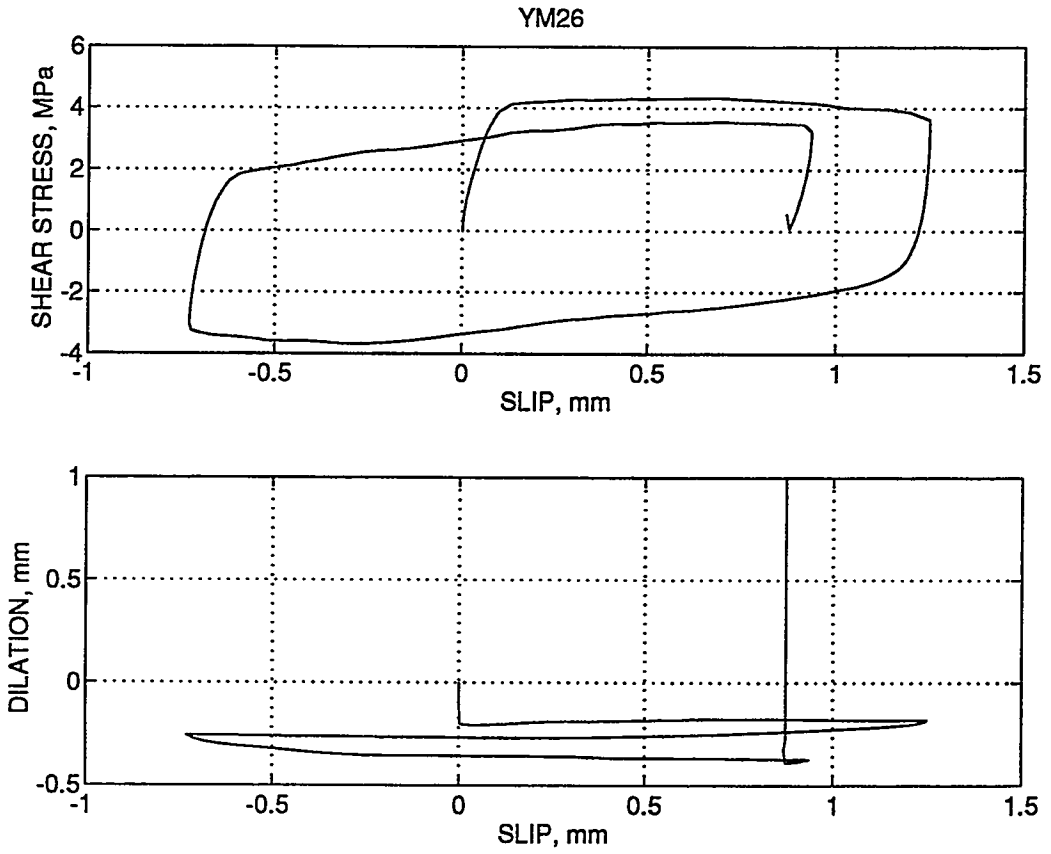

Figure 51: Shear strength and dilation data for YM26.

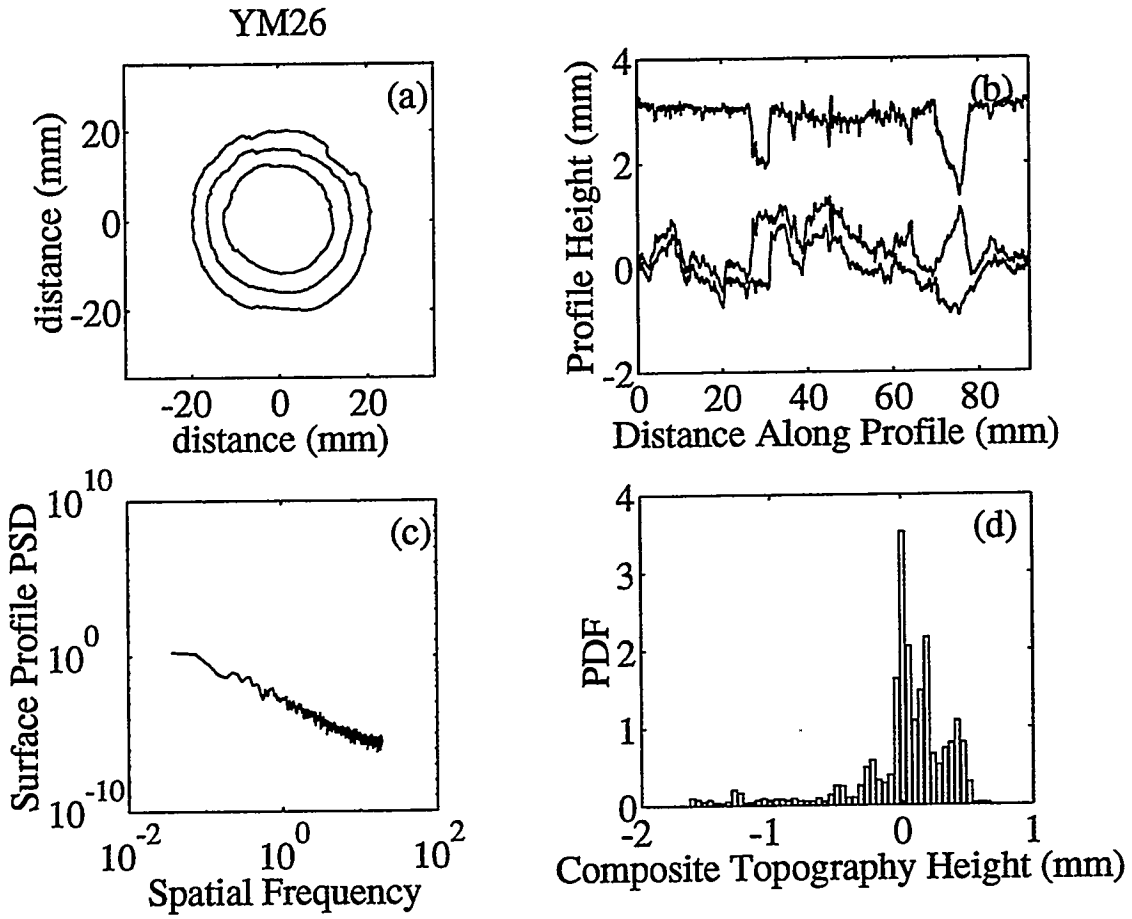

Figure 52: Profilometer data for YM26.

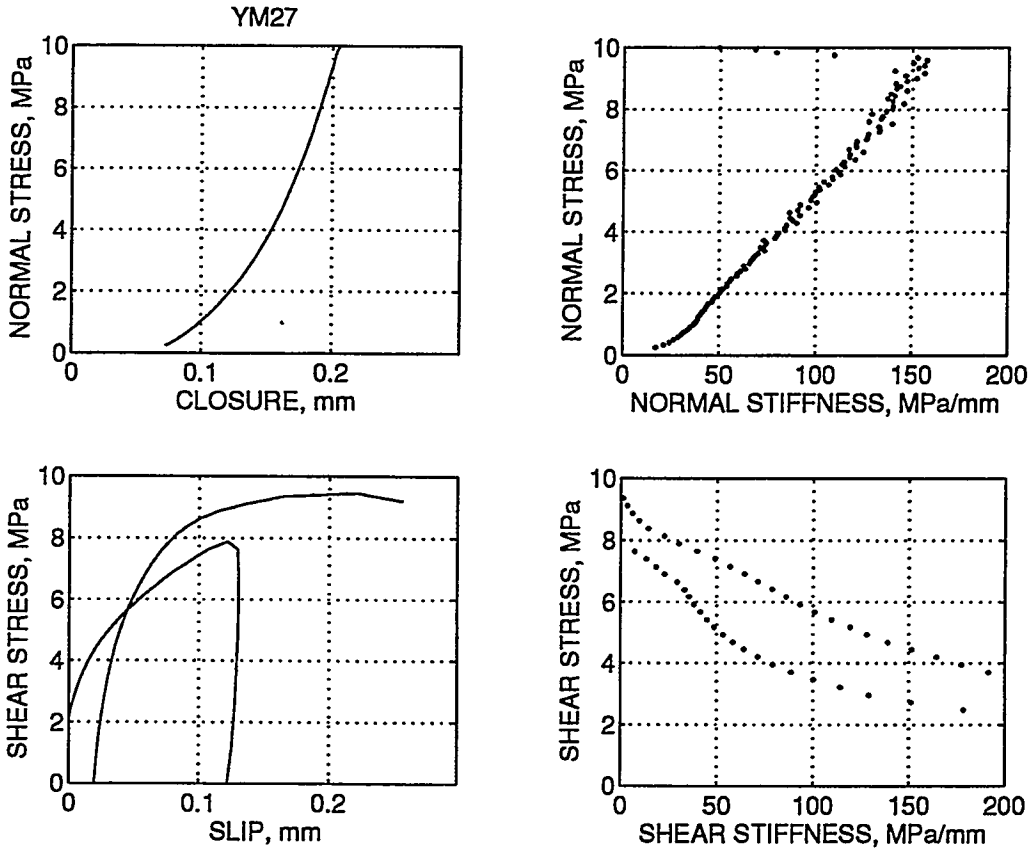

Figure 53: Shear and normal stiffness data for YM27.

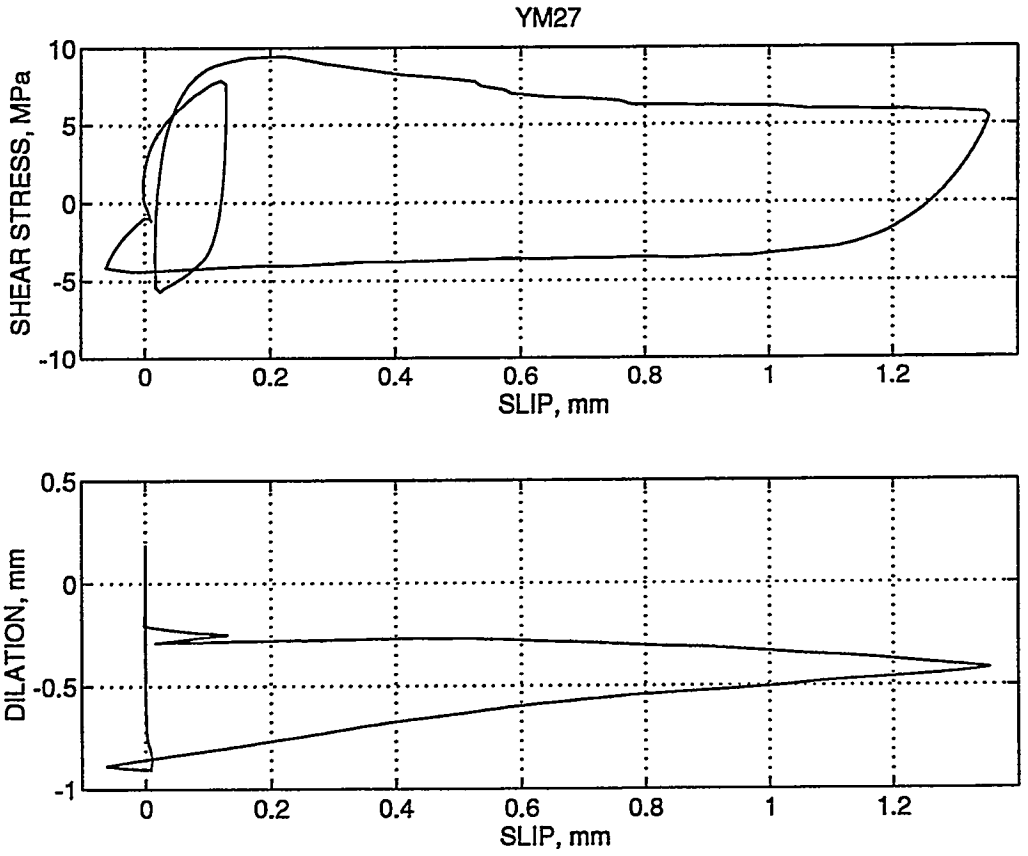

Figure 54: Shear strength and dilation data for YM27.

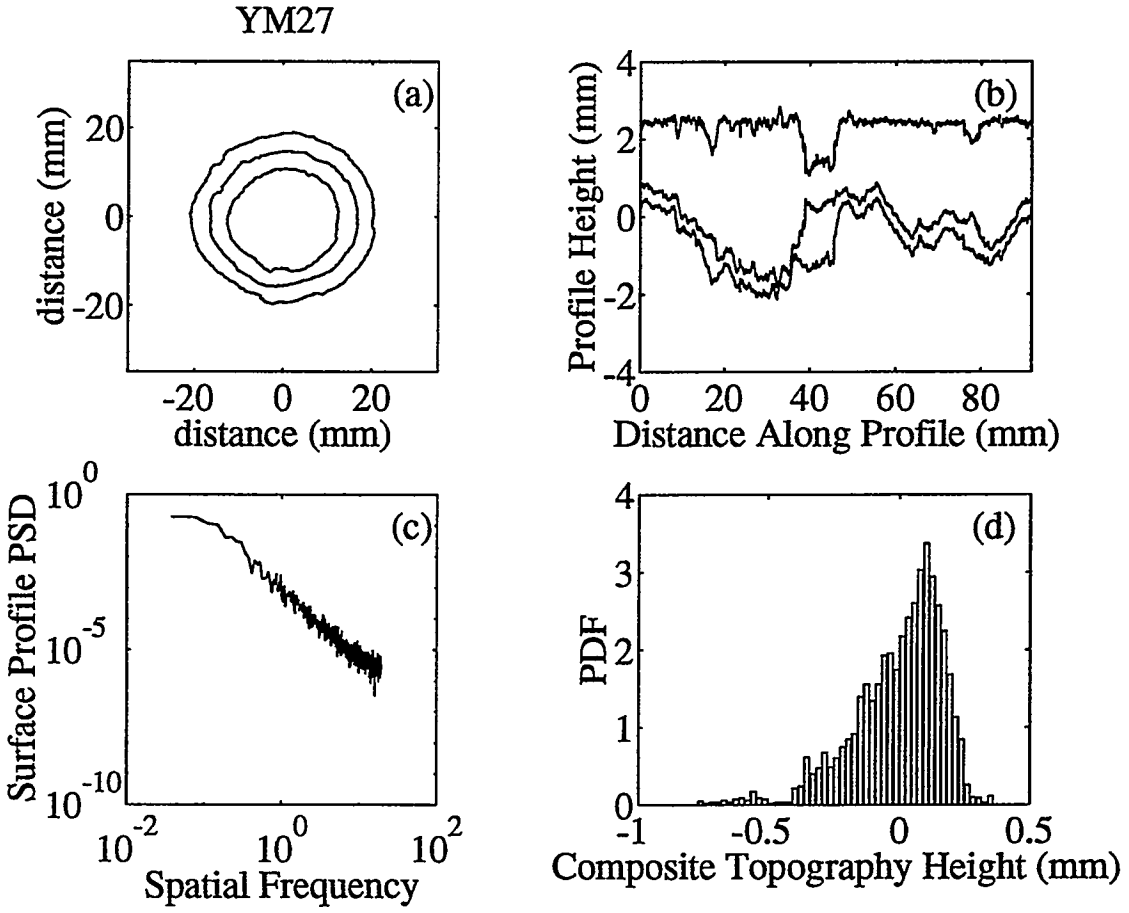

Figure 55: Profilometer data for YM27.

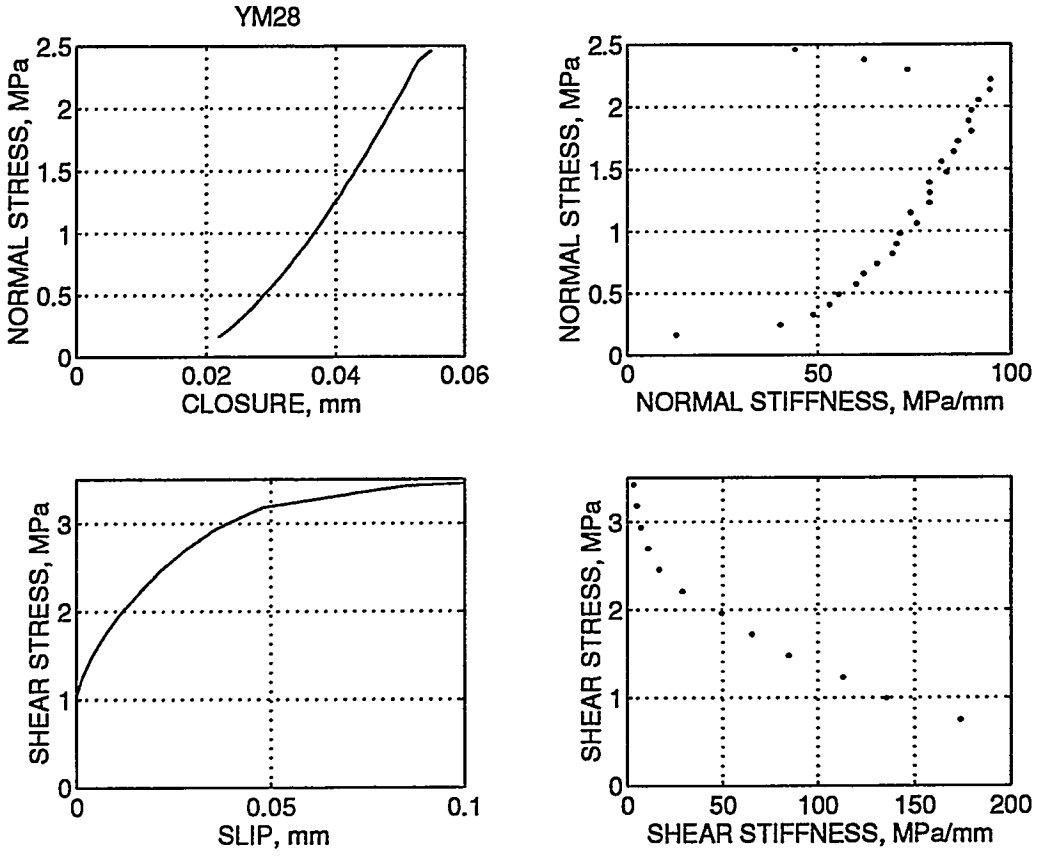

Figure 56: Shear and normal stiffness data for YM28.

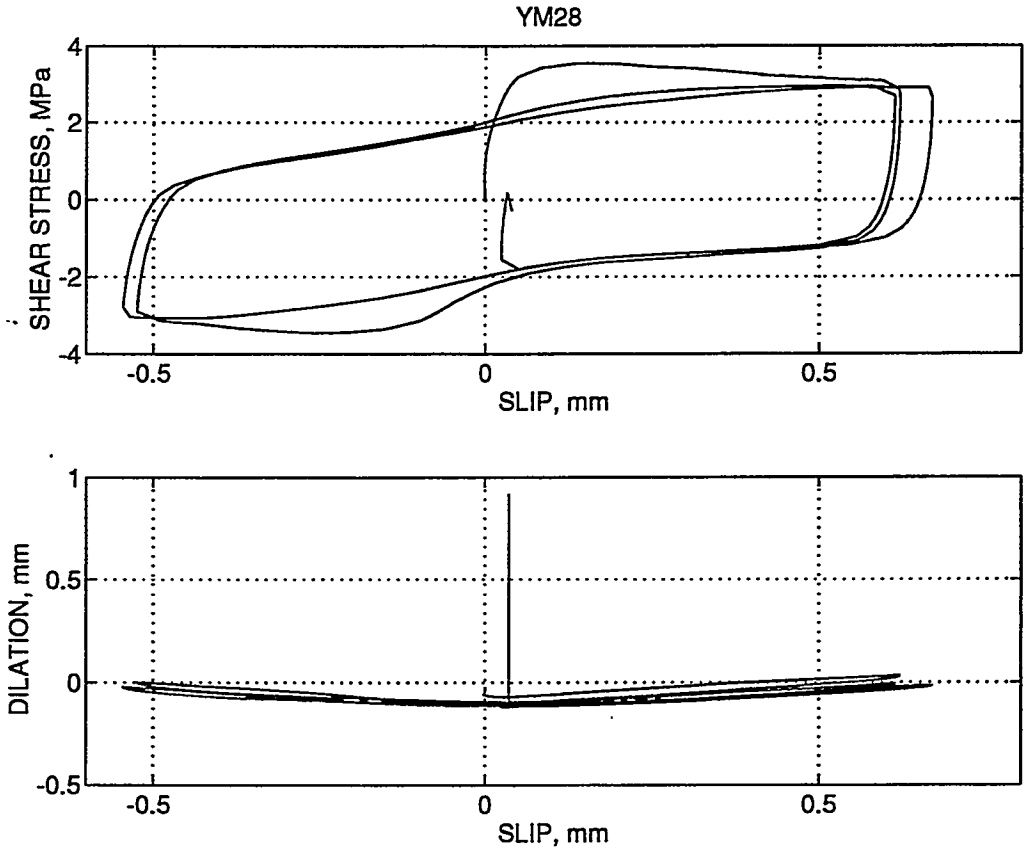

Figure 57: Shear strength and dilation data for YM28.

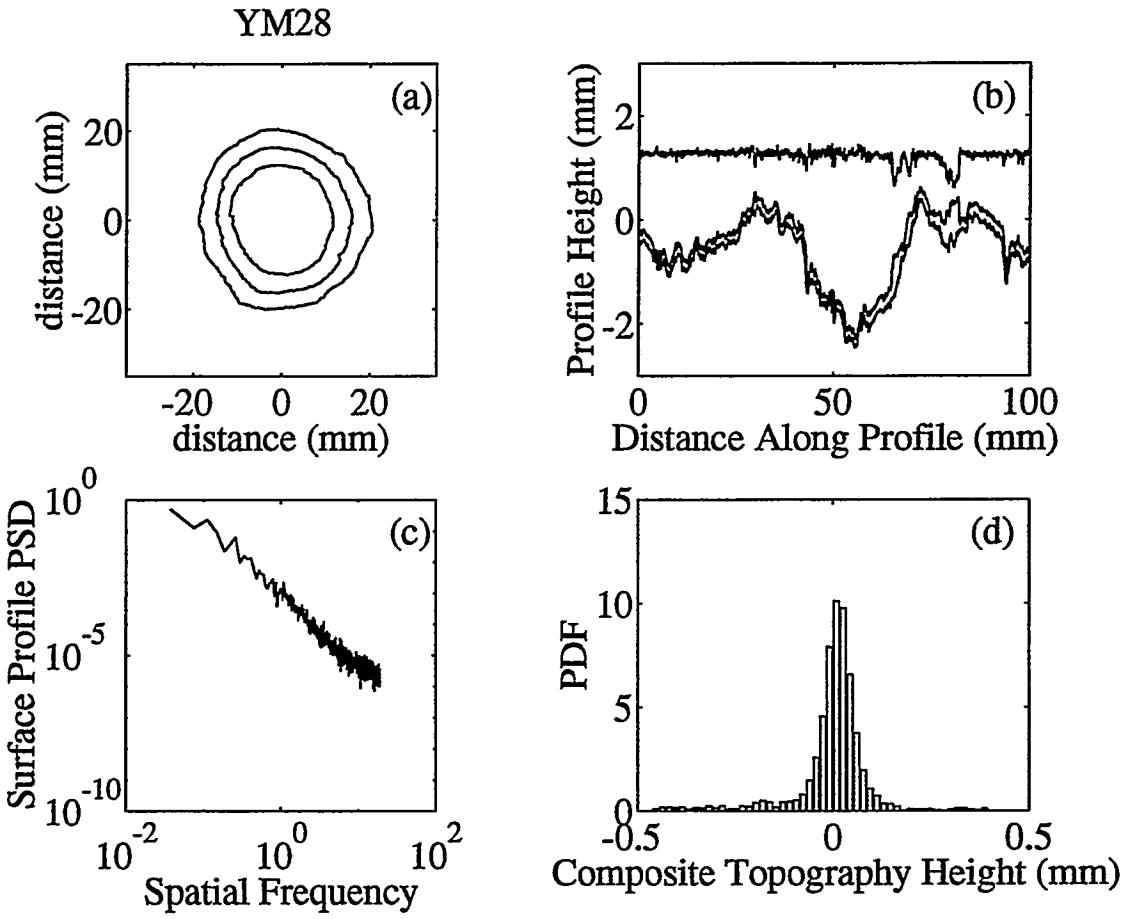

Figure 58: Profilometer data for YM28.

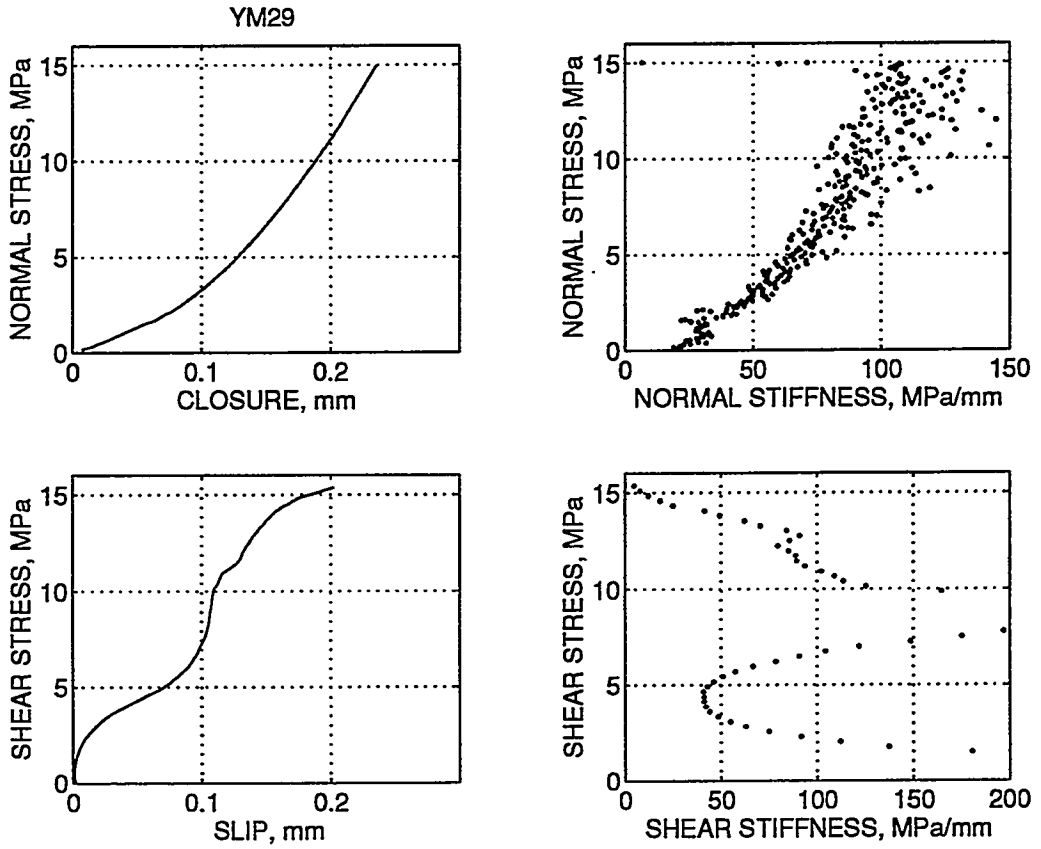

Figure 59: Shear and normal stiffness data for YM29.

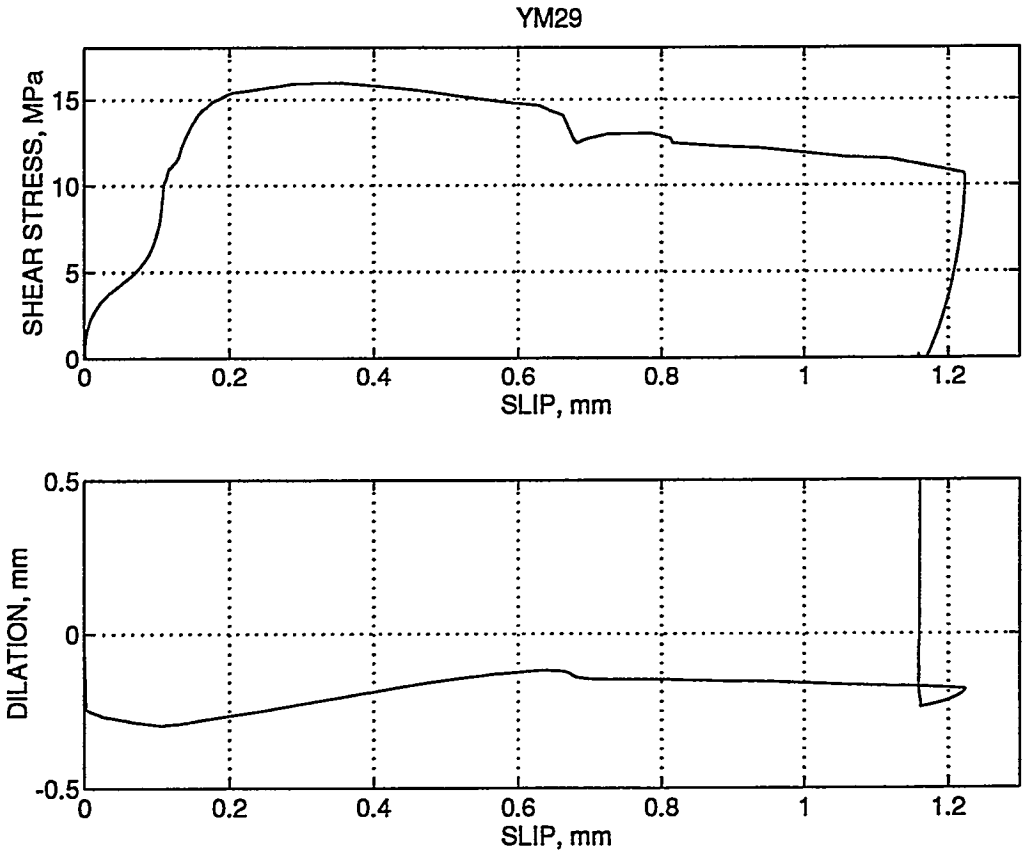

Figure 60: Shear strength and dilation data for YM29.

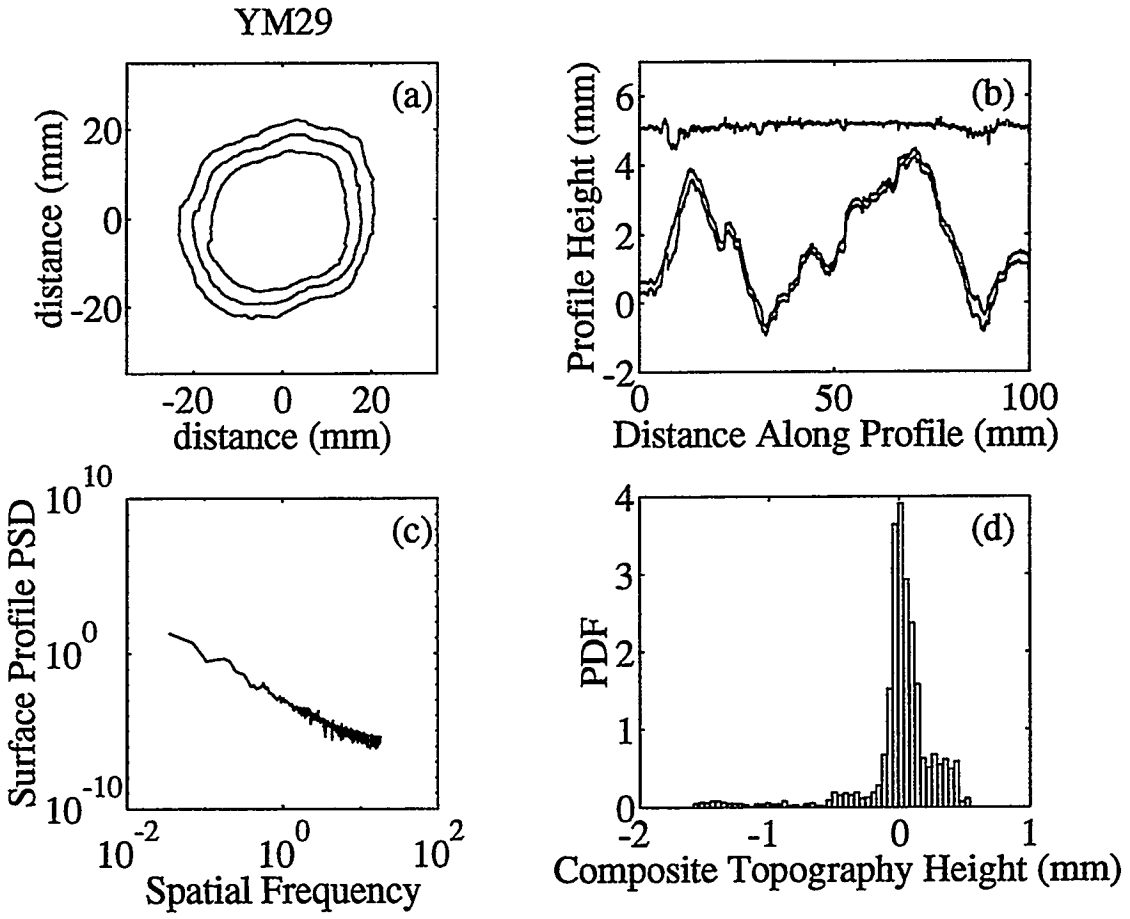

Figure 61: Profilometer data for YM29.

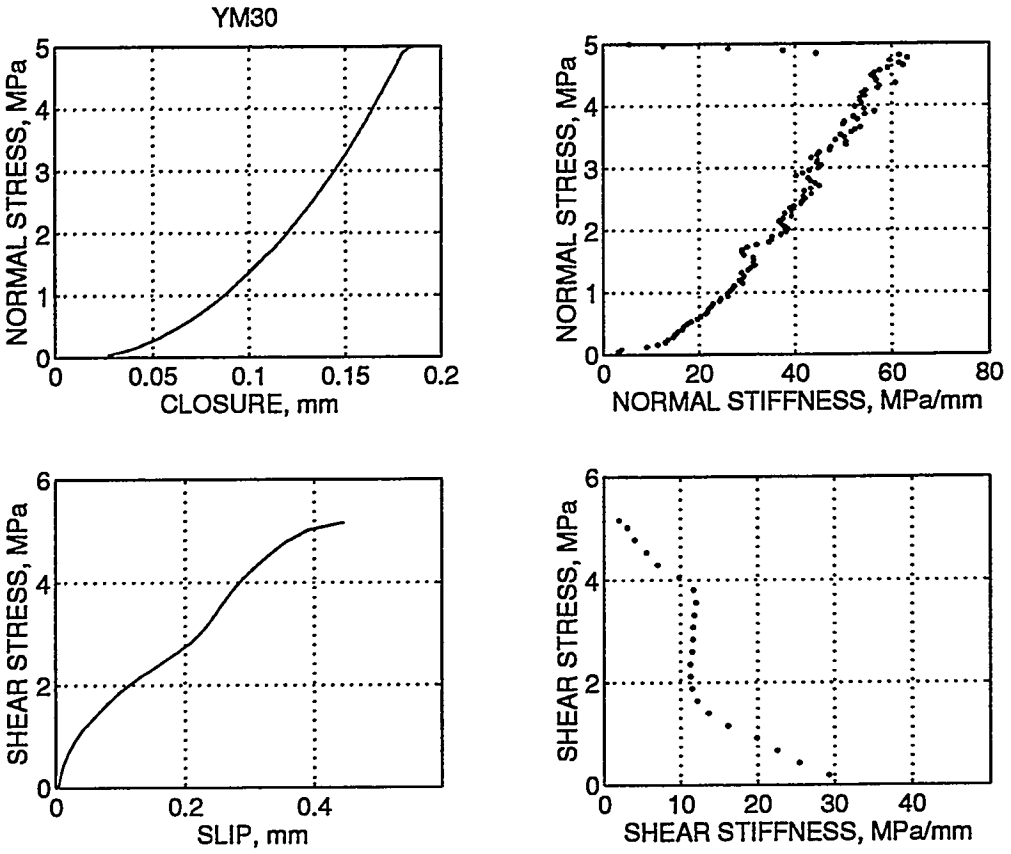

Figure 62: Shear and normal stiffness data for YM30.

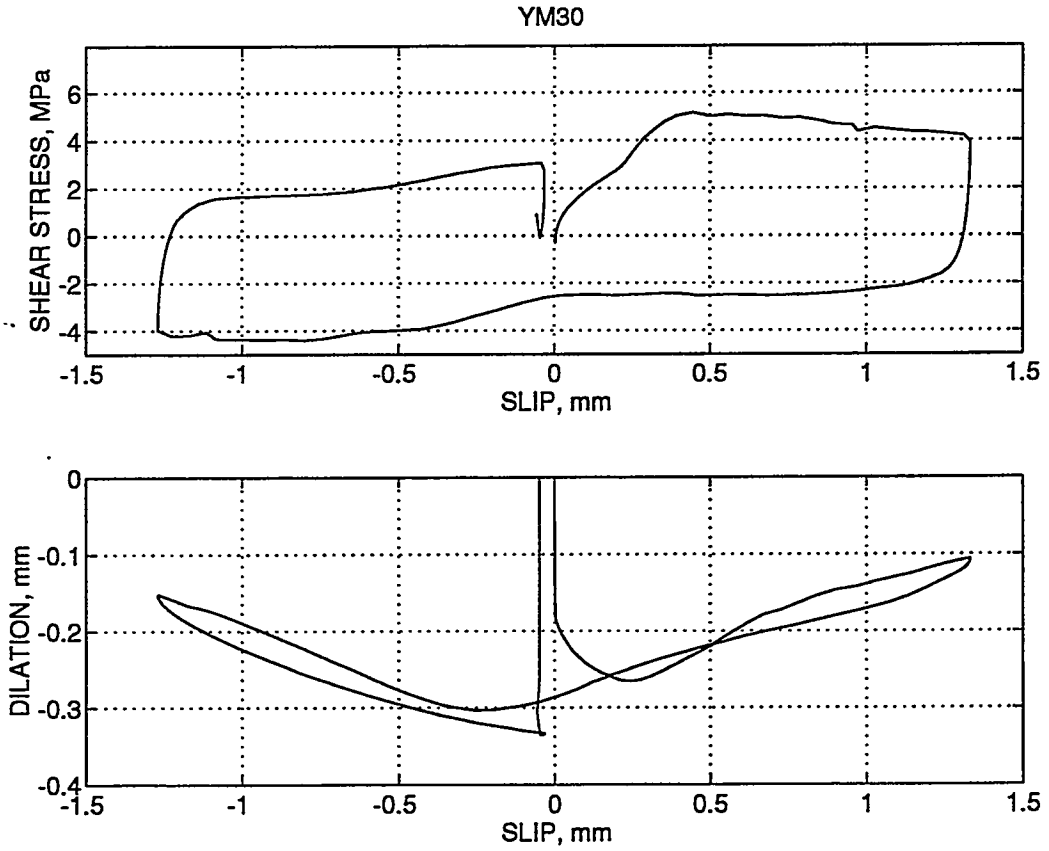

Figure 63: Shear strength and dilation data for YM30.

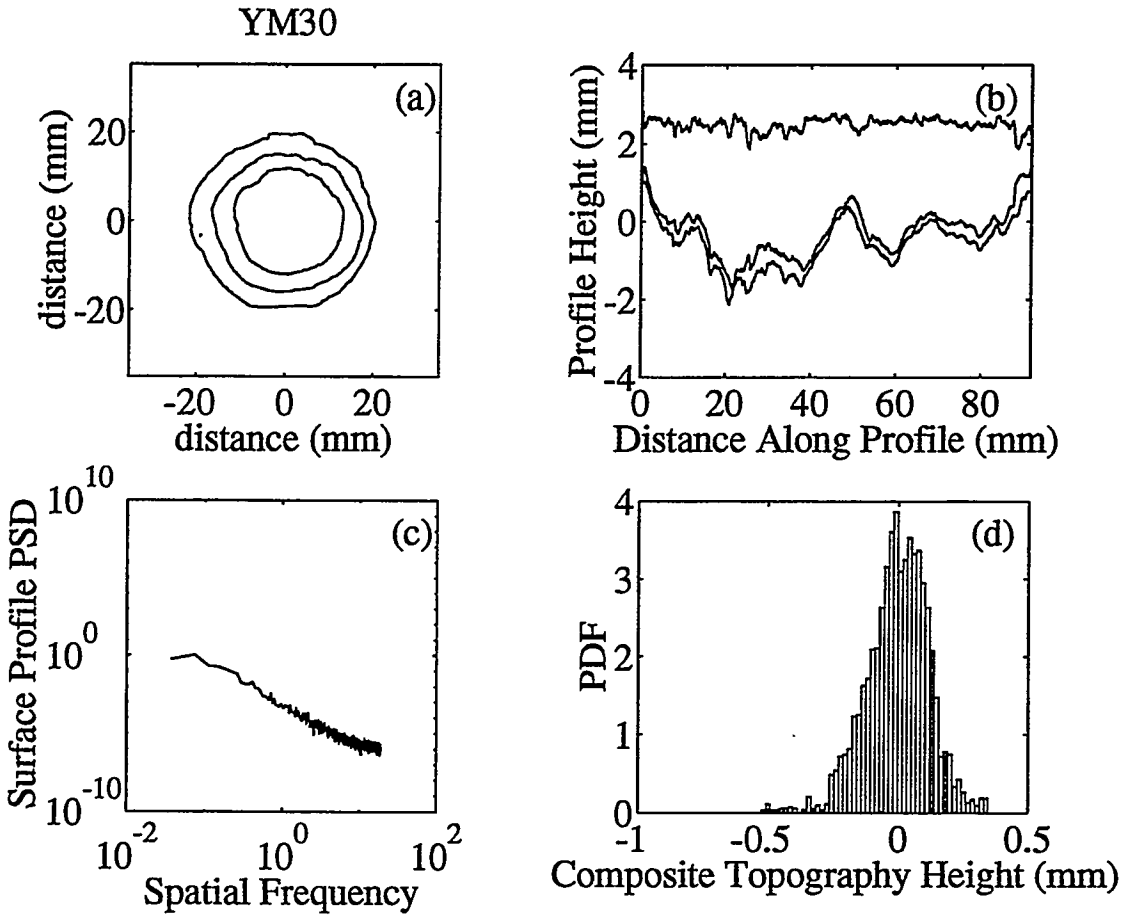

Figure 64: Profilometer data for YM30.

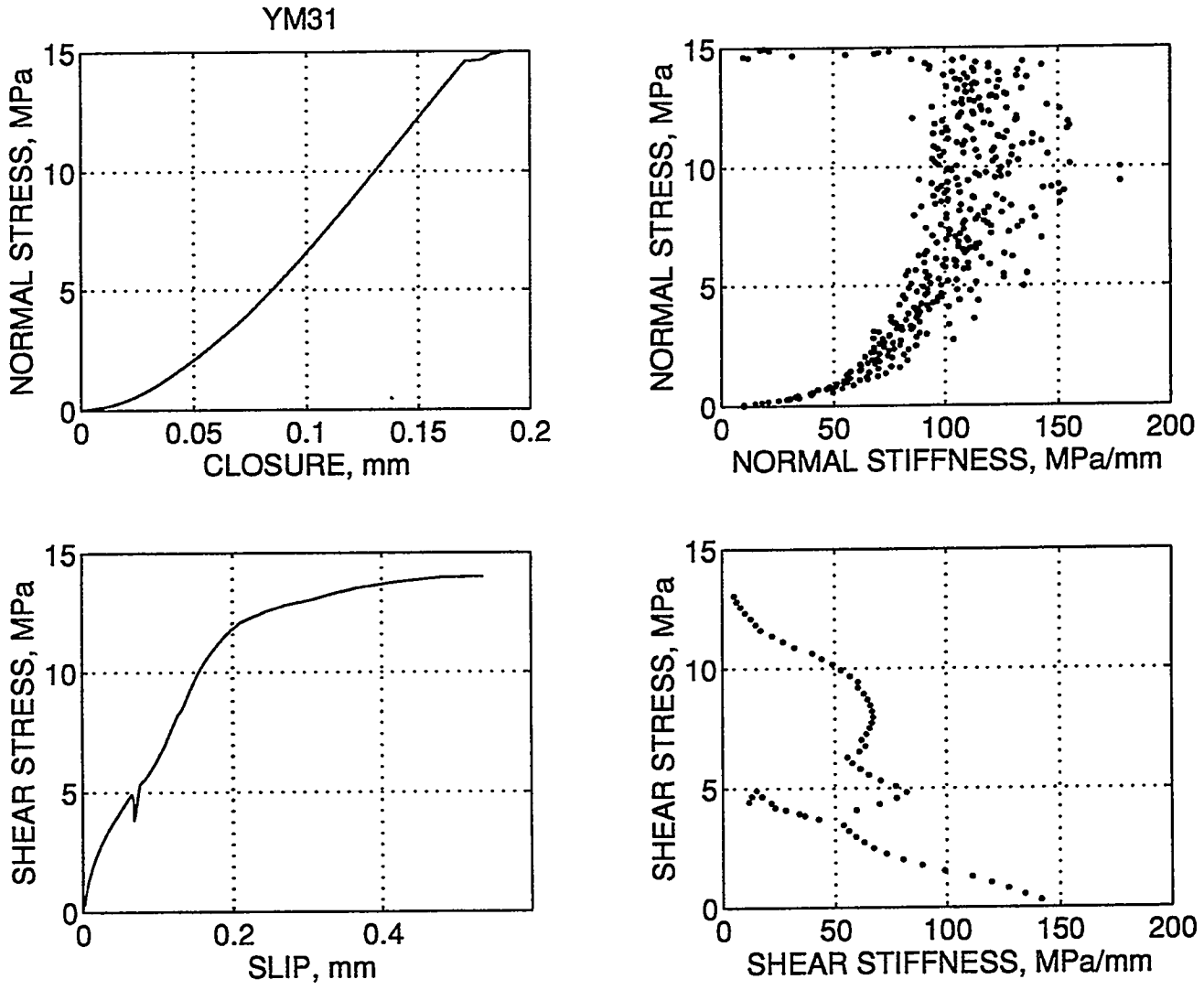

Figure 65: Shear and normal stiffness data for YM31.

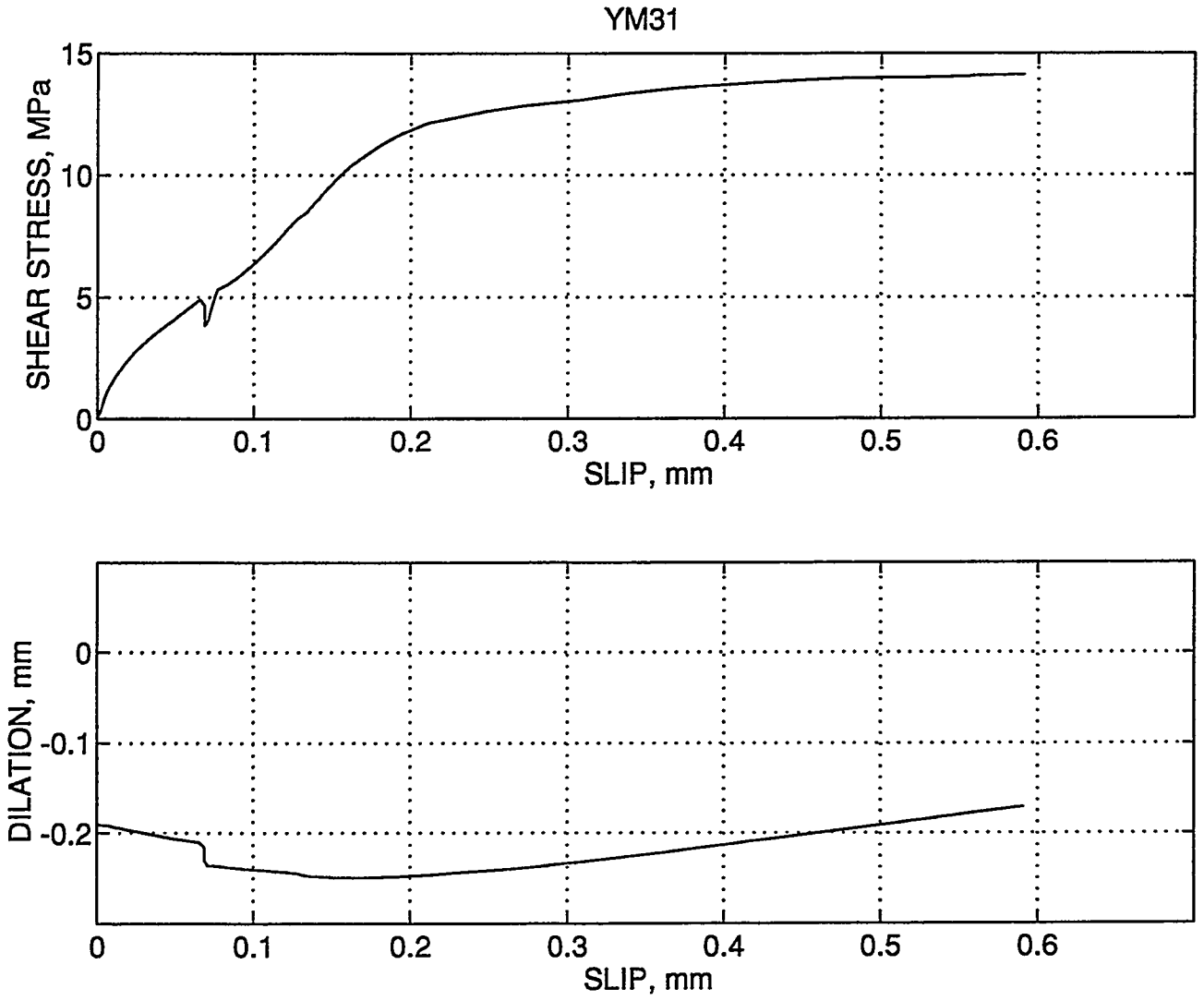

Figure 66: Shear strength and dilation data for YM31.

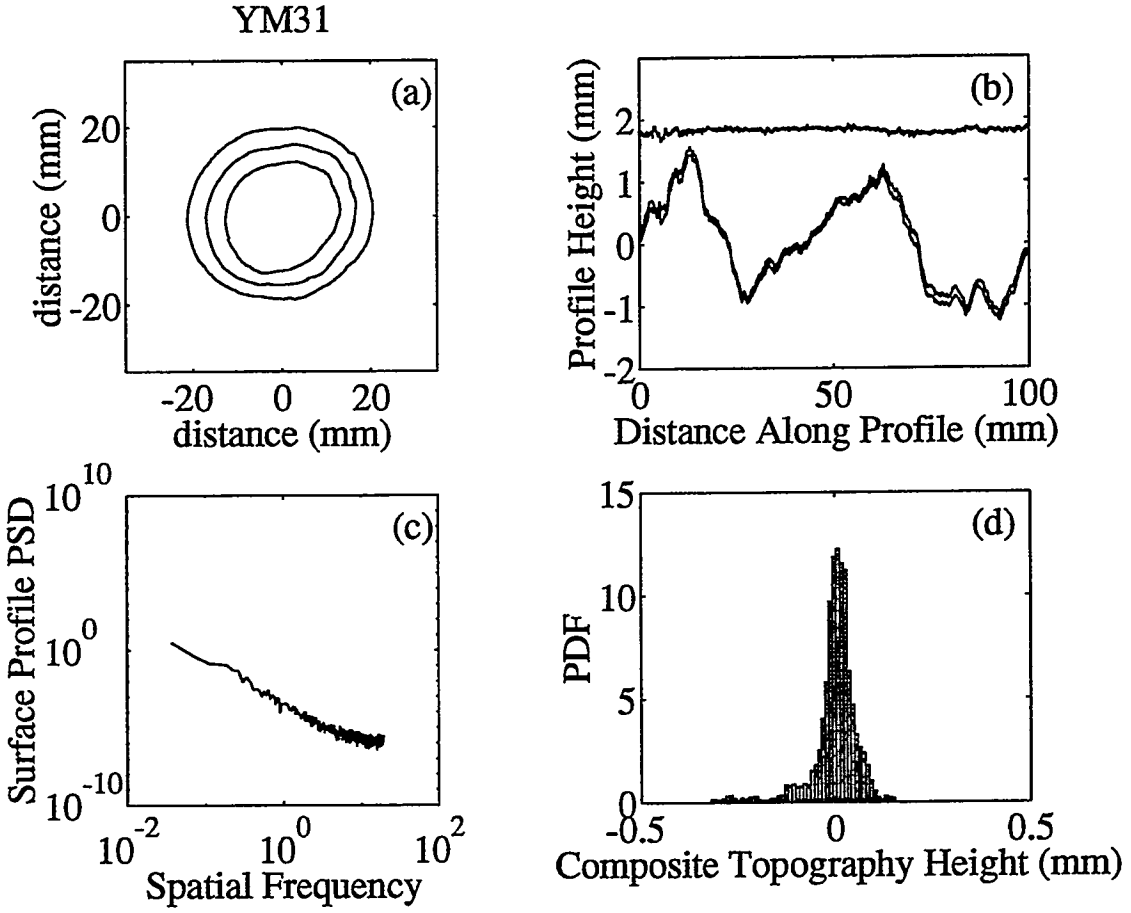

Figure 67: Profilometer data for YM31.

YUCCA MOUNTAIN SITE CHARACTERIZATION PROJECT
UC814 - DISTRIBUTION LIST
SAND95-1736

1 D. A. Dreyfus (RW-1)
Director
OCRWM
US Department of Energy
1000 Independence Avenue SW
Washington, DC 20585

1 L. H. Barrett (RW-2)
Acting Deputy Director
OCRWM
US Department of Energy
1000 Independence Avenue SW
Washington, DC 20585

1 S. Rousso (RW-40)
Office of Storage and Transportation
OCRWM
US Department of Energy
1000 Independence Avenue SW
Washington, DC 20585

1 R. A. Milner (RW-30)
Office of Program Management
and Integration
OCRWM
US Department of Energy
1000 Independence Avenue SW
Washington, DC 20585

1 D. R. Elle, Director
Environmental Protection Division
DOE Nevada Field Office
US Department of Energy
P.O. Box 98518
Las Vegas, NV 89193-8518

1 T. Wood (RW-14)
Contract Management Division
OCRWM
US Department of Energy
1000 Independence Avenue SW
Washington, DC 20585

4 Victoria F. Reich, Librarian
Nuclear Waste Technical Review Board
1100 Wilson Blvd., Suite 910
Arlington, VA 22209

1 Wesley Barnes, Project Manager
Yucca Mountain Site Characterization
Office
US Department of Energy
P.O. Box 98608--MS 523
Las Vegas, NV 89193-8608

1 Director, Public Affairs Office
c/o Technical Information Resource Center
DOE Nevada Operations Office
US Department of Energy
P.O. Box 98518
Las Vegas, NV 89193-8518

8 Technical Information Officer
DOE Nevada Operations Office
US Department of Energy
P.O. Box 98518
Las Vegas, NV 89193-8518

1 J. R. Dyer, Deputy Project Manager
Yucca Mountain Site Characterization Office
US Department of Energy
P.O. Box 98608 -- MS 523
Las Vegas, NV 89193-88608

1 M. C. Brady
Laboratory Lead for YMP
M&O/Sandia National Laboratories
1261 Town Center Drive
Bldg. 4, Room 421A
Las Vegas, NV 89134

1 J. A. Canepa
Laboratory Lead for YMP
EES-13, Mail Stop J521
M&O/Los Alamos National Laboratory
P.O. Box 1663
Los Alamos, NM 87545

1 Repository Licensing & Quality
Assurance
Project Directorate
Division of Waste Management, MS T7J-9
US NRC
Washington, DC 20555

1 Senior Project Manager for Yucca
Mountain
Repository Project Branch
Division of Waste Management, MS T7J-9
US NRC
Washington, DC 20555

1 NRC Document Control Desk
Division of Waste Management, MS T7J-9
US NRC
Washington, DC 20555

1 Chad Glenn
NRC Site Representative
301 E Stewart Avenue, Room 203
Las Vegas, NV 89101

1 Center for Nuclear Waste
Regulatory Analyses
Southwest Research Institute
6220 Culebra Road
Drawer 28510
San Antonio, TX 78284

2 W. L. Clarke
Laboratory Lead for YMP
M&O/ Lawrence Livermore Nat'l Lab
P.O. Box 808 (L-51)
Livermore, CA 94550

1 Robert W. Craig
Acting Technical Project Officer/YMP
US Geological Survey
101 Convention Center Drive, Suite P-110
Las Vegas, NV 89109

1 J. S. Stuckless, Chief
Geologic Studies Program
MS 425
Yucca Mountain Project Branch
US Geological Survey
P.O. Box 25046
Denver, CO 80225

1 L. D. Foust
Technical Project Officer for YMP
TRW Environmental Safety Systems
101 Convention Center Drive
Suite P-110
Las Vegas, NV 89109

1 A. L. Flint
U. S. Geological Survey
MS 721
P. O. Box 327
Mercury, NV 89023

1 Robert L. Strickler
Vice President & General Manager
TRW Environmental Safety Systems, Inc.
2650 Park Tower Dr.
Vienna, VA 22180

1 Jim Krulik, Geology Manager
US Bureau of Reclamation
Code D-8322
P.O. Box 25007
Denver, CO 80225-0007

1 B. T. Brady
Records Specialist
US Geological Survey
MS 421
P.O. Box 25046
Denver, CO 80225

1 M. D. Voegele
Deputy of Technical Operations
M&O/SAIC
101 Convention Center Drive
Suite P-110
Las Vegas, NV 89109

2 A. T. Tamura
Science and Technology Division
OSTI
US Department of Energy
P.O. Box 62
Oak Ridge, TN 37831

1 P. J. Weeden, Acting Director
Nuclear Radiation Assessment Div.
US EPA
Environmental Monitoring Sys. Lab
P.O. Box 93478
Las Vegas, NV 89193-3478

1 John Fordham, Deputy Director
Water Resources Center
Desert Research Institute
P.O. Box 60220
Reno, NV 89506

1 The Honorable Jim Regan
Chairman
Churchill County Board of
Commissioners
10 W. Williams Avenue
Fallon, NV 89406

1 R. R. Loux
Executive Director
Agency for Nuclear Projects
State of Nevada
Evergreen Center, Suite 252
1802 N. Carson Street
Carson City, NV 89710

1 Brad R. Mettam
Inyo County Yucca Mountain
Repository Assessment Office
P. O. Drawer L
Independence, CA 93526

1 Vernon E. Poe
Office of Nuclear Projects
Mineral County
P.O. Box 1600
Hawthorne, NV 89415

1 Les W. Bradshaw
Program Manager
Nye County Nuclear Waste Repository
Project Office
P.O. Box 1767
Tonopah, NV 89049

1 Florindo Mariani
White Pine County Coordinator
P. O. Box 135
Ely, NV 89301

1 Tammy Manzini
Lander County Yucca Mountain
Information Officer
P.O. Box 10
Austin, NV 89310

1 Jason Pitts
Lincoln County Nuclear Waste
Program Manager
P. O. Box 158
Pioche, NV 89043

1 Dennis Bechtel, Coordinator
Nuclear Waste Division
Clark County Dept. of Comprehensive
Planning
P.O. Box 55171
Las Vegas, NV 89155-1751

1 Juanita D. Hoffman
Nuclear Waste Repository
Oversight Program
Esmeralda County
P.O. Box 490
Goldfield, NV 89013

1 Sandy Green
Yucca Mountain Information Office
Eureka County
P.O. Box 714
Eureka, NV 89316

1 Economic Development Dept.
City of Las Vegas
400 E. Stewart Avenue
Las Vegas, NV 89101

1 Community Planning & Development
City of North Las Vegas
P.O. Box 4086
North Las Vegas, NV 89030

2 Librarian
YMP Research & Study Center
101 Convention Center Drive, Suite P-110
Las Vegas, NV 89109

1 Library Acquisitions
Argonne National Laboratory
Building 203, Room CE-111
9700 S. Cass Avenue
Argonne, IL 60439

1 Glenn Van Roekel
Manager, City of Caliente
P.O. Box 158
Caliente, NV 89008

1 G. S. Bodvarsson
Head, Nuclear Waste Department
Lawrence Berkeley National Laboratory
1 Cyclotron Road, MS 50E
Berkeley, CA 94720

1 Steve Hanauer (RW-2)
OCRWM
U. S. Department of Energy
1000 Independence Ave.
Washington, DC 20585

5 Stephen Brown
Applied Research Associates
New England Division
R. R. 1 Box 120A Waterman Rd.
South Royalton, VT 05068

	MS	
2	1330	K. Hart, 6811 100/_(1232714SAND95-1736QA)
20	1330	WMT Library, 6752
1	9018	Central Technical Files, 8940-2
5	0899	Technical Library, 4414
2	0619	Review and Approval Desk, 12690, For DOE/OSTI
1	1325	R. H. Price, 6852
5	1325	N. Brodsky, 6852
1	1325	L. S. Costin, 6852
5	1399	D. S. Kessel, 6850
5	0751	W. Olsson, 6117